

https://dspace.org/

Highly resilient fibrous matrices for rapid drug delivery

Dott, Clare

2011-11-23
http://hdl.handle.net/10539/10831

Downloaded from a DSpace repository. https://dspace.org/

HIGHLY RESILIENT FIBROUS MATRICES FOR RAPID DRUG DELIVERY

CLARE DOTT

A dissertation submitted to the Faculty of Health Sciences, University of the Witwatersrand, in fulfillment of the requirements for the degree of Master of Pharmacy

Supervisor:

Professor Viness Pillay

University of the Witwatersrand, Department of Pharmacy and Pharmacology, Johannesburg, South Africa

Co-Supervisors:

Doctor Yahya Essop Choonara

University of the Witwatersrand, Department of Pharmacy and Pharmacology, Johannesburg, South Africa

and

Ms. Lisa Claire du Toit

University of the Witwatersrand, Department of Pharmacy and Pharmacology, Johannesburg, South Africa

Johannesburg

2011

DECLARATION

I, Clare Dott, declare that this dissertation is my own work. It has been submitted for the degree of Master of Pharmacy in the Faculty of Health Sciences in the University of the Witwatersrand, Johannesburg. It has not been submitted before for any degree or examination at this or any other University.

.....

This**.....**day of January 2011

RESEARCH PRESENTATIONS

POSTERS

Glycerol monostearate and hypromellose-based sheaths for drug delivery.
Clare Dott, Viness Pillay, Yahya E. Choonara and Lisa C. du Toit.
29th Annual Conference of the Academy of Pharmaceutical Sciences, Rustenburg, South Africa, 22-26 September 2008.

Asymmetrical mesophasic cellulose membranes for oramucosal drug delivery.
Nosipho Gwala, Clare Dott, Viness Pillay, Yahya E. Choonara and Lisa C. du Toit.
29th Annual Conference of the Academy of Pharmaceutical Sciences, Rustenburg, South Africa, 22-26 September 2008.

Electrospun fibrous PVA membranes for rapid transmucosal drug delivery.
Clare Dott, Viness Pillay, Yahya E. Choonara and Lisa C. du Toit.
5th International Conference on Pharmaceutical and Pharmacological Sciences, Potchefstroom, South Africa, 23-26 September 2009.

Casted cellulosic films for application in oramucosal drug delivery.
Clare Dott, Viness Pillay, Yahya E. Choonara and Lisa C. du Toit.
American Association of Pharmaceutical Sciences Annual Meeting and Exposition, Los Angeles, California, USA, 8-12 November 2009.

PODIUM

Elucidating structural morphology of electrospun PVA fibres intended for drug delivery.

Clare Dott, Viness Pillay, Yahya E. Choonara and Lisa C. du Toit.

School of Therapeutic Sciences Research Day, University of the Witwatersrand, Johannesburg, South Africa, 12 August 2009.

PATENT

A fibrous matrix system for oramucosal drug delivery.

Viness Pillay, Clare Dott, Yahya E. Choonara, Lisa C. du Toit, South Africa, Patent Application drafted, 2010.

ABSTRACT

The oral delivery of drugs has several disadvantages, particularly in pediatrics, geriatrics and other patients experiencing difficulty in swallowing tablets or capsules. A frequent approach to this problem is the use of liquid formulations or buccal drug delivery systems. However, with liquid formulations, many drugs have an undesirable solubility or stability in appropriate solvents and dosing accuracy is compromised due to the patient being required to measure doses. Current rapidly disintegrating buccal drug delivery systems, such as buccal tablets, are able to dissolve rapidly within the oral cavity; however the short residence time at the absorption surface is a limiting factor in the effectiveness of these delivery systems. Furthermore, buccal tablet and wafer systems tend to be brittle and fragile and hence require special protective packaging. A rapidly disintegrating, flexible, mucoadhesive fibrous matrix system (FMS) with drug-loaded electrospun fibers incorporated onto a polymeric backing film may be capable of overcoming some of the innate disadvantages of the non-invasive delivery of various drugs, especially those requiring a rapid onset of action.

Various electrospinnable polymers were investigated for suitability in the development of the electrospun fibrous layer of the FMS, and it was determined that polyvinylalcohol (PVA) produced drug-loaded fibers with the most acceptable morphology and a desirable disintegration time. An ideal drug-loaded fiber formulation was obtained by design of experiments and employed in further investigations. The original model drug, zidovudine (AZT), exhibited less than 1% permeation after 90 minutes. Permeation was not adequately increased by penetration enhancers, and AZT was therefore tested against diphenhydramine (DPH), which exhibited 42-82% permeation after 5 minutes.

The polymeric backing film layer was developed by investigating various film-forming polymers and methods of film or membrane preparation. Acceptable films were produced by film-casting of solutions containing combinations of PVA and hydroxypropylmethylcellulose (HPMC), and variables for an Experimental Design were obtained. The variables were fill volume (40-100mL), HPMC concentration (0-0.5%$^{w}/_{v}$) and concentration of glycerol (10-15%$^{w}/_{w}$ of total polymer mass). The film layer was optimized according to a Box-Behnken experimental design, employing the responses disintegration time, work of adhesion, maximum detachment force, dissolution and *ex vivo* permeation.

In vitro physicochemical and physicomechanical characterization, as well as *ex vivo* analysis, was performed on the optimized FMS in order to assess the suitability of the system for rapid oramucosal drug delivery. The FMS was deemed to be suitable for buccal drug delivery and able to overcome some of the inherent limitations of current drug delivery systems.

ACKNOWLEDGEMENTS

I would like to acknowledge and express appreciation to all those without whom the completion of this work would not have been possible. I express my gratitude to the following people:

My truly wonderful parents, James M. and Rosalind C. Dott, for your invaluable role in everything I have accomplished, the sacrifices you have made to provide the best for me and your continuing love and support of me, even when I have made bad choices.

My dear brother, Gregory Dott, for believing in me, putting up with me, understanding me and always making me laugh.

My supervisor, Professor Viness Pillay, for the guidance and funding. Furthermore, thank you for encouraging me to continue with this work to completion. My co-supervisors, Dr Yahya E. Choonara and Ms Lisa C. du Toit, thank you for your valuable input and direction.

My amazing, fun, adventurous, good friend, Danielle de Waal, for the vast quantities of friendship, listening, inspiring, encouraging, laughing, exploring, road-tripping and photographing. Your friendship has gone a long way in keeping me on track and seeing this through to the end.

My friend, Deshika Reddy, for the copious research help and advice, laughter that made the unpleasant moments that much more bearable, shared humor (long live Charlie and the Impetuous Membranes of Fury!), listening to me, the more serious conversations and, of course, for helping me keep Lulu's in business.

My friends, Kovanya Moodley and Ameena Wadee, for listening to me, laughing with me and making laboratory work more bearable.

My friends, Wayne and Maureen Holgate, Costa and Jenni Repanis, and Quinton and Bronwyn Chambers, for the thoughts, prayers, listening, encouragement and advice.

My colleagues, Oluwatoyin Adeleke, Priya Bawa, Shivaan Cooppan, Yusuf Dawood, Yasien Docrat, Pius Fasinu, Derusha Frank, Thiresen Govender, Sheri-Lee Harilall,

Deanne Hazle, Teboho Kgesa, Zaheeda Khan, Pradeep Kumar, Martina Manyikana, Felix Mashingaidze, Caragh Murphy, Valence Ndesendo, Ndidi Ngwuluka, Rubina Shaikh, Bongani Sibeko, Meng Meng Sun and Tong-Sheng Tsai – thank you for the help and advice and making campus a better place.

My good friends: Brett Beverley, Nic Fester, Matthew Figueira, Sarah Gebers, Monika Isaacs, Greg McDonald, Ruth McDonald, Phethedi Mokgohloa, Dean Naidoo, Benji Pienaar, Gareth Pon, Jason Pon, Tessa Quin, Lexi Repanis, Liz Repanis, Clayton Schult, Amber Smith, Eric Thornton, Robs Thornton and Brian Wylie – thank you for all the encouragement, prayers and friendship that has been monumental in getting me to this point.

My friend, Kershnee Chetty, for listening, understanding and helping me take my mind off everything when needed.

Thank you to Professor Michael P. Danckwerts for being so accommodatingyou're your willingness to help.

Thank you to David N. Bayever for listening, understanding and all the advice.

Thank you to the support staff in the Department of Pharmacy and Pharmacology for keeping the laboratories clean, providing me with the chemicals I needed and your willingness to help.

Thank you to the Central Animal Services staff of Wits University for always being willing to help me out, even when you didn't have to.

Thank you to the National Research Foundation (NRF) for the research grants that have been of huge financial help to me.

DEDICATION

This work is dedicated to my God and my Savior, Jesus Christ. Without His strength in me, this would not have been possible and I would not be where I am today.

"I can do all things through Him who strengthens me."

Philippians 4:13 (ESV)

TABLE OF CONTENTS

Chapter 1 ..... **1**
Introduction **1**
1.1. Background to this Study 1
1.2. Rationale for this Study 3
1.3. Aim and Objectives of this Study 5
1.4. Novelty of this Study 5
1.5. Overview of this Dissertation 6
Chapter 2 ..... **7**
Drug delivery applications of electrospinning and processing parameters affecting fiber production **7**
2.1. Introduction 7
2.2. Process of Electrospinning 9
2.2.1. Applied Voltage 9
2.2.2. Solution Flow-Rate 11
2.2.3. Polymer Concentration and Solution Viscosity 12
2.2.4 Solvent 13
2.2.5. Solution Conductivity 19
2.2.6. Distance between Capillary and Collector 20
2.2.7. Addition of Surfactants 20
2.3. Electrospinning in Drug Delivery 21
2.3.1. Drug-Loading and Drug Release 21
2.3.1.1. Effect of Drug Dissolved in the Polymer Solution 21
2.3.1.2. Effect of Drug Solubilized Prior to Addition to Polymer Solution 23
2.3.1.3. Effect of Co-Axial Electrospinning 25
2.3.1.4. Effect of Emulsion Electrospinning 27
2.3.1.5. Effect of Drug-Loading by Immersion in Drug Solution 29
2.3.2. Electrospun Fibers in Drug Delivery 30
2.3.3. Polymers Employed for Drug Delivery Applications 30
2.3.4. Crosslinking of Fibers 31
2.4. Other Applications of Electrospun Fibers 31
2.4.1. Biomedical Applications 31
2.4.1.1 Composite Scaffolds Prepared by Electrospinning 31
2.4.2. Electronic Applications 34
2.4.3. Adsorption Applications 34

2.4.4. Sensor and Drug Content Determination Applications 35
2.4.5. Filtration Applications 35
2.5. Concluding Remarks 35
Chapter 3 37
Development and preformulation of a polymeric, mucoadhesive backing film layer and a drug-loaded electrospun fibrous layer 37
3.1. Introduction 37
3.2. Materials and Methods 38
3.2.1. Materials 38
3.2.2. Preparation of Crosslinked HPC Membranes 39
3.2.3. Preparation of Polymeric Films from High Concentration Polymer Solutions 39
3.2.4. Preparation of Polymeric Films Employing a Molding and Film-Casting Technique 39
3.2.4.1. HPC Films 39
3.2.4.2. HPMC Films 39
3.2.4.3. PVA and HPMC Films 40
3.2.5. Preparation of Fibers by Electrospinning 40
3.2.6. Investigation of Various Polymers for Electrospinning 40
3.2.6.1. PVA in Water 40
3.2.6.2. PVA in a 2:1 Mixture of Water and Propan-2-ol 41
3.2.6.3. HPC in Water 41
3.2.6.4. HPC in a 2:1 Mixture of Water and Propan-2-ol 41
3.2.6.5. PEO in Water 41
3.2.6.6. PAA in Water 41
3.2.7. Morphological Surface Structure Analysis of the Electrospun Fiber Layer ... 42
3.2.8. Rheological Characterization of PVA Solutions Employed in Electrospinning 42
3.2.9. Calibration Curves for UV Spectrophotometric Determination of AZT and DPH 42
3.2.10. Drug Entrapment 42
3.2.11. Disintegration Time of the PVA Fiber Layer and Backing Film Layer 43
3.2.12. Drug Permeation by *ex vivo* Studies 43
3.3. Results and Discussion 43
3.3.1. Crosslinked HPC Membranes 43
3.3.2. Polymeric Films Prepared from Viscous Polymer Solutions 44
3.3.3. Polymeric Films Prepared Employing a Molding and Film-Casting Technique 44

3.3.3.1. HPC Films *44*
3.3.3.2. HPMC Films *44*
3.3.3.3. PVA and HPMC Films *44*
3.3.4. Investigation into Various Polymers for Electrospinning 45
3.3.4.1. PVA in Water *45*
3.3.4.2. PVA in a 2:1 Mixture of Water and Propan-2-ol *45*
3.3.4.3. HPC in Water *45*
3.3.4.4. HPC in a 2:1 Mixture of Water and Propan-2-ol *45*
3.3.4.5. PEO in Water *46*
3.3.4.6. PAA in Water *46*
3.3.5. Morphological and Surface Structure Analysis of the Electrospun Fiber Layer 46
3.3.6. Rheological Characterization of PVA Solutions Employed in Electrospinning 47
3.3.7. Calibration Curves for UV Spectrophotometric Determination of AZT and DPH 51
3.3.7.1. AZT in Simulated Saliva (pH 6.75) *51*
3.3.7.2. AZT in PBS (pH 7.4) *51*
3.3.7.3. DPH in Simulated Saliva (pH 6.75) *52*
3.3.7.4. DPH in PBS (pH 7.4) *53*
3.3.8. Drug Entrapment 54
3.3.9. Disintegration Time of the PVA Fiber Layer and Backing Film Layer 55
3.3.10. Drug Permeation by *ex vivo* Studies 55
3.4. Concluding Remarks 56
Chapter 4 57
Preparation, characterization and optimization of an electrospun fibrous matrix system for rapid oramucosal drug delivery 57
4.1. Introduction 57
4.2. Materials and Methods 59
4.2.1. Materials 59
4.2.2. Preparation of polymeric backing films by film-casting 59
4.2.3. Experimental Design 60
4.2.4. Preparation of fibers by electrospinning 61
4.2.5. Morphological and Surface Structure Analysis of the Drug-loaded Fiber Layer 62
4.2.6. Drug Entrapment of Experimental Design Formulations 62
4.2.7. Disintegration Time of Experimental Design Formulations 62

4.2.8. *In vitro* Drug Release 62
4.2.9. *Ex vivo* Drug Permeation Studies 63
4.2.10. Mucoadhesion of Experimental Design Formulations 63
4.3. Results and Discussion 63
4.3.1. Morphological and Surface Structure Analysis of the Drug-loaded Fiber Layer 64
4.3.1. Drug Entrapment of Experimental Design Formulations 64
4.3.2. Disintegration Time of Experimental Design Formulations 65
4.3.3. *In vitro* Drug Release by Dissolution 67
4.3.4. Drug Permeation by *ex vivo* Studies 70
4.3.5. Mucoadhesion of Experimental Design Formulations 73
4.3.6. Analysis of Main Effects and Interaction Effects on Responses 77
4.3.6.1. Disintegration Time 77
4.3.6.2. Work of Adhesion 78
4.3.6.3. Maximum Detachment Force 79
4.3.6.4. AUC_D at 1 minute 80
4.3.6.5. AUC_P at 3 minutes 81
4.3.7. Analysis of the Box-Behnken Experimental Design 82
4.3.8. Response Optimization 86
4.4. Concluding Remarks 88
Chapter 5 89
Physicochemical and physicomechanical investigation of an optimized fibrous matrix system for rapid oramucosal drug delivery 89
5.1. Introduction 89
5.2. Materials and Methods 89
5.2.1. Materials 89
5.2.2. Preparation of Polymeric Backing Films by Film-Casting 90
5.2.3. Preparation of Fibers by Electrospinning 90
5.2.4. Morphological and Surface Structure Analysis of the Drug-loaded Fiber Layer 90
5.2.5. Drug Entrapment of the Optimized FMS and Drug-Loaded Films 90
5.2.6. Disintegration Time of the Optimized FMS and Drug-Loaded Films 90
5.2.7. *In vitro* Drug Release by Dissolution Testing 91
5.2.8. Drug Permeation by *ex vivo* Studies 91
5.2.9. Mucoadhesion of the Optimized FMS and Drug-Loaded Films 91
5.2.10. Determination of Micro-Environmental Surface pH Variation within the FMS 91

5.2.11. Determination of FMS Toughness and Bi-Axial Extensibility 91
5.2.12. Determination of Tensile Properties of the Optimized FMS and Drug-Loaded Films 92
5.2.13. Analysis of the Stress-Strain Rheological Parameters of the Components of the FMS 92
5.2.14. Vibrational Chemical Structure Analysis 93
5.3. Results and Discussion 93
5.3.1. Physical Dimensions of the Films and Fiber Layer 93
5.3.2. Morphological and Surface Structure Analysis of the Electrospun Fiber Layer 93
5.3.3. Drug Entrapment of the Optimized FMS and Drug-Loaded Films 94
5.3.4. Disintegration Time of the Optimized FMS and Drug-Loaded Films 94
5.3.5. *In vitro* Drug Release by Dissolution 95
5.3.6. Drug Permeation by *ex vivo* Studies 97
5.3.7. Mucoadhesion of the Optimized FMS and Drug-Loaded Films 99
5.3.8. Micro-Environmental Surface pH Variation within the FMS 100
5.3.9. FMS Toughness and Bi-Axial Extensibility 101
5.3.10. Determination of Tensile Properties by Nanotensile Testing 102
5.3.11. Analysis of the Stress-Strain Rheological Parameters of the Components of the FMS 106
5.3.11.1. Rheological Analysis of the Optimized FMS and Drug-Loaded Film Formulations 106
5.3.11.2. Rheological Analysis of the Electrospinning Solution 109
5.3.12. Vibrational Chemical Structure Analysis 112
5.4. Concluding Remarks 113
Chapter 6 115
Conclusions and recommendations 115
6.1. Conclusions 115
6.2. Recommendations 116
References 117

LIST OF FIGURES

		Page
Figure 1.1:	Schematic representing the dissolution of the fibrous matrix system (FMS)	4
Figure 2.1:	Schematic illustrating the set-up of the electrospinning process	8
Figure 2.2:	Varying PEO fiber morphology from beaded to smooth fibers as the ratio of ethanol is increased (Reproduced from Fong et al., 1999)	16
Figure 2.3:	Scanning electron micrographs of electrospun polystyrene fibers formed from solutions using 1,2-dichloroethane, dimethylformamide (DMF), ethylacetate, methylethylketone (MEK) and tetrahydrofuran (THF) as solvents (Reproduced from Jarusuwannapoom et al., 2005)	18
Figure 2.4:	Schematic of the drug-loading and electrospinning process from drug-loaded polymer solutions	21
Figure 2.5:	Schematic of the drug-loading and electrospinning process for co-axial electrospinning	26
Figure 2.6:	Schematic of the emulsion electrospinning process	27
Figure 2.7:	Schematic of immersion drug-loading of electrospun fibers	30
Figure 3.1:	Scanning electron micrograph of PVA fibers	47
Figure 3.2:	Rheological profiles of (a) 15%$^{w}/_{v}$, (b) 20%$^{w}/_{v}$, (c) 25%$^{w}/_{v}$ and (d) 30%$^{w}/_{v}$ PVA solutions in 2:1 deionized water and propan-2-ol	48
Figure 3.3:	Rheological profile of 25%$^{w}/_{v}$ PVA solution in deionized water	49
Figure 3.4:	Comparison of average shear force for the electrospinning solutions with varying PVA concentrations	50
Figure 3.5:	Comparison of average viscosity for the electrospinning solutions with varying PVA concentrations	50
Figure 3.6:	Calibration curve for AZT dissolved in simulated saliva (pH 6.75) at λ_{267nm} (in all cases SDs < 0.02, N = 3)	51
Figure 3.7:	Calibration curve for AZT dissolved in PBS (pH 7.4) at λ267nm (in all cases SDs < 0.02, N = 3)	52
Figure 3.8:	Calibration curve for DPH dissolved in simulated saliva (pH 6.75) at λ_{254nm} (in all cases SDs < 0.02, N = 3)	53
Figure 3.9:	Calibration curve for DPH dissolved in PBS (pH 7.4) at λ_{254nm}	

(in all cases SDs < 0.02, N = 3) 54
Figure 3.10: Flux profiles of diphenhydramine (DPH) and zidovudine (AZT) (in all cases SDs < 0.02, N = 3) 56
Figure 4.1: Visualization of a Box-Behnken cube with points on the middle of each edge and in the center. X_1, X_2 and X_3 represent the independent variables in the design (Adapted from Ferreira et al., 2007) 61
Figure 4.2: SEM image of electrospun PVA fibers loaded with DPH 64
Figure 4.3: Vertical bar chart depicting the average disintegration times of the experimental design formulations (in all cases SDs < 0.02, N = 3) 66
Figure 4.4: Contour plot depicting the relationship between the disintegration time, HPMC concentration and fill volume 66
Figure 4.5: Drug release profiles of formulations (a) 1-5, (b) 6-10 and (c) 11-15 (in all cases SDs < 0.02, N = 3) 68
Figure 4.6: Scatter plot depicting AUC of dissolution (AUC_D) at 1 minute for the 15 experimental design formulations 69
Figure 4.7: Contour plot depicting the relationship between the HPMC concentration in film formulations, fill volume and AUC_D at 1 minute 70
Figure 4.8: Flux profiles displaying the flux over time of formulations (a) 1-5, (b) 6-10 and (c) 11-15 72
Figure 4.9: Scatter plot depicting AUC of permeation (AUC_P) at 3 minutes for the 15 experimental design formulations 72
Figure 4.10: Typical textural profile showing the peak force (MDF) (N) and work of adhesion (AUC_{FD}) (mJ) used to determine mucoadhesive properties of the experimental design formulations 74
Figure 4.11: Vertical bar chart depicting the average work of adhesion (WA) 74
Figure 4.12: Vertical bar chart depicting the average maximum detachment force (MDF) 75
Figure 4.13: Contour plot depicting the relationship between the HPMC concentration in film formulations, fill volume and work of adhesion 76
Figure 4.14: Contour plot depicting the relationship between HPMC

concentration, glycerol concentration and work of adhesion 77
Figure 4.15: Diagnostic plots of the design showing (a) main effects plot and (b) interactions plot for disintegration time 78
Figure 4.16: Diagnostic plots of the design showing (a) main effects plot and (b) interactions plot for work of adhesion 79
Figure 4.17: Diagnostic plots of the design showing (a) main effects plot and (b) interactions plot for maximum detachment force 80
Figure 4.18: Diagnostic plots of the design showing (a) main effects plot and (b) interactions plot for AUC_D at 1 minute 81
Figure 4.19: Diagnostic plots of the design showing (a) main effects plot and (b) interactions plot for AUC_P at 3 minutes 82
Figure 4.20: Diagnostic plots of the design showing residual plots for disintegration time 83
Figure 4.21: Diagnostic plots of the design showing residual plots for work of adhesion 83
Figure 4.22: Diagnostic plots of the design showing residual plots for maximum detachment force 84
Figure 4.23: Diagnostic plots of the design showing residual plots for AUC_D at 1 minute 84
Figure 4.24: Diagnostic plots of the design showing residual plots for AUC_P at 3 minutes 85
Figure 4.25: Final optimization plot for the response optimization of the polymeric film formulation 87
Figure 5.1: SEM image of the electrospun fiber layer, showing average fiber diameter of 0.36µm and visible pore size of 0.69-1.91µm 94
Figure 5.2: Vertical bar chart depicting the disintegration times of the fibrous matrix system (FMS), fiber layer of the FMS, drug-loaded optimized film (F_D) and film formed from the same components as the electrospinning solution (F_E) (in all cases SDs < 0.02, N = 3) 95
Figure 5.3: Drug release profiles of the fibrous matrix system (FMS), DPH-loaded film formulation (F_D) and film formed from the same components as the electrospinning solution (F_E) (in all cases SDs < 0.02, N = 3) 96
Figure 5.4: Drug release profiles of the fibrous matrix system (FMS) and Sleepeze-PM® tablets (in all cases SDs < 0.02, N = 3) 96

Figure 5.5: AUC_D comparison between the FMS, comparator DPH-loaded film formulations (F_D and F_E) and Sleepeze-PM® tablets (in all cases SDs < 0.02, N = 3) 97

Figure 5.6: Flux profiles of the fibrous matrix system (FMS), DPH solution, DPH-loaded film formulation (F_D) and film formed from the same components as the electrospinning solution (F_E) 98

Figure 5.7: Scatter plot depicting AUC_P at 3 minutes for the fibrous matrix system (FMS), DPH solution, DPH-loaded film formulation (F_D) and film formed from the same components as the electrospinning solution (F_E) 98

Figure 5.8: Typical textural profile used to determine MDF (peak) and WA (AUC_{FD}) for assessing mucoadhesion 100

Figure 5.9: Average pH variation over time for the FMS hydrated in simulated saliva (pH 6.75) 101

Figure 5.10: Typical textural extensibility profile for the FMS, showing 3 distinct regions: linear extensibility (A), maximum extensibility (B) and fracture point (C) 102

Figure 5.11: Vertical bar chart outlining average maximum force and distance values for the film of the fibrous matrix system (FMS), the complete FMS, drug-loaded FMS film (F_D) and film containing the same components as the electrospinning solution (F_E) (in all cases SDs < 0.02, N = 3) 102

Figure 5.12: Stress-strain nanotensile profiles of the (a) drug-loaded fiber layer, (b) FMS film, (c) FMS, (d) drug-loaded F_D film and (e) drug-loaded F_E film 106

Figure 5.13: Linear rheological profiles of the (a) FMS, (b) F_D film and (c) F_E film 108

Figure 5.14: Linear rheological profile of the 25%$^w/_v$ PVA electrospinning solution 109

Figure 5.15: Thixotropy curve for the 25%$^w/_v$ PVA solution used for electrospinning 110

Figure 5.16: Rheology plot depicting the yield stress (at 0.3782Pa) of a 25%$^w/_v$ PVA solution intended for electrospinning 111

Figure 5.17: Rheological plot depicting the yield point in a stress sweep of a 25%$^w/_v$ PVA solution 111

Figure 5.18: Stress sweep of 25%$^w/_v$ PVA solution intended for

electrospinning 112
Figure 5.19: Molecular structures of (a) DPH and (b) PVA 113
Figure 5.20: FTIR profiles of the drug-loaded fibers (DF), placebo fibers (PF) and DPH 113

LIST OF TABLES

		Page
Table 2.1:	Solvent properties and the resulting fiber morphology in electrospinning	14
Table 2.2:	Polymers, drugs and solvents for application in drug delivery	32
Table 3.1:	Total percentage of drug permeated after 90 minutes	55
Table 4.1:	Polymer concentrations and volumes used in film preparation according to the Box-Behnken design	60
Table 4.2:	Variables employed in the Box-Behnken design	61
Table 4.3:	Drug entrapment per 1.5cm^2 section of electrospun fibrous membrane system (FMS)	65
Table 4.4:	Calculated apparent permeability coefficient (P_{app}) and steady-state flux values (J_{ss}) for the 15 experimental design formulations	73
Table 4.5:	ANOVA analysis for the measured responses investigated in the Box-Behnken experimental design	85
Table 4.6:	Targeted response values employed in formulation optimization	87
Table 4.7:	Predicted and experimental values for optimization of the responses	88
Table 5.1:	Test parameters employed in bi-axial extensibility testing	92
Table 5.2:	Drug entrapment per 1.5cm^2 section of fibrous matrix system (FMS), drug-loaded optimized film (F_D) and film produced from ratios in electrospinning solution (F_E)	94
Table 5.3:	Calculated apparent permeability coefficient (P_{app}) and steady-state flux (J_{ss}) values for the FMS, DPH solution, F_D and F_E	99
Table 5.4:	Maximum detachment force (MDF) and work of adhesion (WA) for the FMS film, fiber layer of the FMS and the drug-loaded films, F_E and F_D	100
Table 5.5:	Experimental values obtained from nanotensile analysis of the FMS and various films	103
Table 5.6:	Average rheological parameters of the FMS, F_D film and F_E film in 1mL simulated saliva (pH 6.75)	107

LIST OF EQUATIONS

		Page
Equation 4.1:	Determination of the apparent permeability coefficient (P_{app}) of diphenhydramine released from drug-loaded formulations	63
Equation 4.2:	Determination of the steady-state flux (J_{ss}) of diphenhydramine released from drug-loaded formulations	63
Equation 4.3:	Regression equation for disintegration time	86
Equation 4.4:	Regression equation for work of adhesion	86
Equation 4.5:	Regression equation for maximum detachment force	86
Equation 4.6:	Regression equation for AUC_D at 1 minute	86
Equation 4.7:	Regression equation for AUC_P at 3 minutes	86

CHAPTER 1

INTRODUCTION

1.1. Background to this Study

Oral drug delivery in pediatric patients is an area of concern in the pharmaceutical industry. The majority of formulations designed for pediatric use are in the form of liquids. Liquid formulations have a few advantages over solid formulations. These advantages include a faster onset of action, due to drug that is either dissolved or suspended in the form of small particles, and convenience of pediatric administration. Liquid formulations are easier to swallow than large tablets or capsules, particularly for infants, young children and geriatric patients, who experience difficulty with swallowing. However, liquid formulations are not always ideal for drug delivery, especially when the drug to be delivered has an undesirable stability or is poorly soluble in an appropriate liquid, or where loss of drug may occur due to measurement (Winfield, 2004). Examples of such drugs include those used in the treatment of HIV/AIDS, Tuberculosis (TB) and Malaria. Liquid formulations are also not ideal in terms of dosing accuracy because of the necessity for the patient or care-giver to accurately measure the prescribed dose (Winfield, 2004; Dixit and Puthli, 2009). Furthermore, there are very few solid drug delivery systems designed for pediatric use (Standing and Tuleu, 2005).

The oral administration of a drug, using a liquid or solid drug delivery system, poses several challenges. The patient is required to be compliant and able to swallow the drug delivery system. Swallowing tablets or capsules can be particularly challenging in HIV/AIDS patients who suffer from dysphagia, elderly patients and pediatric patients (Sastry et al., 2000). When administered orally, a drug is subjected to the harsh environment of the stomach and small intestine, where it comes into contact with varying pH and high enzymatic activity, and may be degraded. If the drug remains intact and is absorbed, it may then undergo hepatic first pass metabolism. Exposure to the harsh gastrointestinal environment and hepatic first pass metabolism may result in the drug having a low bioavailability and a lower than optimal plasma concentration (Sudhakar et al., 2006). If these factors are bypassed, a superior bioavailability may be achieved as well as the possibility of lowering doses and decreasing dosing frequencies (Sudhakar et al., 2006; Dixit and Puthli, 2009). There may also be a reduction in the

side-effects related to high doses and gastrointestinal transit, and toxicity related to high doses (Stanley and Ashburn, 1992; Dixit and Puthli, 2009).

One of the diseases of concern in this study was HIV/AIDS and the novel delivery of model drug, zidovudine (AZT). There is currently no cure for HIV/AIDS, and treatment, according to the World Health Organization (WHO), is aimed at preserving or restoring immunological function, keeping the viral load minimal, thereby reducing the incidence of opportunistic infections, and enhancing patient quality of life (WHO, 2007). The treatment for HIV/AIDS involves complicated regimens of antiretroviral agents, where the patient is required to take at least three different drugs at different times during the day (WHO, 2007). For the successful treatment of HIV/AIDS, the drug plasma concentration needs to be relatively high in order to completely suppress viral replication (Aungst, 1999). AZT is a nucleoside reverse transcriptase inhibitor (NRTI) that is often used in HIV treatment regimens (WHO, 2007). When selecting a first line regimen for the treatment of HIV in infants and children, the preferred option is a combination of two NRTIs and one non-nucleoside reverse transcriptase inhibitor (NNRTI), for example, AZT (NRTI), lamivudine (NRTI) and nevirapine (NNRTI) (WHO, 2007). Zidovudine has an oral bioavailability of approximately 65% that is relatively low due to hepatic first pass metabolism (Aungst, 1999). The World Health Organization (WHO) encourages the development of formulations, for the treatment of HIV, that are suited for use in pediatric patients, particularly solid formulations (WHO, 2007).

Bypassing the harsh gastrointestinal environment and first pass metabolism can be achieved by formulating a drug delivery system that permits the dissolution and absorption of drug within the oral cavity (Cappello et al., 2006). The absorption sites within the oral cavity are the buccal (cheek), sublingual (under the tongue) and gingival (gums) areas. Drug is absorbed most readily from the sublingual area and least readily from the gingival area (Stanley and Ashburn, 1992). The oral mucosa is an attractive site for drug absorption due to good permeability, a high level of vascularization and minimal enzymatic activity compared to the enzymatic activity present in the stomach and small intestine that may result in degradation of certain drugs (Giannola et al., 2007). Another advantage is the fact that a drug delivery system administered via the oramucosal route does not need to be swallowed (Hoogstraate and Wertz, 1998). The majority of the dose administered would be absorbed from the oral cavity. Drug that is not absorbed in the oramucosal region would pass into the gastric region and be absorbed via normal gastro-intestinal absorption, but this would be a minimal quantity. Current rapidly disintegrating buccal drug delivery systems, such as buccal tablets, are

able to dissolve rapidly within the oral cavity. However, the short residence time at the absorption surface is a limiting factor in the effectiveness of these delivery systems (Madhav et al., 2009). Furthermore, buccal tablet and wafer systems tend to be brittle and fragile and hence require special protective packaging (Dixit and Puthli, 2009).

In previous studies, electrospun fibers have been loaded with drug and studied for their potential application in controlled drug delivery (Verreck et al., 2003a; Zeng et al., 2003; Kim et al., 2004; Kenawy et al., 2007; Tungprapa et al., 2007; Yang et al., 2007; Ranganath and Wang, 2008; Kenawy et al., 2009; Loh et al., 2010; Tiwari et al., 2010). It has been found that, depending on polymers or combination of polymers used, fibrous matrices may demonstrate controlled release of drug and therefore have the potential to control the delivery of drugs (Sill and von Recum, 2008). Furthermore, fine control over drug release kinetics may be achieved by the use of different electrospinning and drug-loading techniques (Sill and von Recum, 2008). The incorporation of drug into a low density, porous carrier system may result in an enhanced matrix-solvent interaction, leading to faster drug dissolution, enhanced bioavailability and an improvement in therapeutic effect (Szepes et al., 2007). Methods of formulating porous matrix systems include lyophilization (Bredenberg et al., 2003), freeze-casting (Szepes et al., 2007), compaction (Carli et al., 1984), electrospinning (Liu et al., 2006) and use of a porogen (Vidaurre et al., 2007).

This study therefore proposed to develop a novel, porous, polymeric fibrous matrix system (FMS) with electrospun fibers incorporated onto a mucoadhesive, flexible film for the oral transmucosal delivery of drugs to infants, children and geriatrics as well as other patients experiencing difficulty with swallowing or patients that may be in a comatose state. It should be noted that the aim of this study was to design a platform for the delivery of various drugs and it is not limited in its application to the delivery of AZT. It is proposed to be flexible and versatile enough for the oramucosal delivery of various other drugs requiring a rapid onset of action, such as anaglesics, anxiolytics and sleep inducers.

1.2. Rationale for this Study

The FMS comprised two components and was formed by electrospinning for the fibrous layer and film-casting for the backing film layer, which were proposed to result in high drug-loading, high mechanical strength, high porosity, large surface area for hydration, mucoadhesion and taste-masking. The high porosity was achieved by the fibrous

network that the electro-spun fibers formed. The formulation of the FMS may be an alternative to the formulation of low density, porous matrices, such as wafers, produced by other methods. The porous, low density matrices were proposed to enhance the dissolution of drugs that are sparingly soluble in an aqueous environment by increasing the surface area for hydration. The FMS is a solid drug delivery system, resulting in a greater dosing accuracy than that of a liquid formulation because the necessity for the patient or care-giver to measure doses is not required. The main area that was targeted for drug absorption was the buccal region of the oral cavity. Suitable excipients, such as citric acid, were employed to mask the taste of the drug. Absorption of drug via the buccal mucosa bypasses gastro-intestinal and first pass metabolism and therefore could result in a higher bioavailability.

In general, the FMS incorporated drug into a fibrous matrix, from where it was released rapidly once in contact with saliva in the oral cavity. A flexible, mucoadhesive film enabled the FMS to adhere to the buccal mucosa and the membranes were fast dissolving, which resulted in rapid exposure of the drug to saliva (see Figure 1.1). It is considered suitable for the administration of drug to pediatric patients, patients suffering from dysphagia and the elderly, who experience problems with swallowing tablets, capsules and liquids. This was proposed to result in an increase in drug stability as well as patient compliance. The WHO strongly encourages the use of solid drug delivery systems in HIV patients (WHO, 2007). There is therefore a demand for a solid drug delivery system that can be used in pediatric patients, as well as others who experience difficulty with swallowing.

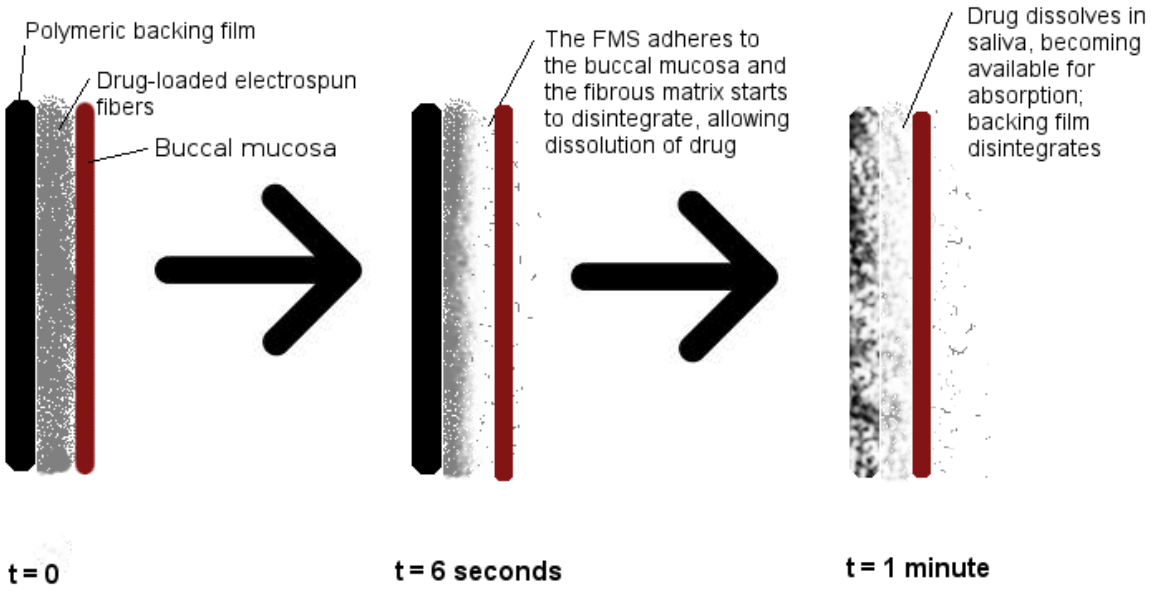


Figure 1.1: Schematic representing the dissolution of the fibrous matrix system (FMS)

1.3. Aim and Objectives of this Study

The overall aim of this study was to design and develop a porous polymeric Fibrous Matrix System (FMS) in the form of a film, which would allow for the immediate release of drugs so that they can be absorbed via the oral mucosa. The drug delivery system is intended to overcome many of the shortcomings of rapidly dissolving oral drug delivery systems, as well as liquid formulations that are designed for pediatric administration.

In order to accomplish this, the following objectives have been outlined:

- To review the application of electrospinning in drug delivery and, in doing so, validate the novelty of the FMS in buccal drug delivery.
- To identify suitable polymers for the design and development of a rapidly disintegrating, porous, polymeric fibrous matrix system (FMS), allowing for the immediate release of drugs to be absorbed via the buccal mucosa.
- To develop drug-loaded fibers by electrospinning and backing films by film-casting.
- To combine the fibers and films in order to develop a FMS to deliver drug to the buccal mucosa.
- To perform *in vitro* disintegration and dissolution studies to determine the disintegration and drug release characteristics of the system.
- To perform *ex vivo* permeation studies to determine the permeation of the model drug through the oral mucosa.
- To optimize the FMS, employing a three-level Box-Behnken experimental design.
- To perform physicochemical and physicomechanical investigations on the formulated FMS.

1.4. Novelty of this Study

Porous matrices for oramucosal drug delivery have been formulated by numerous methods, however the FMS is novel in the fact that:

- It comprises electrospun fibrous structures that are carefully engineered and highly porous.
- Fibers were formed by an electrospinning technique, which is unique in buccal drug delivery.
- The fibers were electrospun directly onto a polymeric film to form the FMS.
- The FMS is mucoadhesive and intended for delivering drug to the buccal mucosa.

1.5. Overview of this Dissertation

Chapter 1 provides an introduction and outlines the background to the study, delineating the challenges faced with current rapidly dissolving oramucosal drug delivery systems, particularly for pediatric and geriatric patients, and explores the rationale for the study. It also covers the aim and objectives of the study.

Chapter 2 is a literature review, focusing on electrospinning and the employment of this technique in drug delivery. Solution and processing parameters affecting fiber formation during electrospinning are outlined. Furthermore, various methods of drug-loading and effects on drug release are elucidated.

Chapter 3 describes the development of the drug-loaded fiber layer, by electrospinning, and the polymeric backing film layer, by film-casting, of the FMS. Preliminary investigations, where various polymers were assessed for suitability in the development of the components of the FMS, are outlined. Variables for an experimental design were obtained. Furthermore, the investigation into permeation enhancement is delineated in this chapter.

Chapter 4 is a description of the analysis and optimization of the backing film layer produced according to three-factor Box-Behnken experimental design. The dependent variables assessed in the experimental design were the fill volume, HPMC concentration and glycerol concentration. Formulations were analyzed according to five responses, namely disintegration time, work of adhesion, maximum detachment force, dissolution and permeation. An optimized formulation was determined employing the quadratic model.

Chapter 5 describes the *in vitro* physicochemical and physicomechanical analysis of the optimized FMS as well as *ex vivo* permeation studies.

Chapter 6 expounds the conclusions and future recommendations of the study.

CHAPTER 2

DRUG DELIVERY APPLICATIONS OF ELECTROSPINNING AND PROCESSING PARAMETERS AFFECTING FIBER PRODUCTION

2.1. Introduction

Electrospinning of polymers is a unique technology that is used to produce very fine fibers in the nano- and micrometer size range (Liang et al., 2007). Electrostatic repulsive forces result in a reduced fiber diameter and increased fiber length, unlike fibers produced by other methods such as conventional spinning or mechanical drawing (Li et al., 2004). Fibers produced by conventional spinning methods are lengthened and thinned by being subjected to rheological, gravitational, tensile, inertial and aerodynamic forces (Reneker and Chun, 1996). Electrospinning produces thin, continuous fibers without using contact, but rather by applying an electrical potential to a liquid (Reneker and Chun, 1996; Li et al., 2004; Baji et al., 2010). When an electrical potential is applied to a drop of polymer solution at the end of a capillary tube, the rounded drop elongates, becoming conical in shape (Baumgarten, 1971; Doshi and Reneker, 1995; Sill and von Recum, 2008), termed the Taylor cone (Figure 2.1) (Sill and von Recum, 2008). When the electrical field exceeds the surface tension of the liquid, a fine fiber jet is ejected from the tip of the Taylor cone (Zeleny, 1935; Liang et al., 2007; Sill and von Recum, 2008; Baji et al., 2010), travelling through the atmosphere, the solvent evaporates, depositing solid polymer fibers on a grounded collector (Sill and von Recum, 2008). The gap between the capillary tube and the collector is closed by the charges carried in the fiber jet, thereby completing the circuit (Deitzel et al., 2001; Baji et al., 2010). The resultant product is a porous fibrous scaffold with a very high surface area to volume ratio (Liang et al., 2007; Reneker and Yarin, 2008).

Electrospinning is related to the process of electrospraying, which involves the application of an electrical potential to a low viscosity liquid, causing a jet of the liquid to accelerate from a capillary tip towards a grounded collector (Deitzel et al., 2001). Electrospraying has been used in the production of very fine aerosol particles in the sub-micron size range (Jaworek, 2007). Due to the low viscosity of the liquid used in electrospraying, the jet will possess a low degree of chain entanglement (Shenoy et al., 2005; Baji et al., 2010) and the surface tension will cause it to break up (Deitzel et al., 2001; Hogan and Biswas 2008). Polymer chain entanglement increases with increasing

solution concentration and molecular weight (Shenoy et al., 2005; Munir et al., 2009, Bhardwaj and Kundu, 2010). A jet of polymer solution exhibiting a low viscosity will break up into droplets due to the insufficient chain entanglement density (McKee et al., 2004; Munir et al., 2009; Baji et al., 2010). Conversely, when the viscosity of the solution is increased, and hence adequate chain overlap and entanglements occur, the jet will undergo a whipping motion, stretching the fiber and reducing the diameter (McKee et al., 2004; Shenoy et al., 2005; Munir et al., 2009).

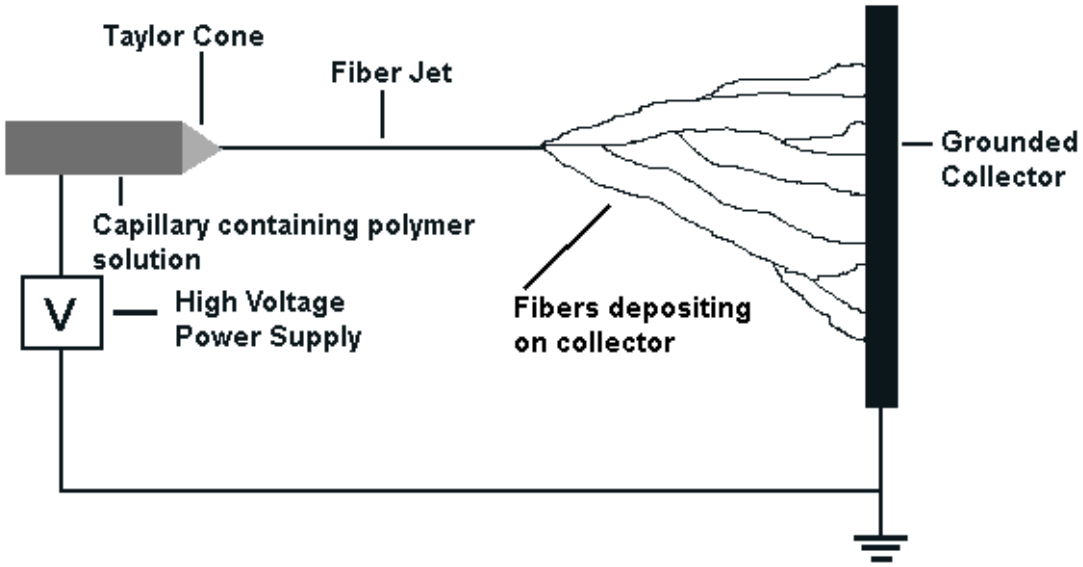


Figure 2.1: Schematic illustrating the set-up of the electrospinning process

Zeleny (1914, 1917 and 1935) investigated the surface instability of liquids when subjected to an electrical potential and found that fine threads were produced from the conical surface of the drop at the end of a capillary when the applied potential was large enough, although the fine threads eventually broke up into fine droplets as they moved away from the capillary. However, it wasn't until Formhals (1934) solved a few technical issues, that electrospinning became feasible. Formhals (1934) combined a moveable fiber-collecting device with the electrode that attracted the fibers so that the collecting device could attract the fibers, although due to the short distance between the jet and collector electrodes, fibers were not able to dry completely before reaching the collector, resulting in the fibers sticking together and to the collector. In 1939, Formhals improved on this (Formhals, 1939), which resulted in greater control over the length of the fibers that were produced and the possibility for the formation of composite fibers by an electrospinning process that involved the deposition of spun fibers onto a base fiber (Formhals, 1940) and succeeding to increase the fiber strength by drawing fibers through a rotating funnel (Formhals, 1943).

Electrospinning has been applied in several varied fields. In electronics, electrospun nanofibers have been used in electronic micro- and nano-devices (Xin et al., 2008), as fine conducting fibers (MacDiarmid et al., 2001; Viswanathamurthi et al., 2003; Allaoui et al., 2008), as magnetic materials (Ju et al., 2008), as anode material in lithium ion batteries (Yao et al., 2008a; Yao et al., 2008b) and as optical and electrical nano-materials (Tan et al., 2008). In catalysis, electrospun fibers have application in the fabrication of catalytic electrodes (Gong et al., 2003; Bai et al., 2008; Li et al., 2008a). Electrospinning has been employed in the fabrication of High Efficiency Particulate Air (HEPA) filters (Park et al., 2003; Ahn et al., 2006) and filters with a high filtration efficiency and low air resistance (Tsai et al., 2002). Nanofibrous materials have been investigated for their superior potential in absorption and adsorption and may be applied for absorption of water (Ali, 2008) and adsorption of pollutants such as toluene and benzene (Oh et al., 2008), as well as for the fabrication of sensors for the detection of gases (Ding et al., 2004; Li et al., 2008c), substances such as urea (Sawicka et al., 2005) or drugs (such as anti-cancer drug, daunorubicin) (Song et al., 2008). Electrospun polymer mats have been employed in the fabrication of micro-air vehicle wing skin (Pawlowski et al., 2003). Biomedically, electrospun fibers have received much attention in the areas of drug delivery (Kenaway et al., 2007; Tungprapa et al., 2007; Sill and von Recum, 2008), gene delivery (Liang et al., 2005; Chu et al., 2006; Sill and von Recum, 2008), prevention of post-operative adhesions (Zong et al., 2004), wound dressing (Khil et al., 2003; Chen et al., 2008) and tissue engineering (Yoshimoto et al., 2003; Xu et al., 2007; Sill and von Recum, 2008). Applications relating to tissue engineering include artificial vascular grafts (Xu et al., 2004; Ma et al., 2005; Vaz et al., 2005), neural tissue engineering (Yang et al., 2005; Schnell et al., 2007; Chew et al., 2008), tendon and ligament tissue engineering (Lee et al., 2005; Sahoo et al., 2006) and bone tissue engineering (Liao et al., 2008; Yang et al., 2008). This chapter will delve into the pharmaceutical applications of electrospinning as well as the processing parameters affecting the production of electrospun fibers.

2.2. Process of Electrospinning

2.2.1. Applied Voltage

Taylor (1969) observed that the difference between the applied voltage that would cause a drop to become unstable and that which would cause it to become conical in shape is very small. In general, as the applied voltage increases, the fiber diameter

decreases initially and after a certain point, increases once again (Sill and von Recum, 2008).

In a study by Baumgarten (1971), the jet length of a polymer solution at the optimal feed rate increased when the applied voltage was increased. At a capillary-to-collector gap of 50mm, the fiber diameter initially decreased to a minimum and then increased with increasing voltage. At a gap of 75mm, the decrease in fiber diameter to a minimum was not so apparent and the diameter increased slightly in response to an increase in applied voltage. The optimum capillary feed rate also increased with an increase in voltage.

Deitzel and co-workers (2001) examined the effect of applied voltage on a poly(ethylene oxide) (PEO)/water system and observed that the applied voltage has a significant effect on the shape of the droplet from which the fiber jet originates. Charge is transported from the capillary to the collector by the flow of polymer and, if all other variables remain constant, an increase in the applied voltage, and hence current, would therefore generally reflect an increase in the flow-rate between the capillary and collector. An increase in applied voltage resulted in an increase in the spinning current for the PEO/water system. At an applied voltage of 5.5kV, jet initiation occurred and fibers were found to be straight and free of defects and, as the applied voltage increased to 7kV, the current slowly increased. At these lower voltages, the fiber jet was ejected from a cone which was formed at the bottom of the droplet on the end of the capillary and fibers had fewer bead defects and a cylindrical morphology. Although above 7kV, the current increased dramatically ejecting the jet from the liquid surface within the capillary tip. Beads on the fibers began to become prevalent and were found to be high in density at 9kV, where the jet was ejected from inside the capillary tip. Therefore it appears that bead defect formation may be related to current.

In a study undertaken by Zong and co-workers (2002), the effect of applied voltage on the morphology of resulting electrospun poly(lactic acid) (PLA) fibers was investigated. Jet formation began to occur at 16kV; however the jet was not stable at voltages below 20kV. At 20kV, the jet originated from the tip of the Taylor cone and very few beads were formed; as the voltage was increased to 25kV, the droplet volume became smaller and bead formation became more likely. The beads had smaller diameters and the distances between beads were shorter. When voltage was increased to 30kV, the droplet completely disappeared and the jet emerged from the tip of the capillary, with fibers possessing a larger diameter and beads becoming more spherical in shape.

Meechaisue and co-workers (2006) used desaminotyrosyl-tyrosine ethyl ester (DTE) to synthesize poly(DTE carbonate) and investigated the effect of the applied voltage on the electrospun fibers of the synthesized polymer. At applied voltages between 10 and 15kV/10cm, mostly beaded fibers were formed with the bead density decreasing as the voltage increased, while, at voltages between 20 and 25kV/10cm, the produced fibers were generally smooth. It was found that the fiber diameter increased, while the fiber density decreased with increasing voltage.

Beachley and Wen (2009) investigated the effect of the applied voltage on the diameter and length of electrospun polycaprolactone (PCL) fibers. It was observed that both the length and diameter of the fibers decreased with increasing voltage. There was also an increase in the uniformity of the electrospun fibers with increasing voltage.

2.2.2. Solution Flow-Rate

At a high applied voltage, where the fiber jet is ejected from inside the capillary and bead defects become more prevalent, it may be necessary to increase the pressure which causes the drop to protrude from the capillary, thereby replacing the solution which was lost when the fiber jet was ejected (Zeleny, 1935). As flow-rate increases, the pore size and fiber diameter increase, but when the flow-rate is too high, fibers are unable to dry completely before reaching the collector, resulting in one of two things, either bead defects occur or the fibers may become flattened (Sill and von Recum, 2008). A study conducted by Baumgarten (1971), showed that solution flow-rate had little effect on fiber diameter, but an increase in flow-rate resulted in an increase in jet length.

In a study by Zong and co-workers (2002), it was shown that the lower the solution flow-rate, the smaller the diameter of the resultant electrospun fibers and beads. Beads and larger fiber diameters occurred at higher flow-rates. This could be attributed to the larger droplet at the end of the capillary, due to the higher flow-rate, resulting in the solution being carried away faster amounting to incomplete drying and formation of beads. Theron and co-workers (2004), investigated the effect of solution flow-rate on electric current and surface charge density. They found that, as flow-rate increased, electric current increased and surface charge density decreased.

Beachley and Wen (2009) investigated the effect of the solution flow-rate on the length and diameter of PCL fibers formed by electrospinning. It was found that the flow-rate did

not have any significant effect on the length, diameter or uniformity of the fibers. Furthermore, it was concluded that once the flow-rate was great enough for fiber formation to occur, any further increases only resulted in more solution than necessary at the capillary tip.

2.2.3. Polymer Concentration and Solution Viscosity

It has been shown that the concentration of polymer in the solution to be electrospun has an effect on both the viscosity and surface tension of the liquid (Sill and von Recum, 2008). A higher polymer concentration results in a greater viscosity (Baumgarten, 1971; Meechaisue et al., 2006), greater conductivity (Meechaisue et al., 2006), greater chain entanglement density (Shenoy et al., 2005; Munir et al., 2009) and a larger fiber diameter (Huang et al., 2003; Yang et al., 2004; Bhardwaj and Kundu, 2010).

Doshi and Reneker (1995) investigated the effect of viscosity on the electrospinning of aqueous PEO solutions and found that fibers were formed from solutions with viscosities between 800 and 4000mPa.s. Below 800mPa.s, the fiber jet broke up into droplets and above 4000mPa.s, fiber formation was difficult because the solution dried at the tip of the capillary. Fong and co-workers (1999) investigated the effect of viscosity of PEO solutions on bead formation in electrospun fibers. They found that a more viscous solution was less likely to form beads, but as viscosity increased, the bead diameter and distance between beads increased with the bead shape becoming less spherical and more spindle-like. Viscoelastic forces competed with surface tension in the fiber jet and an increase in viscosity therefore favored the formation of smooth fibers. In another study, it was shown that fiber formation from polyacrylonitrile solutions occurred between 170 and 21500mPa.s, with viscosities in the upper range resulting in incomplete drying of the polymer fiber. As the viscosity increased, jet length and fiber diameter increased and the drop at the end of the capillary changed from a hemispherical to a conical shape (Baumgarten, 1971).

Deitzel and co-workers (2001) found that electrospinning of aqueous PEO solutions between 4 and 10%$^{w}/_{v}$ (~100-2000mPa.s) resulted in the formation of fibers. Whereas below 4%$^{w}/_{v}$, surface tension was the main determinant of fiber morphology and a combination of fibers and droplets was formed. At lower concentrations within this range, fibers were found to have irregular morphologies as well as bundles and junctions due to inadequate drying before reaching the collector. At higher concentrations within this range, the fibers were found to be straight and cylindrical, with fewer junctions and bundles because fibers were able to dry before reaching the

collector due to the lower solvent content. Above 10%$^{w}/_{v}$, the flow of polymer solution through the capillary could not be controlled due to cohesion, and fiber formation was inhibited by the high viscosity. It can therefore be concluded that viscosity and surface tension often determine the useful range of polymer concentrations in electrospinning for a given polymer.

Zong and co-workers (2002) attempted to electrospin PLA solutions of different concentrations and then examined the effects on resulting fiber morphology. They observed that electrospinning solutions with concentrations below 20%$^{w}/_{v}$ resulted in the formation of a mixture of large beads and fibers. Solutions with concentrations above 40%$^{w}/_{v}$ were highly viscous and difficult to electrospin. As the concentration, and hence viscosity, increased between these two extremes, the fibers produced became more uniform and the beads had larger diameters and became more spindle-shaped.

Meechaisue and co-workers (2006) examined the effect of different poly(DTE carbonate) concentrations on electrospun fiber formation. At 5%$^{w}/_{v}$ (25mPa.s), mainly droplets were formed because the viscoelastic force at this concentration was not large enough to overcome the repulsive forces of charge, resulting in the fiber jet breaking up into droplets. At higher polymer concentrations, the jet was more stable because the viscoelastic force exceeded the repulsive forces. Beaded and smooth fibers were formed at 10%$^{w}/_{v}$ (148mPa.s) and almost completely smooth fibers were formed at 15%$^{w}/_{v}$ (505mPa.s). It was proposed that the repulsive forces from the charge within the fiber jet resulted in stretching and therefore a smaller diameter. At 20%$^{w}/_{v}$ (1960mPa.s), the fiber jet could better resist the stretching repulsive forces of charge and fiber diameter was hence greater. In this instance, polymer concentration had little effect on surface tension.

2.2.4 Solvent

In order to allow for sufficient solvent evaporation to occur before the fiber reaches the collector, a volatile solvent is required. The choice of solvent therefore plays an important role in fiber formation (Sill and von Recum., 2008). Besides the actual formation of fibers, the choice of solvent also influences the morphology of the fibers (Megelski et al., 2002). The effect of commonly used solvents in electrospinning is highlighted in Table 2.1.

Table 2.1: Solvent properties and the resulting fiber morphology in electrospinning

Solvent	Boiling Point (˚C)	Fiber Morphology	Other Properties	Reference
Dichloromethane (DCM)	39.8	Beaded, large diameter	Low dielectric constant, high surface tension	Yang et al., 2004; Meechaisue et al., 2006
Chloroform	61.2	Beaded at very low polymer concentration, smooth at higher concentration	High intrinsic viscosity	Son et al., 2004
Methanol	64.7	Small fiber diameter with ↑ methanol concentration until 50% then ↑ fiber diameter	High dielectric constant	Meechaisue et al., 2006
Tetrahydrofuran (THF)	66	Smooth and beaded, ribbon-like, high pore density	High dipole moment, good conductivity	Jarusuwannapoom et al., 2005; Megelski et al., 2002
Ethylacetate	77.1	Smooth and beaded, ribbon-like	High dielectric constant, fair conductivity	Jarusuwannapoom et al., 2005
Ethanol	78.3	Smooth, large diameter	Low surface tension, high intrinsic viscosity	Fong et al., 1999; Son et al., 2004; Yang et al., 2004
Methylethylketone (MEK)	79.6	Flat, ribbon-like, very few beads	High dipole moment, good conductivity	Jarusuwannapoom et al., 2005
Dichloroethane	83.5	Smooth and beaded, C-shaped	High dipole moment, fair conductivity	Jarusuwannapoom et al., 2005
Deionized Water	100	Beaded, small diameter	Low intrinsic viscosity	Fong et al., 1999; Son et al., 2004
Dimethylformamide (DMF)	153	Smooth and beaded, round	High dipole moment, high conductivity, low intrinsic viscosity	Son et al., 2004; Jarusuwannapoom et al., 2005

Fong and co-workers (1999) electrospun PEO fibers using pure water and a mixture of ethanol and water. By keeping the PEO concentration constant and increasing the ratio of ethanol to water, the solution viscosity increased, resulting in the formation of smoother fibers with larger diameters as depicted in Figure 2.2, where the electric field was 0.5kV/cm and the weight fraction of PEO was 3.0%. This is most probably due to the fact that ethanol is more volatile than water and therefore combinations with higher ethanol:water ratios would have evaporated faster, resulting in a greater viscosity, thereby facilitating fiber solidification, and a slower rate of bead formation (Theron et al., 2004).

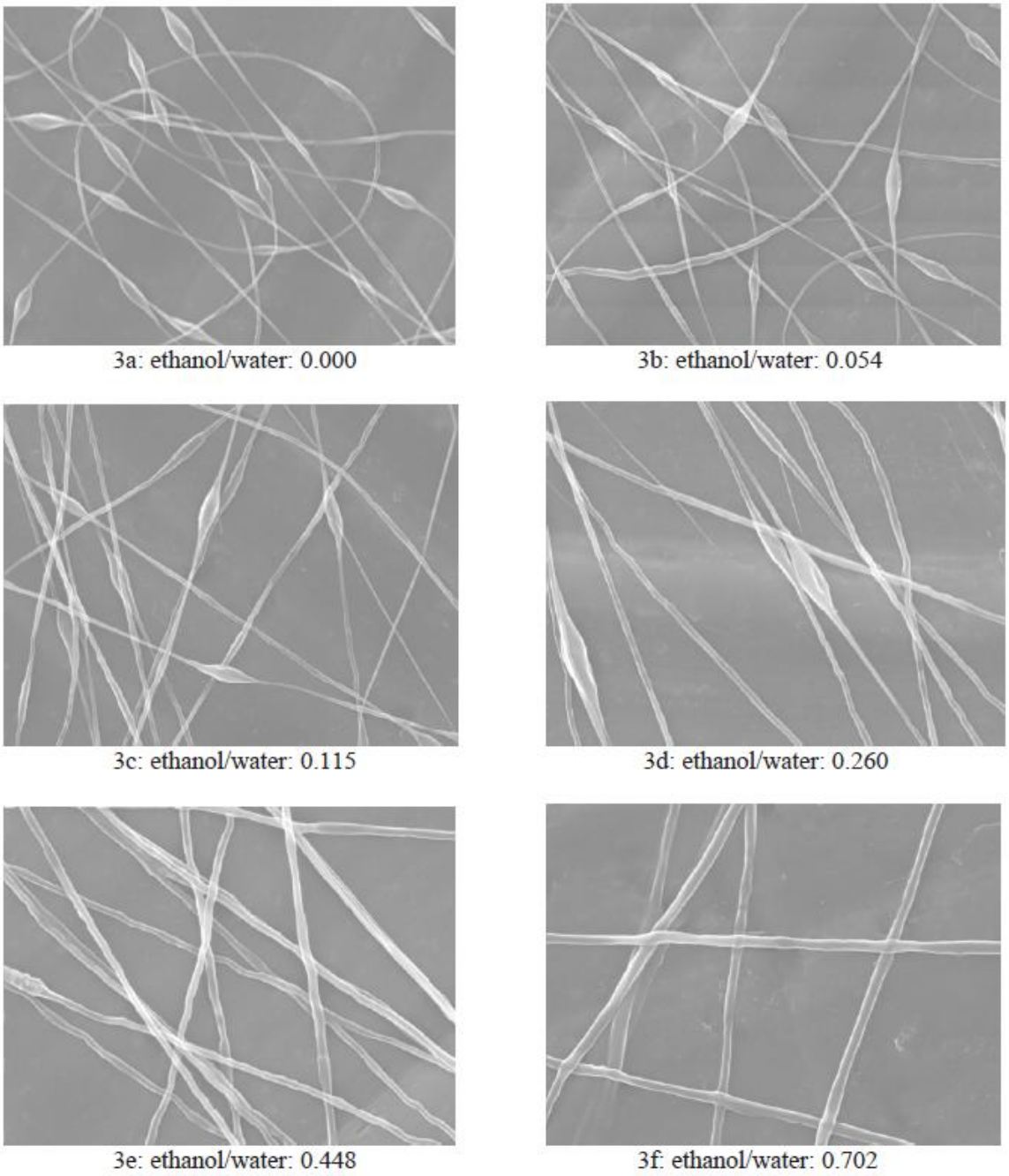


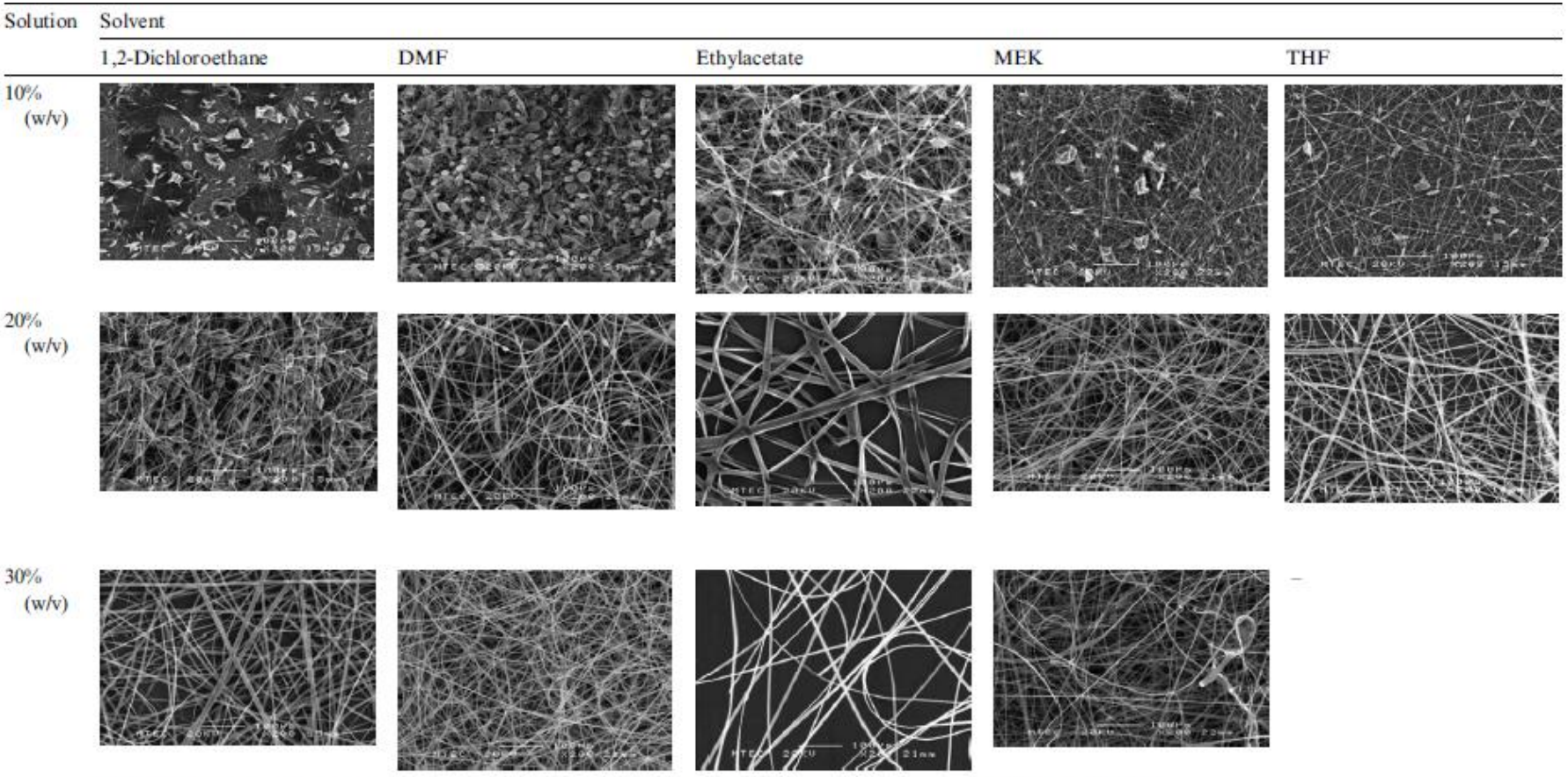
Figure 2.2: Varying PEO fiber morphology from beaded to smooth fibers as the ratio of ethanol is increased (Reproduced from Fong et al., 1999)

Megelski and co-workers (2002) investigated the effect of different solvents on fiber diameter and pore formation in electrospun polymer fibers. Various solvents with different boiling points and vapor pressures were used to electrospin polymer fibers and the effect on the fiber diameter and porosity of the fibers was examined. Polystyrene fibers were electrospun from tetrahydrofuran (THF), dimethylformamide (DMF) and combinations of the two. Fibers electrospun using THF, the more volatile of the two, resulted in fibers with very high pore density whereas fibers obtained using DMF

resulted in almost completely smooth fibers. The combination of solvents in varying ratios resulted in a decrease in pore density as the ratio of DMF:THF was increased.

Son and co-workers (2004) examined the influence of employing water, chloroform, DMF and ethanol as solvents on the electrospinning of PEO fibers. They observed that fibers that were electrospun using DMF required a higher applied voltage and a longer capillary to collector distance than when the other three solvents were used, which could be attributed to the higher boiling point of DMF. The minimum polymer concentrations for the formation of fibers that were free of beads were 3, 4, 7 and 10%$^{w}/_{v}$ for chloroform, ethanol, DMF and water, respectively. Employing water as the solvent resulted in the production of fibers with the smallest diameter in relation to the other three solvents. In another study by Yang and co-workers (2004), the effects of employing different solvents for the electrospinning of poly(vinyl pyrrolidone) (PVP) were investigated. The solvents investigated were DCM, ethanol and DMF. Ethanol produced smooth fibers, whereas beaded fibers were formed upon using DCM or DMF. A combination of ethanol and DMF resulted in fibers with diameters as small as 20nm. However, a combination of ethanol and DCM resulted in the formation of fibers with diameters as large as 300nm.

Jarusuwannapoom and co-workers (2005) also investigated the effects of using different solvents on the electrospinning of polystyrene solutions. Of the eighteen solvents that were tested, only five of them (DMF, THF, ethylacetate, 1,2-dichloroethane and methylethylketone [MEK]) were optimal for electrospinning polystyrene. All the solvents had a high dipole moment value, displayed relatively good conductivity and their polystyrene solutions had relatively good conductivity values, which are important factors for electrospinnability. The qualitative differences in the morphology of the fibers formed using these solvents and various solution concentrations were as depicted in Figure 2.3.



Remark: the applied potential and the collection distance were 20 kV and 10cm and the scale bar in each micrograph is for 100 μm.

Figure 2.3: Scanning electron micrographs of electrospun polystyrene fibers formed from solutions using 1,2-dichloroethane, dimethylformamide (DMF), ethylacetate, methylethylketone (MEK) and tetrahydrofuran (THF) as solvents (Reproduced from Jarusuwannapoom et al., 2005)

Meechaisue and co-workers (2006) investigated the use of methanol, dichloromethane (DCM) and a combination of the two in the electrospinning of poly(DTE-*co*-20%DT carbonate) fibers. Employing pure DCM, which is more volatile than methanol, resulted in the formation of beaded fibers; this can be attributed to its low dielectric constant and higher surface tension. As the methanol content increased, the fibers became smoother. When 10-30% methanol was used, the diameter of the fibers decreased due to the higher dielectric constant of methanol, leading to greater charge repulsion. However, when 50% of the solvent was methanol, the fiber diameter increased due to the increase in electrostatic force, causing the fiber to reach the collector faster.

2.2.5. Solution Conductivity

Generally, it has been observed that an increase in solution conductivity results in a decrease in fiber diameter (Sill and von Recum, 2008). A greater charge carrying capacity has been observed in solutions with high conductivity than those with low conductivity and the fiber jet produced from a solution of high conductivity is therefore subjected to a greater tensile force when exposed to an applied voltage (Sill and von Recum, 2008). Thus, conductivity of a solution is a very important factor in determining whether a solution can be electrospun (Jarusuwannapoom et al., 2005).

Fong and co-workers (1999) investigated the influence of adding sodium chloride (NaCl) to a solution of PEO in distilled water on electrospun fibers. The net charge density of the fiber jet was increased by the addition of NaCl to the solution. This resulted in a decrease in resistivity of the fiber jet due to the increased charge flowing into the jet. The increased charge resulted in an increased force within the jet and smooth fibers were formed. When the charge of the fiber jet was neutralized with ions of opposite polarity, electrical forces were reduced and beads were formed.

Zong and co-workers (2002) conducted a study to investigate the effects of adding different salts (KH_2PO_4, NaH_2PO_4 and NaCl) to PLA solutions for electrospinning. Each salt was added separately at $1\%^{w}/_{v}$ to PLA solutions. The resulting electrospun fibers were smooth, free of beads and had smaller diameters than fibers electrospun from salt-free solutions. Solutions containing NaCl produced fibers with the smallest diameter, while KH_2PO_4-containing solutions produced fibers with the largest diameter. The size of the ions was found to have an effect on the fiber diameter, where ions with smaller radii have a higher charge density and impose greater forces of elongation on electrospun

fibers. The small diameter obtained by the addition of NaCl is due to the fact that sodium and chloride ions are smaller than potassium or phosphate ions.

Son and co-workers (2004) investigated the influence of adding small amounts of polyelectrolytes, poly(allylamine hydrochloride) (PAH) and poly(acrylic acid) (PAA) on the conductivity of PEO in water solutions. The viscosity and surface tension of the formed solution increased only slightly, whereas conductivity and charge density increased significantly when small amounts of PAH and PAA were added. The diameters of the resulting electrospun fibers were decreased on addition of the polyelectrolytes. In a study by Beachley and Wen (2009), the effect of addition of NaCl to PCL solutions was investigated. It was observed that the electrospun fiber diameter decreased as the concentration of NaCl in the solution was increased. Solutions that were electrospun without NaCl produced beaded fibers, whereas fibers electrospun from NaCl-containing solutions were smooth.

2.2.6. Distance between Capillary and Collector

Generally, the diameter of electrospun fibers decreases as the distance between the capillary and the collector increases, which results in beaded fibers being formed at smaller distances (Sill and von Recum, 2008).

In a study conducted by Baumgarten (1971), the effect of increasing the distance between the capillary and the collector on fiber diameter (when applied voltage was increased) was investigated. At a distance of 50mm between capillary and collector, the fiber diameter initially decreased to a minimum and then increased with increasing voltage. At a gap of 75mm, the decrease in fiber diameter to a minimum was not so apparent and the diameter increased slightly in response to an increase in applied voltage. Doshi and Reneker (1995) investigated the influence of the distance between the capillary and collector on the diameter of electrospun fibers. Fiber diameter decreased as the distance increased although at distances greater than 30mm, the fiber jet became too small and unstable. Megelski and co-workers (2002) noted no significant change in fiber diameter with a change in distance between the capillary and the collector. However, bead formation began to occur as the distance decreased.

2.2.7. Addition of Surfactants

Zeng and co-workers (2003) examined the influence of surfactants and drugs on the uniformity and diameter of electrospun PLA fibers. Various cationic, anionic and non-ionic surfactants and drugs were added to the PLA solution. The surfactants employed

were triethyl benzyl ammonium chloride (TEBAC), sodium dodecyl sulfate (SDS) and aliphatic PPO-PEO ether (AEO10). Reduction of fiber diameter and improvement of fiber uniformity was observed with addition of all three types of surfactant.

2.3. Electrospinning in Drug Delivery

2.3.1. Drug-Loading and Drug Release

Drug-loading of electrospun fibers can be achieved in various ways (Chew et al., 2005; Luong-Van et al., 2006; Tungprapa et al., 2007; Ranganath and Wang, 2008; He et al., 2009). If the drug and the polymer are soluble in the same solvents, the drug can be dissolved directly into the polymer solution (Luong-Van et al., 2006; Tungprapa et al., 2007; Ranganath and Wang, 2008). If the drug and polymer are not soluble in the same solvents, the drug can be solubilized in a small amount of another solvent before being added to the polymer solution (Luong-Van et al., 2006; Kenawy et al., 2007; Kim et al., 2007) or the drug can be dissolved in a solvent that is immiscible with that in which the polymer is dissolved and emulsion electrospun (Xu et al., 2005; Li et al., 2008b), or the two solutions can be co-axial electrospun (He et al., 2006; Huang et al., 2006). Electrospun fibers can also be immersed in a drug solution for drug-loading (Chunder et al., 2007).

2.3.1.1. Effect of Drug Dissolved in the Polymer Solution

Figure 2.4 is a schematic of the drug-loading and electrospinning process when drug is dissolved in the same solution as the polymer prior to electrospinning, which results in the drug being encapsulated within the electrospun fibers.

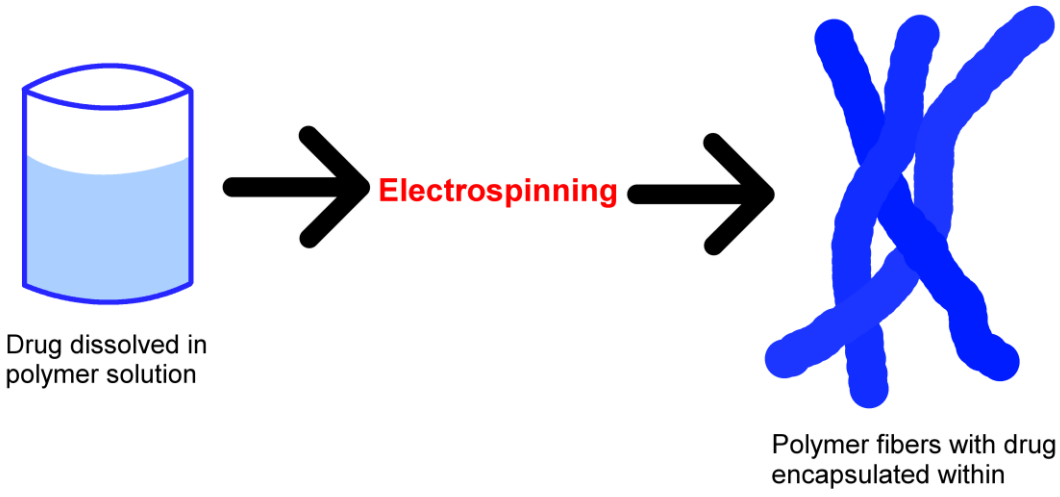


Figure 2.4: Schematic of the electrospinning process from drug-loaded polymer solutions

Zeng and co-workers (2005) investigated the influence of compatibility between the polymer solution and drug on the release kinetics of electrospun fiber formulations. Paclitaxel, doxorubicin hydrochloride and doxorubicin base were employed as model drugs. PLA was dissolved in a mixture of chloroform and acetone. The drugs were added to solutions separately. Drugs were encapsulated by PLA fibers and the encapsulation was studied. Paclitaxel and doxorubicin base were found to have a good compatibility with PLA and good solubility in the chloroform/acetone solvent that was used, which resulted in even drug encapsulation. Doxorubicin hydrochloride was not adequately encapsulated and was found near or on the surface of the PLA fibers. The release rate of paclitaxel and doxorubicin base was nearly zero-order due to fiber erosion. A burst release of doxorubicin hydrochloride was observed due to diffusion at the surface of the sample. It was concluded that drug solubility and compatibility with solvents and polymers are important factors to consider for encapsulation. Lipophilic polymers should be used to produce fibers for the encapsulation of lipophilic drugs and hydrophilic polymers for hydrophilic drugs in order to ensure that the drug is completely encapsulated and hence avoid burst release.

Taepaiboon and co-workers (2006) incorporated four different non-steroidal anti-inflammatory drugs (NSAIDs) into electrospun PVA fibrous mats for transdermal drug delivery. PVA was dissolved in distilled water and the model drugs, sodium salicylate, diclofenac sodium, naproxen and indomethacin, were added individually to PVA solutions. These solutions were electrospun and the fibers were collected on a rotating metal drum. Drug encapsulation efficiency ranged from 81 to 98%. Sodium salicylate-loaded fibrous mats displayed a burst release due to its high water solubility. As the fibrous matrix absorbed water and swelled, the drug was solvated and rapidly leached out of the matrix. The total percentage of drug release from the fibrous mats at 24 hours was 98, 97, 76, and 42% for naproxen, sodium salicylate, diclofenac sodium and indomethacin, respectively. Drug-loaded PVA mats were assessed for potential in transdermal drug delivery by an *ex vivo* diffusion study.

Suwantong and co-workers (2007) prepared curcumin-loaded cellulose acetate fibrous mats. Cellulose acetate was dissolved in a mixture of acetone and DMAc. Curcumin was dissolved in the polymer solution at 5, 10, 15 and 20%$^{w}/_{w}$ based on the cellulose acetate content and the resulting solution was electrospun. Drug encapsulation efficiency was 101.9±0.8%, 95.6±2.5%, 91.4±0.4% and 90.8±0.4% for the 5, 10, 15 and 20%$^{w}/_{v}$ solutions respectively. The maximum curcumin release was greatest for the 20%$^{w}/_{v}$ solution and lowest for the 5%$^{w}/_{v}$ solution. An initial burst release of curcumin

occurred followed by a gradual increase in curcumin release over 50 hours. It was concluded, from the study, that curcumin-loaded fibrous mats may have potential application as transdermal or topical patches or as wound dressings.

In another study conducted by Taepaiboon and co-workers (2007), cellulose acetate mats were loaded with vitamins and investigated for *in vitro* release characteristics. Solutions were made by dissolving 17%$^{w}/_{v}$ cellulose acetate and vitamin A or vitamin E in a mixture of acetone and dimethylacetamide (DMAc). The solution was electrospun and fibers were collected on a rotating metal drum. Drug encapsulation efficiency was 82.9±2.2% for vitamin E and 44.5±1.1% for vitamin A. There was a gradual increase in the rate of release of vitamin A and E from the fibrous mats. After 6 hours, a maximum of about 34% of vitamin A had been released. After 24 hours, a maximum of about 52% of vitamin E had been released. The proposed application of the vitamin-loaded fibrous mats was for transdermal drug delivery.

Ranganath and Wang (2008) fabricated poly(lactic-*co*-glycolic acid) (PLGA) microfiber implants by electrospinning. PLGA was dissolved in a mixture of DCM and DMF at 30%$^{w}/_{v}$. Paclitaxel, which was employed as the model drug, was dissolved in the polymer solution and the resulting solution was electrospun. Fibers were collected as mats on a rotating drum covered with aluminum foil. The mats were cut into sheets or punched as discs. Paclitaxel encapsulation efficiency was found to be 98±4.9% for PLGA 85:15 fibers and 94±0.57% for PLGA 50:50 fibers. Drug release occurred over 80 days and there was low initial burst release. Paclitaxel release was nearly zero order for the discs, although drug was released faster from PLGA 50:50 fibers than from PLGA 85:15 fibers due to the higher glycolic acid content of the former. From *in vitro* cellular apoptosis and *in vivo* tumor inhibition studies, it was concluded that PLGA mats may have application as implants for chemotherapy against brain tumors.

2.3.1.2. Effect of Drug Solubilized Prior to Addition to Polymer Solution

When the drug is not soluble in the same solvent as the one used for the polymer solution, it may be solubilized prior to addition to the polymer solution and the resulting solution then electrospun.

Kenawy and co-workers (2002) investigated electrospun fiber mats as drug delivery systems for the controlled delivery of tetracycline hydrochloride which was used as a model drug. Poly(ethylene-co-vinyl acetate) (PEVA), poly(lactic acid) (PLA) and a 50:50 blend of PEVA and polyvinylalcohol (PVA) were dissolved individually in chloroform.

Tetracycline was dissolved in a small amount of methanol for solubilization and then added to the polymer solutions. These solutions were electrospun and fibers were collected on a stainless steel sheet on a metal drum. PEVA mats had the fastest drug release rate. They released approximately 65% of drug content within 5 days. The 50:50 PLA/PEVA mats released 50% of drug content within 5 days. PLA mats exhibited an initial burst release effect arising from the drug that was on the surface of fibers and thereafter a negligible release over the next 50 hours.

Kim and co-workers (2004) investigated the release of hydrophilic drug, cefoxitin sodium, from PLGA-based electrospun fibrous scaffolds. PLGA was dissolved in DMF at 33%$^{w}/_{v}$. Cefoxitin sodium was dissolved in a small amount of water and this aqueous drug solution was slowly added to the polymer solution. The drug/polymer solution was electrospun and the fibers were collected on a rotating metal drum. The drug concentration was found to influence the morphology and density of the scaffolds. As the drug concentration increased, the density decreased and the fiber morphology changed from beaded fibers to smooth fibers. Adding poly(ethylene glycol) (PEG)-PLA block copolymer resulted in sustaining of the drug release to up to one week. It was concluded that the scaffolds may have potential in the prevention of post-surgical infections and adhesions.

In a study by Luong-Van and co-workers (2006), heparin loaded fibrous PCL mats were fabricated by electrospinning. Heparin was dissolved in a small amount of water and methanol was added. This solution was added to DCM and the resulting solution was used to dissolve PCL. The polymer/drug solution was electrospun and the fibers were collected on glass microscope slides. Heparin was released from the fibrous mats in a sustained manner over a period of 14 days. The released heparin was found to maintain biological functionality and it was concluded that the fibers had potential application for the delivery of heparin at the site of vascular grafts.

In another study, Kenawy and co-workers (2007) developed new systems of controlled drug release by electrospinning. Partially and fully hydrolyzed PVA was dissolved in deionized water. Ketoprofen was dissolved in a small amount of methanol and the solution was added to the polymer solution. The surfactant, Triton X-100 was added to the fully hydrolyzed PVA solution before addition of the drug in methanol. The solutions were electrospun and the resulting fibers were collected on a metal collector as fibrous mats. It was found that fully hydrolyzed PVA with entrapped ketoprofen could only be electrospun when combined with a small amount of surfactant and acetic acid.

Stabilization treatment with methanol or ethanol resulted in crosslinks within the fibers. Fibers that were not treated with alcohol showed a fast initial release of a large percentage of the drug content. Fibers treated with methanol showed a fast initial release of a much lower percentage of the drug content as well as a slow drug release over a period of two weeks. However, the overall drug release was lower from treated fibers. The degree of hydrolysis of PVA also affected the drug release rate.

Kim and co-workers (2007) examined the controlled release of a protein drug from electrospun fiber meshes composed of a blend of poly(ε-caprolactone) (PCL) and PEO. Lysozyme was employed as a model protein. A blend of PCL and PEO was dissolved in chloroform at varying ratios. Salt-free and dried lysozyme were dissolved in dimethylsulphoxide (DMSO) and the resulting solution was mixed with the polymer blend solution. The polymer/lysozyme solution was electrospun and the fiber meshes were collected on a rotating metal drum. Protein release studies were carried out and it was found that blends containing a high proportion of PEO demonstrated a more rapid protein release; therefore lysozyme release can be readily controlled by varying the polymer blend ratio. It was concluded that this protein delivery strategy may find application in wound dressing and tissue engineering.

2.3.1.3. Effect of Co-Axial Electrospinning

Co-axial electrospinning involves the electrospinning of two separate solutions simultaneously such that the inner solution is ejected from the capillary tip inside the outer solution to essentially produce a fiber within a fiber (Sill and von Recum, 2008). A schematic of the co-axial electrospinning process is shown in Figure 2.5.

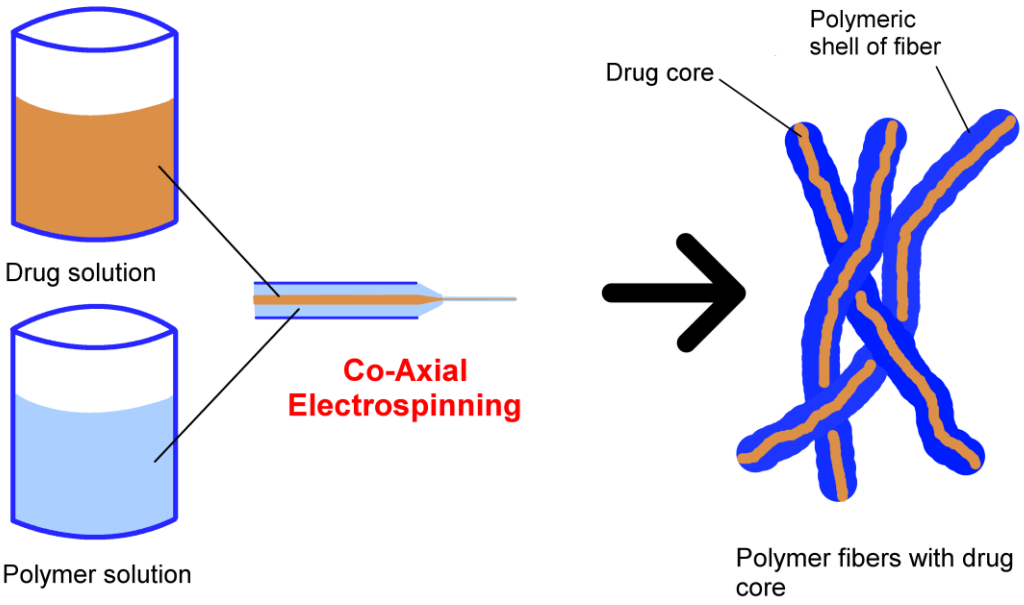


Figure 2.5: Schematic of the drug-loading and electrospinning process for co-axial electrospinning

In a study by He and co-workers (2006), drug loaded core-sheath fibers were produced by co-axial electrospinning. PLA was dissolved in a mixture of chloroform and acetone and the model drug, tetracycline hydrochloride, was dissolved in a mixture of methanol and chloroform with a small amount of PLA. Triallyl isocyanurate was added to the polymer solution as a crosslinking agent. Drug concentration was kept constant while polymer concentration was varied. The drug solution was fed through the inner needle and the polymer solution through the outer needle. The fibers were collected on a grounded metal screen. A lower polymer concentration resulted in the formation of more uniform fibers with narrower diameter distribution, whereas higher polymer concentrations resulted in the formation of fibers with larger diameters. Sustained drug release was observed over a period of 32 days. Thus, drug release rate may be adjusted by changing the polymer concentration and hence sheath thickness. It was concluded that these fibrous membranes may have potential application in drug delivery or as sutures and wound dressings.

Huang and co-workers (2006) fabricated drug-loaded core-sheath poly(ε-caprolactone) (PCL) fibers by co-axial electrospinning for application in wound dressing. PCL was dissolved in a mixture of chloroform and ethanol and the model drugs, resveratrol and gentamycin sulfate were dissolved in ethanol and water, respectively. The polymer concentration was kept constant and the drug concentrations varied. The drug and polymer solutions were fed through co-axial needles, with the drug solution in the inner needle and the polymer solution in the outer needle. An electrical potential was applied

to the inner solution and nanofibers, with a drug core and an outer polymer sheath, were collected on a grounded metal screen. It was found that when the drug and polymer solutions were miscible (resveratrol loaded fibers), an increase in drug concentration resulted in a decrease in bead formation, but when the drug and polymer solutions were immiscible (gentamycin sulfate loaded fibers), the opposite was true. On testing the erosion and drug release rate, no burst release was observed for either drug and release was observed to be smooth over seven days. However, this study did not include tissue studies.

2.3.1.4. Effect of Emulsion Electrospinning

When the drug and polymer are not soluble in the same solvent or miscible solvents, the solutions of drug and polymer can be formulated into an emulsion and emulsion electrospun to form drug-loaded fibers. Figure 2.6 is a schematic of the emulsion electrospinning process.

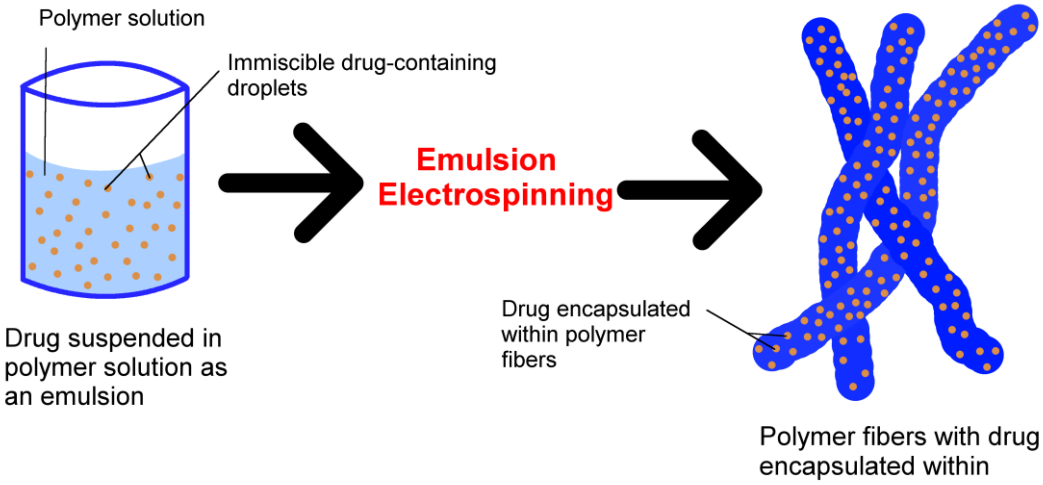


Figure 2.6: Schematic of the emulsion electrospinning process

Xu and co-workers (2005) electrospun ultra-fine fibers containing a water-soluble drug from water-in-oil (W/O) emulsions. The model drug was doxorubicin hydrochloride, which was dissolved in water to form the aqueous phase. Amphiphilic PEG-PLA diblock copolymer was dissolved in chloroform to form the oily phase. Sodium dodecyl sulfate (SDS) was added to the polymer solution as an emulsifying agent. The drug solution was slowly added to the polymer solution and emulsified. The resulting W/O emulsion was electrospun and the fibers were collected on a grounded target. The drug was completely encapsulated inside the fibers because it was dissolved in the aqueous phase of a stable emulsion. The release of the drug was controlled by diffusion and enzymatic degradation and was found to occur slowly over 10 hours. An *in vitro*

cytotoxicity assay was performed and it was found that the doxorubicin hydrochloride fibers exhibited satisfactory cytotoxicity against tumor cells.

Qi and co-workers (2006) produced PLA composite fibers through electrospinning from W/O emulsions. A surfactant called sodium bis(2-ethylhexyl) sulfosuccinate was dissolved in DCM. Alginate was dissolved in water to which bovine serum albumin (BSA), the model drug, was added. The aqueous solution was slowly added to the DCM phase and the mixture was vortexed. A calcium chloride solution was added to cross-link the alginate to form calcium alginate gel beads. PLA was then added to this emulsion and dissolved in the DCM phase. The final emulsion was electrospun and fibers were collected as mats on grounded aluminum foil. The calcium alginate beads were the drug reservoirs within the fibers and became spindle-shaped on electrospinning. An initial burst release was observed due to protein adsorbed or loosely associated on the fiber surface. A slow release over 120 hours followed the burst release.

In a study that was conducted by Li and co-workers (2008b), proteinase K was loaded inside PEG-PLA fibers by emulsion electrospinning. PEG-PLA and SDS were dissolved in chloroform, and an aqueous proteinase K solution was slowly added to the polymer solution to form a W/O emulsion. The emulsion was electrospun and fibers were collected on a metal drum covered with aluminum foil. The formed fibers were found to have a core-sheath structure, with proteinase K forming the core and PEG-PLA forming the sheath. The fiber, core and sheath diameters could be adjusted by changing the size of emulsion droplets before electrospinning. Almost 100% mass loss occurred after 7 days of *in vitro* biodegradation.

Maretschek and co-workers (2008) prepared highly hydrophobic nanofibers that were loaded with protein. Cytochrome C, the hydrophilic model protein was dissolved in water and PLA in chloroform. Hydrophilic polymers such as poly(ethylene imine) (PEI) or poly(l-lysine) (PLL) were added to the aqueous phase before emulsification in order to reduce the hydrophobicity of the fibers. Emulsions were prepared and electrospun, and fibers were collected on a round steel plate covered with aluminum foil. Protein encapsulation efficiency was between 85 and 95%. Generally, protein release appeared to be dependent on the surface tension of the release medium. PLA fibers demonstrated very slow controlled release behavior. Nanofibers prepared with higher PLA concentrations showed no burst release whereas lower concentrations resulted in an increased release rate. Incorporation of hydrophilic polymers into the aqueous phase

resulted in a larger fiber diameter and an adjustable protein release rate. However, potential drug delivery applications were not explored in this study.

In another study, Xu and co-workers (2008) prepared doxorubicin hydrochloride-loaded PEG-PLA nanofibers by emulsion electrospinning. The model drug was doxorubicin hydrochloride which was dissolved in water at various concentrations. PEG-PLA was dissolved in chloroform with SDS as a surfactant. These two solutions were emulsified and homogenized to produce a homogenous W/O emulsion. The emulsion was electrospun and the fiber mats were collected and freeze-dried to remove residual chloroform. The drug was incorporated inside the nanofibers, which had a core-sheath structure. A higher doxorubicin concentration in the aqueous phase resulted in a thinner core, which was due to the inward movement of the aqueous phase being related to the drug content in the drops. The drug release rate was found to decrease as drug content increased because of the drug distribution within the fibers forming a reservoir-type system.

2.3.1.5. Effect of Drug-Loading by Immersion in Drug Solution

An alternative method of drug-loading is to immerse electrospun polymer fibers in a drug solution. Drug release from such systems may be controlled by coating of the fibers after drug-loading (Chunder et al., 2007). Figure 2.7 is a schematic of the immersion drug-loading process.

Chunder and co-workers (2007) fabricated fibers by electrospinning PAA and PAH, both of which are weak polyelectrolytes. The fibers were studied for their potential in controlling the release of cationic molecules, using methylene blue as a model drug. The fibers were loaded with methylene blue by crosslinking, immersion in a sodium hydroxide solution, drying and then immersion in a solution containing methylene blue. Controlled drug release was due to the negatively charged carboxylate groups in the fibers bounded to the positively charged drug. The degree of ionization of PAA was dependent on the pH of the dissolving medium and therefore drug release could be controlled by pH. As the pH of the non-buffered dissolving medium decreased below 6, protons began to bind to carboxyl groups, resulting in methylene blue being released. When the fibers were placed in phosphate buffered saline (PBS), methylene blue underwent a fast release due to swelling caused by the PBS. It was also observed that drug release could be further controlled by coating the fiber surfaces. Coating the fibers with a perfluorosilane network, that would not swell in PBS, resulted in obstruction of the diffusion of methylene blue and therefore a sustained release. Coating the fibers with

multilayers of PAA and poly(N-isopropylacrylamide) (PNIPAAM), resulted in a temperature-controlled release of methylene blue. It was concluded that these polyelectrolyte fibers had potential application in drug delivery; however, specific applications were not explored.

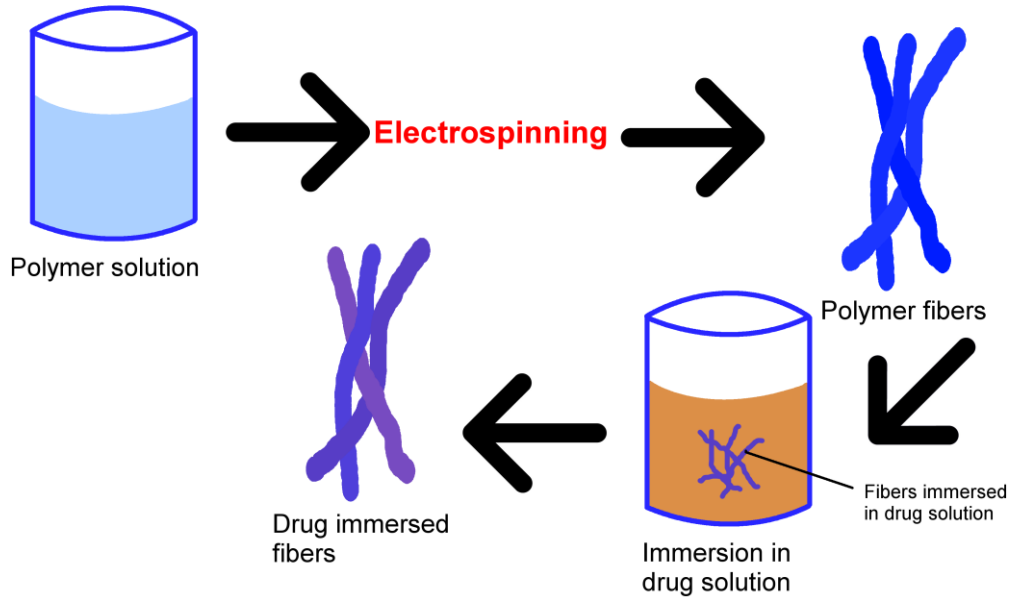


Figure 2.7: Schematic of immersion drug-loading of electrospun fibers

2.3.2. Electrospun Fibers in Drug Delivery

Electrospun fibers have been examined for various pharmaceutical applications. Drug delivery implants that release an anticancer drug in a sustained manner at a tumor site have been produced by electrospinning (Xu et al., 2005; Ranganath and Wang, 2008). Another example of a site specific drug delivery system fabricated by electrospinning is one where heparin can be delivered to the site of a vascular graft (Luong-Van et al., 2006). Electrospun fibrous mats have been assessed for their application in trans-dermal drug delivery systems or as wound dressings (Verreck et al., 2003a; He et al., 2006; Taepaiboon et al., 2006; Suwantong et al., 2007; Taepaiboon et al., 2007; Tungprapa et al., 2007). The prevention of post-surgical abdominal adhesions and infections has been investigated using antibiotic-loaded electrospun fibrous scaffolds (Kim et al., 2004; Zong et al., 2004).

2.3.3. Polymers Employed for Drug Delivery Applications

Various polymers have been electrospun and applied in drug delivery as exemplified in Table 2.2. Polymer, solvent and drug compatibility are important parameters when attempting to achieve stable and reproducible drug delivery, as a general rule, lipophilic

polymers should be used with lipophilic drugs while hydrophilic polymers should be used with hydrophilic drugs in order to obtain a stable release profile (Zeng et al., 2005).

2.3.4. Crosslinking of Fibers

Yang and co-workers (2007) prepared gelatin/PVA nanofibers and investigated their potential application in controlled drug release. An aqueous solution of PVA was added to a gelatin/formic acid solution, using different ratios. Raspberry ketone, the model drug, was added to the gelatin/PVA solutions, which were subsequently electrospun. It was found that, as the ratio of PVA increased, fiber diameter and tensile strength increased. Due to the water solubility of raspberry ketone, gelatin and PVA, an initial burst drug release was obtained. It was further observed that when the drug concentration increased, the percentage release was lower. Glutaraldehyde was employed as a crosslinking agent and an increase in crosslinking time resulted in a decrease in the rate of drug release. It was concluded that these crosslinked electrospun fibers may have application in controlled drug delivery. Specific potential drug delivery applications were, however, not explored in this study.

2.4. Other Applications of Electrospun Fibers

2.4.1. Biomedical Applications

2.4.1.1 Composite Scaffolds Prepared by Electrospinning

Composite scaffolds are useful in tissue engineering for the reconstruction of structural tissues, multi-tissue organs and tissue interfaces (Maquet et al., 2004; Schek et al., 2005; Chan and Leong, 2008). Hydroxyapatite/PLA composites have a high mechanical strength, good osteo-conductivity, osteo-inductivity and biodegradability (Liao et al., 2005; Miao et al., 2008). An ideal three-dimensional scaffold for tissue engineering should have a highly porous structure with a large surface area (Chen et al., 2006; Viswanath and Ravishankar, 2007). Such a scaffold can be prepared by electrospinning (Deng et al., 2007; Xu et al., 2007).

Table 2.2: Polymers, drugs and solvents for application in drug delivery

Polymer	Solvent	Drug(s)	Reference
Cellulose acetate	2:1 Acetone/DMAc	Naproxen, indomethacin, ibuprofen, sulindac	Tungprapa et al., 2007
		Curcumin	Suwantong et al., 2007
		Vitamin A, vitamin E	Taepaiboon et al., 2007
Poly(ε-caprolactone) (PCL)	7:3 DCM/methanol	Heparin	Luong-Van et al., 2006
	3:1 Chloroform/ethanol	Resveratrol, gentamycin sulfate	Huang et al., 2006
Poly(ethylene oxide)/poly(ε-caprolactone) (PEO/PCL) blend	Chloroform	Lysozyme	Kim et al., 2007
Poly(vinyl alcohol) (PVA)	Deionized water	Ketoprofen	Kenawy et al., 2007
		Sodium salicylate, diclofenac sodium, naproxen, indomethacin	Taepaiboon et al., 2006
Gelatin/PVA blend	Gelatin in formic acid, PVA in deionized water	Raspberry ketone	Yang et al., 2007
Poly(lactic-*co*-glycolic acid) (PLGA)	DCM/DMF	Paclitaxel	Ranganath and Wang, 2008
	DMF	Cefoxitin sodium	Kim et al., 2004
Polyurethane	DMF	Itraconazole	Verreck et al., 2003a
	DMAc	Ketanserin	
Poly(lactic acid) (PLA)	2:1 Chloroform/acetone	Doxorubicin hydrochloride	Zeng et al., 2005
		Tetracycline hydrochloride	He et al., 2006
	Chloroform	Cytochrome C	Maretschek et al., 2008
	DCM	Bovine serum albumin (BSA)	Qi et al., 2006
Poly(ethylene-co-vinyl acetate) (PEVA)	Chloroform	Tetracycline hydrochloride	Kenawy et al., 2002
Poly(ethylene glycol)-polylactide (PEG-PLA)	Chloroform	Doxorubicin hydrochloride	Xu et al., 2005, Xu et al., 2008
Poly(acrylic acid)/poly(allylamine hydrochloride) (PAA/PAH) blend	Deionized water	Methylene blue	Chunder et al., 2007

Chu and co-workers (2006) attempted to develop a non-viral gene carrier for a specific target by electrospinning. It was proposed that developing a gene carrier would enable delivering of genes that represent growth factors which could aid the repairing of fractured bones. Plasmid DNA was condensed in a poor solvent mixture. The condensed DNA was then encapsulated in a tri-block copolymer of poly(lactide)-b-poly(ethylene glycol)-b-poly(lactide) (LEL). PLGA and encapsulated DNA solutions were electrospun to form a nano-fibrous scaffold. Promising results were obtained. Thus, it is anticipated that an effective gene carrier could be developed in future using electrospinning.

In a similar study, Deng and co-workers (2007) prepared poly(l-lactic acid)/hydroxyapatite (PLA/HAP) hybrid nanofibrous scaffolds by electrospinning. The structure and morphology of the scaffolds were investigated using SEM, differential scanning calorimetry (DSC) and Fourier transform infrared spectroscopy (FTIR). The results indicated that the average diameter of hybrid nanofibers was similar to that of pure poly(l-lactic acid) fibers, but a new surface bonding (COO^-) was formed in hybrid nanofibers which resulted in the surface of the fibers becoming coarse. The weight loss and water uptake of hybrid scaffolds decreased while the viscosity-average molecular weight decreased in the phosphate buffer solution with time. This was as opposed to the results obtained with pure poly(l-lactic acid) scaffolds where weight loss and water uptake increased continuously and the viscosity-average molecular weight decreased in the phosphate buffer solution with time. A possible explanation is that the dissolving hydroxyapatite particles acted as a physical barrier and blocked off the entry of water. The biocompatibility of these scaffolds has been investigated on human osteosarcoma MG-63 cell culture and the results have shown that the cells could adhere well and proliferate better on the hybrid scaffolds than pure scaffolds.

In a study undertaken by Xu and co-workers (2007), electrospun composite fibrous scaffolds, composed of poly(l-lactide)-grafted hydroxyapatite (PLA-g-HAP) nanoparticles and a polylactide (PLA) matrix were produced. The morphology of the composite fibers, as well as the distribution of PLA-g-HAP nanoparticles in the fibers, was investigated using environmental scanning electron microscope (ESEM) and transmission electron microscopy (TEM). Results showed that at a low PLA-g-HAP content (approximately $4\%^{w}/_{v}$), the nanoparticles dispersed uniformly in the fibers and the composite fibrous mats exhibited higher strength properties, compared to the pristine PLA fiber mats and the simple hydroxyapatite/PLA blend fiber mats. However, as the content of PLA-g-HAP increased, the nanoparticles began to aggregate, which resulted in the deterioration of

the mechanical properties of the composite fiber mats. Thus, degradation behaviors of the composite fiber mats depended entirely on the PLA-g-HAP content. At a low PLA-g-HAP content, degradation was delayed presumably due to the reduction of autocatalytic degradation of PLA while at high PLA-g-HAP content, degradation rate increased, most likely due to the enhanced wettability of the composite fibers and the escape of the nanoparticles from fiber surfaces during incubation.

Ma and co-workers (2008) attempted to capture bone marrow-derived hematopoietic stem cells into nanofiber scaffolds. PLGA was mixed with collagen at a 1:1 ratio and solutions of varying concentrations were prepared. The solutions were electrospun and the resulting fiber scaffolds were dried. The bone marrow-derived hematopoietic stem cells were seeded into wells and exposed to the fiber scaffolds, onto which they became attached. This method of capturing cells showed potential in the design of artificial carriers of bone marrow-derived stem cells.

2.4.2. Electronic Applications

In a study by Bai and co-workers (2008), silver chloride nano-particles were incorporated into PVP nanofibers to produce organic-inorganic composite fibers by electrospinning. The silver chloride particles were dispersed successfully within the PVP matrix. The composite fiber matrices may have potential application as catalyst, electronic and photonic materials. Ju and co-workers (2008) prepared manganese ferrite ($MnFe_2O_4$) nanofibers by electrospinning a mixture of poly(vinyl acetate) (PVAc) and $MnFe_2O_4$. After collecting and drying the fibers at 80˚C for 6 hours, the fibers were oxidized by heating at 400, 600 and 800˚C for 4h to get manganese ferrite fibers. Due to the high electrical resistance and high magnetic permeability of manganese ferrite, it is expected that these fibers may have potential application as magnetic material that may be used in electronic devices, magnetic recording devices and magneto-optical recording.

2.4.3. Adsorption Applications

Oh and co-workers (2008) used electrospinning to produce nanofibers that, when activated, are able to adsorb toluene. Toluene, which is a volatile organic compound, is considered to be a pollutant and therefore the aim is to reduce its level in the atmosphere. Activated carbon nanofibers were prepared by electrospinning polyacrylonitrile-based fibers and activating the fibers at temperatures between 800 and 1000˚C. The high surface area and large micro-pore volume of the activated carbon nanofibers resulted in an excellent toluene adsorption capacity.

2.4.4. Sensor and Drug Content Determination Applications

Sawicka and co-workers (2005) developed an electrospun fibrous mat for urea biosensing. A mixture of urease and PVP was electrospun and the fibers were collected as mats. Urease converted urea to ammonia, which could be measured as a mV value. This system proved to be an excellent biosensing device. Kang and co-workers (2007) developed a method of extracting trazodone from human plasma with an electrospun nanofiber solid-phase extraction sorbent. A polystyrene solution was electrospun and the fiber web was collected on a copper grid. Samples were pushed through this sorbent and trazodone was extracted. The sorbent was then washed with water and analytes were eluted with methanol. The methanol used for elution was analyzed by high performance liquid chromatography (HPLC). This method of extraction and analysis of trazodone was found to be effective.

2.4.5. Filtration Applications

Ahn and co-workers (2006) developed nano-filters by electrospinning Nylon 6. Generally nanofibers have a very large surface area and small pore size compared to conventional textiles. Nylon 6 solutions with concentrations between 15 and 24%$^{w}/_{v}$ were electrospun and the fibers were collected on a drum covered with steel mesh. The filtration efficiency and pressure drop of the nanofibers was compared to that of High Efficiency Particulate Air (HEPA) filters. The nylon 6 nano-filters were found to have a filtration efficiency that was greater than that of commercial HEPA filters. Thus, nylon 6 nano-filters showed the potential for application as high efficiency filters.

2.5. Concluding Remarks

Electrospun fibers have shown great potential in many areas, including drug delivery. Altering the processing parameters and solution constituents used in the electrospinning process can greatly influence the morphology of the fibers formed. Research conducted thus far has shown that it is now possible to produce low-cost, high-value, high-strength fibers from biodegradable and renewable materials. In this regard, electrospun fibers have shown great potential for application in wound dressings, filtration, bone tissue engineering, catalyst supports, non-woven fabrics, reinforced fibers, support for enzymes, fuel cells, conducting polymers and composites, photonics, medicine, fiber mats serving as reinforcing component in composite systems, fiber templates for the preparation of functional nanotubes and drug delivery systems. Drugs can be incorporated inside or on the surface of fibers, using various methods, and may be

released rapidly or in a controlled manner. Therefore electrospun fibers may display a considerable scope for use as potential drug delivery carriers for the treatment of various diseases. The use of electrospun fibers in rapid drug delivery has, however, not been extensively investigated in previous studies.

CHAPTER 3

DEVELOPMENT AND PREFORMULATION OF A POLYMERIC, MUCOADHESIVE BACKING FILM LAYER AND A DRUG-LOADED ELECTROSPUN FIBROUS LAYER

3.1. Introduction

A drug delivery system intended for accelerated oramucosal drug delivery is required to be rapidly disintegrating, releasing drug almost instantaneously to the buccal mucosa for immediate absorption (Rossi et al., 2005). This may be achieved by the use of water-soluble polymers and a large surface area exposed to the dissolution medium (Verreck et al., 2003b; Dokoumetzidis and Macheras, 2006). Electrospun fibers exhibit an exceedingly large surface area to mass ratio (Reneker and Yarin, 2008), which not only enhances the dissolution rate, but also increases the bioavailability and total amount of drug released in comparison to cast-films of the same composition (Agarwal et al., 2008) and may therefore find application in rapid oramucosal drug delivery.

Due to the relatively short residence time of an oramucosally administered drug delivery system at the site of absorption, mucoadhesion is often required (Ponchel, 1994). Mucoadhesive drug delivery systems are advantageous in that the entire system is rendered immobile, an intimate contact between the system and buccal mucosa is created (Andrews et al., 2009) and a high drug concentration at the absorption surface is achieved (Ponchel, 1994). This results in a reduction in the required drug concentration as well as an improved bioavailability (Andrews et al., 2009). Thin, mucoadhesive films are favorable for oramucosal drug delivery due to the flexible nature and high contact surface area of such films (Perioli et al., 2004; Ponchel, 1994).

Several polymers have been electrospun for the purpose of drug delivery (Sill and von Recum, 2008; Bhardwaj and Kundu, 2010), including polyvinylalcohol (PVA) (Taepaiboon et al., 2006; Kenawy et al., 2007), cellulose acetate (Tungprapa et al., 2007), poly (ε-caprolactone) (PCL) (Luong-Van et al., 2006), poly(ethylene oxide) (PEO) (Kim et al., 2007) and poly(acrylic acid) (PAA) (Chunder et al., 2007). Although, not specifically for application in drug delivery, hydroxypropylcellulose (HPC) fibers have also been electrospun and investigated by Shukla and co-workers (2005).

The buccal mucosa is more permeable than skin but less permeable than intestinal mucosa (Nicolazzo et al., 2005). A permeation barrier, composed of lipids, is believed to be present in the upper portion of the buccal epithelium, which results in reduced permeability of certain drugs (Şenel and Hıncal, 2001; Nicolazzo et al., 2005). For drugs with poor permeability, such as zidovudine (AZT), it therefore becomes advantageous to employ permeation enhancers in oramucosally administered formulations (Şenel and Hıncal, 2001). There are various categories of buccal permeation enhancing substances that have different suggested modes of action. These include surfactants, which disrupt the integrity of the protein domain and intercellular lipids; fatty acids, which enhance the fluidity of phospholipids; cyclodextrins, which act as drug inclusion carriers; chelators, which interfere with calcium ions; and cations and polymers with positive charge, which interact with negative ions on the surface of the buccal mucosa (Şenel and Hıncal, 2001).

This chapter details the development of a mucoadhesive polymeric backing film layer and a drug-loaded electrospun fiber layer with the aim of producing a flexible, mucoadhesive fibrous matrix system (FMS) by depositing the latter directly onto the former. The film layer provided a flexible, mucoadhesive backing layer with a large exposed surface area and the drug-loaded fiber layer exhibited an exceedingly high surface area, due to the fiber dimensions, allowing for more rapid disintegration and drug release than what could be achieved from a drug-loaded film formulation. Polymers investigated for the development of the backing layer were selected based on water-solubility and film or membrane-forming propensity. The polymers investigated for the fibrous layer were selected based on water-solubility and electrospinnability. Various penetration enhancing substances were investigated for their effect on the buccal permeation of one of the model drugs, AZT.

3.2. Materials and Methods

3.2.1. Materials

Polyvinylalcohol (PVA) (87-89% hydrolyzed, M_w 13,000-23,000g/mol), poly(ethylene oxide) (PEO), poly(acrylic acid) (PAA) (M_w 1,800g/mol), chitosan (medium molecular weight), β-cyclodextrin and diphenhydramine (DPH) were purchased from Sigma-Aldrich (St. Louis, Missouri, USA). Propan-2-ol, glycerol, citric acid, sodium carbonate, sodium chloride, peppermint oil, spearmint oil, cod liver oil, lemon oil, aniseed oil, oleic acid and ethanol were purchased from Rochelle Chemicals (Johannesburg, South Africa). Hydroxypropylcellulose (HPC) (Klucel Type EF and Type HF) was purchased

from Hercules (Wilmington, Delaware, USA). Hydroxypropylmethylcellulose (HPMC) was purchased from Colorcon Limited (London, England). Zidovudine (3'-azido-3'-deoxythymidine) (AZT) was purchased from Evershine Ind. (Naejar Malad, Mumbai, India).

3.2.2. Preparation of Crosslinked HPC Membranes

Crosslinked membranes were produced by a method based on a study by Pillay and co-workers (2005). HPC (Type HF) was dissolved in deionized water at concentrations between 1 and 3%$^{w}/_{v}$ and the solutions were homogenized. The polymer solution (2mL) was syringed onto the bases of round glass moulds (4cm diameter). The moulds were placed in beakers, into which 25mL of sodium carbonate (2.5-20%$^{w}/_{v}$) or sodium chloride (10-15%$^{w}/_{v}$) solutions were syringed separately. The beakers were covered and the solutions left to crosslink for 24-72 hours, after which the formed membranes were removed and left to dry under an extractor at 21°C.

3.2.3. Preparation of Polymeric Films from High Concentration Polymer Solutions

HPC (Type HF) and HPMC were employed in the preparation of polymeric films. Solutions were prepared by dissolving HPC or HPMC in a 2:1 mixture of 80% ethanol and water at concentrations of 5.5-7%$^{w}/_{v}$. The solutions were semi-solid and exhibited minimal flow properties. The polymer solutions were cast onto smooth, flat glass surfaces with a spatula and oven dried at 50°C for 2 hours.

3.2.4. Preparation of Polymeric Films Employing a Molding and Film-Casting Technique

3.2.4.1. HPC Films

HPC films were prepared from solutions with lower polymer concentrations than those used previously in an attempt to form films with a more even surface morphology. HPC (Type EF) and glycerol were dissolved in a 2:1 mixture of propan-2-ol and water at concentrations of 15%$^{w}/_{v}$ and 8%$^{w}/_{v}$, respectively. The resulting solutions were placed in flat, smooth-surfaced molds and placed under an extractor at 21°C for 48 hours in order for complete solvent evaporation and film formation to occur.

3.2.4.2. HPMC Films

HPMC solutions with lower polymer concentrations than those employed previously were used to produce films with an improved surface morphology. HPMC was dissolved in a 2:1 mixture of deionized water and propan-2-ol at concentrations ranging between 0.5%$^{w}/_{v}$ and 3%$^{w}/_{v}$. Glycerol was added to the solutions as a plasticizer at varying

concentrations between 5 and 70% of the HPMC mass. Solutions were placed in rectangular, flat-bottomed molds and placed under an extractor at 21°C for 48 hours for solvent evaporation and film formation to take place.

3.2.4.3. PVA and HPMC Films

PVA was employed in film preparation with the aim of improving the morphology of the films. PVA/HPMC films were developed by first producing film formulations containing PVA and adding one other component at a time, at varying concentrations, to subsequent formulations in order to determine acceptable ranges for the various constituents. Polymer solutions were prepared by dissolving PVA (0.5-2.5%$^{w}/_{v}$), HPMC (0-1%$^{w}/_{v}$) and glycerol (5-20%$^{w}/_{w}$ of combined polymer mass) in a 4:1 mixture of deionized water and propan-2-ol. Solutions were syringed into rectangular, flat-bottomed molds and placed under an extractor at 21°C for 48 hours in order for complete solvent evaporation and film formation to occur. The feasible mold fill-volume was also investigated by dissolving PVA, at a constant concentration of 1%$^{w}/_{v}$, in the solvent mixture and filling the mold with different volumes ranging between 25-100mL.

3.2.5. Preparation of Fibers by Electrospinning

Solutions, employing different solvents and polymers at varying concentrations, were prepared in order to assess the production of fibers. Once appropriate solvent/polymer combinations were determined, either AZT or diphenhydramine (DPH) was dissolved in the polymer solution in order to assess drug-loading and permeation. Solutions were placed in a 5mL pipette, which was fitted into the adjustable supporting bracket of an electrospinning device. Electrospinning of the solutions was performed at 10-20kV with a tip-to-collector distance of 5-15cm, using a custom-built electrospinning device (RGC Engineering, Johannesburg, South Africa) equipped with a voltmeter and MJ Series High Voltage Power Supply (Glassman High Voltage Inc., New Jersey, USA). Fibers were collected on aluminum foil-lined board or on polymeric backing films secured to the board.

3.2.6. Investigation of Various Polymers for Electrospinning

3.2.6.1. PVA in Water

PVA was dissolved in deionized water at concentrations of 10, 15, 20 and 25%$^{w}/_{v}$, and the solutions were electrospun across distances of 5 and 11cm with applied potentials of 15, 17 and 20kV and investigated for fiber production potential. Drug-loaded and plasticizer-containing solutions were also produced by adding AZT and glycerin to polymer solutions, respectively. Tip-to-collector distances and applied potentials were

dependent on the formation of a Taylor cone at the tip of the pipette, and were adjusted accordingly during the process of electrospinning.

3.2.6.2. PVA in a 2:1 Mixture of Water and Propan-2-ol

PVA was dissolved in a 2:1 mixture of deionized water and propan-2-ol at concentrations of 15, 20, 22, 25 and 30%$^{w}/_{v}$, and solutions were electrospun with tip-to-collector distances of 5 and 11cm at applied potentials of 15, 17, 18, and 20kV. Drug-loaded solutions were produced by dissolving either AZT or DPH in PVA solutions at various concentrations. Glycerol and glycerin were added to the PVA solutions as plasticizers in order to assess their effect on fiber production. Citric acid was employed as a taste-masking agent.

3.2.6.3. HPC in Water

HPC was dissolved in deionized water to make a 15%$^{w}/_{v}$ solution, which was electrospun at an applied voltage of 10kV and a tip-to-collector distance of 10cm. The applied voltage and tip-to-collector distance was determined by the formation of a Taylor cone.

3.2.6.4. HPC in a 2:1 Mixture of Water and Propan-2-ol

HPC was dissolved in a 2:1 mixture of deionized water and propan-2-ol at a concentration of 10%$^{w}/_{v}$. The solution was electrospun with a tip-to-collector distance of 5cm and at an applied voltage of 20kV. Drug-loaded solutions were produced by dissolving AZT and DPH in the solutions, both at concentrations of 2 and 3%$^{w}/_{v}$.

3.2.6.5. PEO in Water

PEO was dissolved in deionized water at a concentration of 10%$^{w}/_{v}$ and electrospun at an applied voltage of 20kV, over a tip-to-collector distance of 10cm. Glycerin was added to the PEO solution at a concentration of 5%$^{v}/_{v}$ in order to assess the effect of plasticizer on fiber formation. This solution was electrospun at an applied voltage of 18kV, across a distance of 7cm.

3.2.6.6. PAA in Water

PAA was dissolved in deionized water at a concentration of 25%$^{w}/_{v}$ and electrospun across a tip-to-collector distance of 10cm at an applied voltage of 15kV.

Further investigations were carried out only on PVA solutions electrospun fibers formed from PVA solutions as this polymer was deemed most suitable for the purposes of this study.

3.2.7. Morphological Surface Structure Analysis of the Electrospun Fiber Layer

The surface morphology of the electrospun fiber layer was analyzed by images produced by scanning electron microscopy (SEM), using a Phenom Microscope (FEI Company, Hillsboro, Oregon, USA). This was also used to confirm the presence of fibers.

3.2.8. Rheological Characterization of PVA Solutions Employed in Electrospinning

The rheological properties of PVA solutions at various concentrations were determined with the use of a Haake Modular Advanced Rheometer System (ThermoFisher Scientific, Karlsruhe, Germany). The stress-strain rheological parameters of the polymer solution have an influence on electrospinning, and are important factors when considering the desired characteristics of a solution to be electrospun. Samples were analyzed by placing the polymer solution on the sample stage and immersing the C35/1° titanium rotor in the fluid while the temperature was maintained at 25°C. The shear rate was ramped from 0 to 500/s and viscosity and shear force were quantified for each solution.

3.2.9. Calibration Curves for UV Spectrophotometric Determination of AZT and DPH

Calibration curves were generated by dissolving known concentrations of AZT and DPH in simulated saliva (pH 6.75) and phosphate buffered saline (PBS) (pH 7.4) and measuring the absorbance using a UV spectrophotometer (Specord 40, Analytik Jena, AG, Germany). Absorbances of AZT and DPH were analyzed at λ_{267nm} and λ_{254nm}, respectively. Concentration was plotted on the x-axis and absorbance on the y-axis to generate a linear curve with $R^2 > 0.95$.

3.2.10. Drug Entrapment

Samples of the drug-loaded fiber layer were cut into sections, dissolved in simulated saliva (pH 6.75) and the drug content of each section was analyzed by UV spectrophotometry (Specord 40, Analytik Jena, AG, Germany).

3.2.11. Disintegration Time of the PVA Fiber Layer and Backing Film Layer

The *in vitro* disintegration times of the PVA fiber layer and film formulations were determined according to a modified method based on the United States Pharmacopoeia (USP) method for tablet disintegration testing using a Type PTZ 1 basket-rack assembly disintegration apparatus (Pharma Test, Hainburg, Germany). According to the USP 32, disintegration is considered to have occurred when there is no longer any solid residue left on the mesh of the basket-rack assembly apparatus (USP 32, 2009). The disintegration medium was 150mL simulated saliva (pH 6.75) in a glass jar placed in a water bath maintained at 37˚C. Samples were cut into sections and placed on the mesh of the basket rack assembly, with a mesh disc placed on top. The basket rack assembly was raised and lowered through a distance of 55mm and at a frequency of 25 cycles per minute and the time taken for sample disintegration to occur was determined by observation and recorded.

3.2.12. Drug Permeation by *ex vivo* Studies

PVA fiber layers, loaded with AZT or DPH, were electrospun directly onto films made up of either PVA or a combination of PVA and HPMC. Chitosan and β-cyclodextrin were incorporated into formulations containing AZT, as permeation enhancers, in an attempt to improve permeation. The resulting fiber-on-film systems were cut into sections and assessed for *ex vivo* drug permeation characteristics. *Ex vivo* drug permeation testing was performed using freshly excised porcine buccal tissue, which is considered to have a closer resemblance to human buccal mucosa than other animal tissues (Langoth et al., 2005; Figueiras et al., 2009). Sections of mucosa were mounted in Franz Type Diffusion Cells (Perme Gear, Inc., Hellertown, Pennsylvania, USA) and equilibrated for 0.5 hours at 37˚C by adding PBS (pH 7.4) to both the acceptor and donor compartments. After equilibration, the PBS in the donor compartment was removed and replaced with a drug-loaded sample in simulated saliva (pH 6.75). Samples were drawn from the acceptor compartment at 20 seconds, 1, 3, 5, 10, 30, 60 and 90 minutes and analyzed by UV spectrophotometry, and the volume removed was replaced with fresh PBS.

3.3. Results and Discussion

3.3.1. Crosslinked HPC Membranes

HPC at 2.5%$^{w}/_{v}$ and sodium carbonate at 15%$^{w}/_{v}$ were recognized as the most ideal reaction components for membrane formation. However, the membranes produced were porous and fragile, and deemed unsuitable for the purposes of this study. Due to

their malapropos nature, no further investigations were carried out on the crosslinked HPC membranes.

3.3.2. Polymeric Films Prepared from Viscous Polymer Solutions

The HPC and HPMC films, which were prepared from 5.5%$^{w}/_{v}$ polymer solutions, displayed an uneven morphology due to the process of film formation by casting with a spatula. HPMC films were slightly more even than HPC films, which exhibited large pores but were poorly formed. Solutions with polymer concentrations above 5.5%$^{w}/_{v}$ were too viscous to be adequately spread onto a flat surface and film formation could therefore not occur. The production of films from less viscous solutions that could be poured into moulds was therefore investigated.

3.3.3. Polymeric Films Prepared Employing a Molding and Film-Casting Technique

3.3.3.1. HPC Films

Films were removed from molds and found to be thin, clear, even and extremely adhesive. Due to the adhesive nature of the HPC films, they were considered unsuitable for the purposes of the present study and no further investigation was carried out.

3.3.3.2. HPMC Films

For the production of HPMC films displaying a desirable thickness and uniformity, HPMC concentrations were found to be between 1 and 2%$^{w}/_{v}$. Without plasticizer, the films were brittle and fragile and the ideal glycerol concentration for the formation of flexible films was found to be between 15 and 30%$^{w}/_{w}$ of the polymer mass. HPMC films were easily torn, which made removal from molds problematic. Further studies, including other polymers in the film formulation, were therefore conducted.

3.3.3.3. PVA and HPMC Films

The films produced were thin, even in thickness and clear or cloudy, depending on the solution constituents. PVA concentrations between 0.5 and 2%$^{w}/_{v}$ produced films of a desirable thickness at a fill volume of 50mL. Films containing more than 2%$^{w}/_{v}$ PVA (50mL fill volume) were too thick for electrospinning as fiber deposition was not uniform on these films. It was found that the optimal glycerol concentration was between 10 and 15%$^{w}/_{w}$ of the total polymer mass. Lower than this, the films were fragile and higher than this, the films were difficult to work with. HPMC could be incorporated into the films at concentrations between 0 and 0.5%$^{w}/_{v}$ without causing breakage on removal of films from molds. The acceptable fill volume was found to be between 40 and 100mL. Below 40mL, film formation was not particularly even.

3.3.4. Investigation into Various Polymers for Electrospinning

3.3.4.1. PVA in Water

The solutions were visibly thin in consistency, particularly at 10%$^{w}/_{v}$ PVA, and fiber formation was generally poor, with a considerable quantity of spraying occurring during electrospinning. Where fibers were formed, they were visible only as a fine layer of discoloration on the aluminum foil, which is not adequate for drug delivery on account of the exceedingly high drug-loading that would be required so that a sufficient dose may be achieved.

3.3.4.2. PVA in a 2:1 Mixture of Water and Propan-2-ol

Solutions of PVA dissolved in a 2:1 mixture of deionized water and propan-2-ol were observed to exhibit the most desirable fiber formation on electrospinning. The solutions were visually thicker than those of PVA dissolved in deionized water and the produced fibers formed a thick layer on the foil or film onto which they were electrospun, which is adequate for drug-loading. Addition of plasticizers to the electrospinning solutions had a significant effect on fiber formation at higher plasticizer concentrations, hindering the production of fibers, whereas at lower concentrations, plasticizer addition resulted in the formation of a more flexible fiber layer without a marked effect on fiber production. The presence of drug in PVA solutions had little or no effect on fiber formation, and PVA fibers, electrospun from solutions using a 2:1 mixture of deionized water and propan-2-ol as the solvent, were therefore deemed to be satisfactory for drug delivery. The ideal PVA concentration for the electrospinning solution was determined to be 25%$^{w}/_{v}$, the DPH concentration was 10%$^{w}/_{v}$ and the excipients were citric acid and glycerol at 2%$^{w}/_{v}$ and 5%$^{v}/_{v}$, respectively.

3.3.4.3. HPC in Water

The formation of fibers from solutions containing HPC dissolved in deionized water was observed as a thin white layer on the film onto which the fibers were electrospun. Fiber production was preferable to that from PVA in water solutions; however, it was not sufficient to be applied in drug delivery.

3.3.4.4. HPC in a 2:1 Mixture of Water and Propan-2-ol

Fiber production from solutions of HPC dissolved in a 2:1 mixture of deionized water and propan-2-ol was somewhat superior to fiber production from HPC in water solutions. A fairly thick, white layer was formed on the collecting surface, suggesting that adequate fiber production had occurred. However, drug-loading of the HPC

solutions with AZT or DPH hindered both fiber production and formation considerably. Therefore, no further studies were conducted on HPC for electrospinning.

3.3.4.5. PEO in Water

Fibers electrospun from PEO solutions formed a thick, white layer on the collecting surface. Nevertheless, fiber deposition was observed to be erratic, with a large amount of deposition occurring in some regions and little or none in others and showing no clear pattern. The erratic nature of fiber deposition obviates the application of PEO in drug delivery for the purposes of this study and no further investigations were conducted.

3.3.4.6. PAA in Water

The PAA solution was not viscous enough for fiber formation to occur. Visually, the polymer solution appeared to have a similar consistency to water, whereas solutions that were adequately electrospun had consistencies similar to that of syrup. During electrospinning, the Taylor cone was not formed and the solution sprayed, in the form of droplets, onto the collecting surface. It was concluded that fiber formation did not occur at a concentration of 25%$^{w}/_{v}$ and no further studies were conducted.

3.3.5. Morphological and Surface Structure Analysis of the Electrospun Fiber Layer

The presence of PVA fibers in the electrospun fiber layer was confirmed by SEM analysis. Figure 3.1 clearly displays fibrous structures. Fibers formed were in the less than 500nm thick and appeared to be somewhat uniform in diameter and structure. Pores were also apparent between individual fibers.

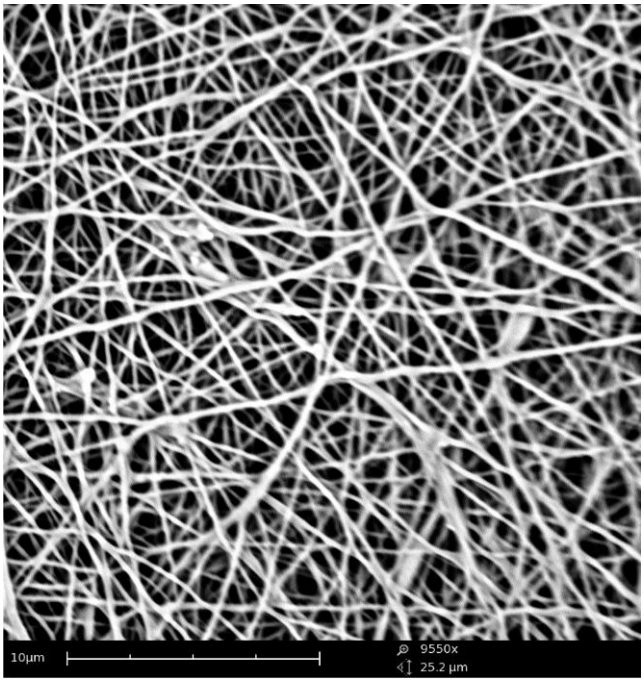


Figure 3.1: Scanning electron micrograph of PVA fibers

3.3.6. Rheological Characterization of PVA Solutions Employed in Electrospinning

The rheological properties of a solution employed for electrospinning can have a substantial effect on the process of electrospinning as well as the quality and morphology of fibers that are formed (Tao and Shivkumar, 2007). The degree of polymer chain entanglements, and hence the polymer concentration, has a considerable influence over the viscosity and electrospinnability of a solution (Ramakrishna et al., 2005). The actual conformation of individual polymer chains also has a significant influence on solution viscosity, considering that solutions containing coiled chains have a lower viscosity than those with extended chains (Ramakrishna et al., 2005). It is therefore important to investigate the rheological properties of polymeric solutions employed in electrospinning.

The rheological properties of PVA solutions for electrospinning were quantified at various PVA concentrations by ramping the shear rate ($\dot{\gamma}$) from 0 to 500/s. The rheological profiles of the 15, 20, 25 and 30%$^{w}/_{v}$ PVA solutions in 2:1 deionized water and propan-2-ol are depicted in Figure 3.2 a, b, c and d, respectively. The rheological profile of the 25%$^{w}/_{v}$ PVA in water solution is depicted in Figure 3.3. The viscosity of the solutions increased with increasing shear rate and appeared to exhibit non-Newtonian, dilatant flow properties.

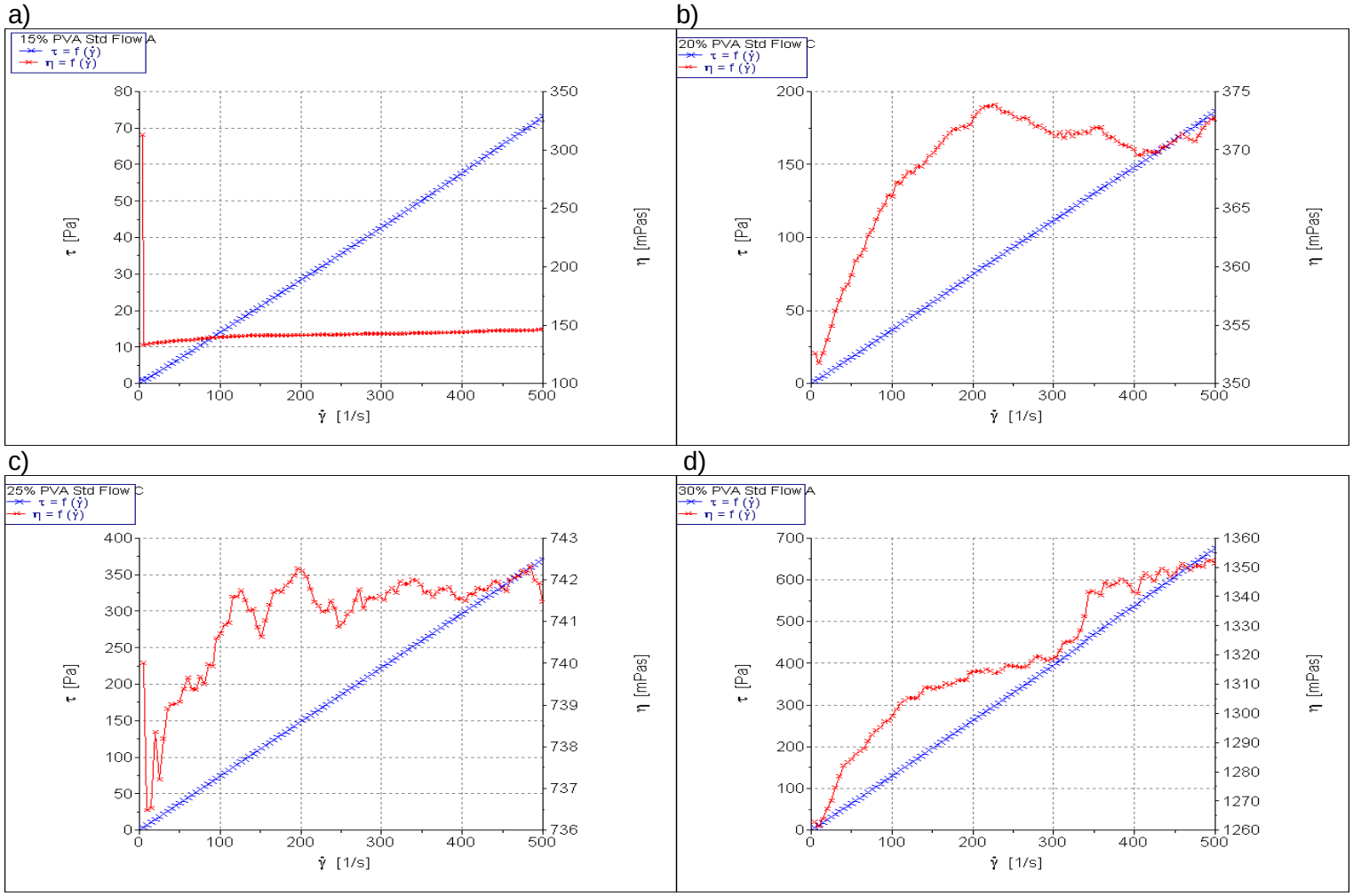


Figure 3.2: Rheological profiles of (a) 15%$^{w}/_{v}$, (b) 20%$^{w}/_{v}$, (c) 25%$^{w}/_{v}$ and (d) 30%$^{w}/_{v}$ PVA solutions in 2:1 deionized water and propan-2-ol

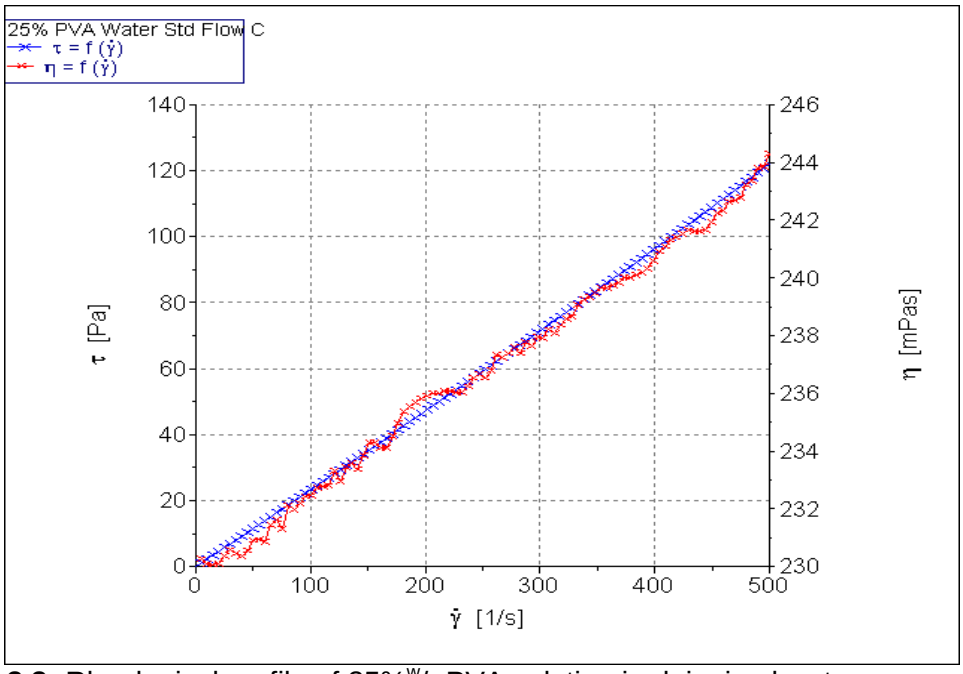


Figure 3.3: Rheological profile of 25%$^{w}/_{v}$ PVA solution in deionized water

The average shear force (τ) and viscosity (η), over the shear rate range, were calculated and plotted against concentration in Figures 3.4 and 3.5, respectively. Figures 3.4 and 3.5 appear to display a similar shaped curve, suggesting that the increase in average viscosity with increasing polymer concentration is proportional to the increase in shear force. At lower PVA concentrations (below 25%$^{w}/_{v}$) and when the solvent used was deionized water, electrospun fibers did form, but spraying of solution droplets also occurred intermittently where the viscosity was too low for constant fiber jet formation. At PVA concentrations above 25%$^{w}/_{v}$, the solution was too viscous to pass through the capillary tip of the pipette consistently. At a PVA concentration of 25%$^{w}/_{v}$, fiber formation was satisfactory and minimal spraying occurred.

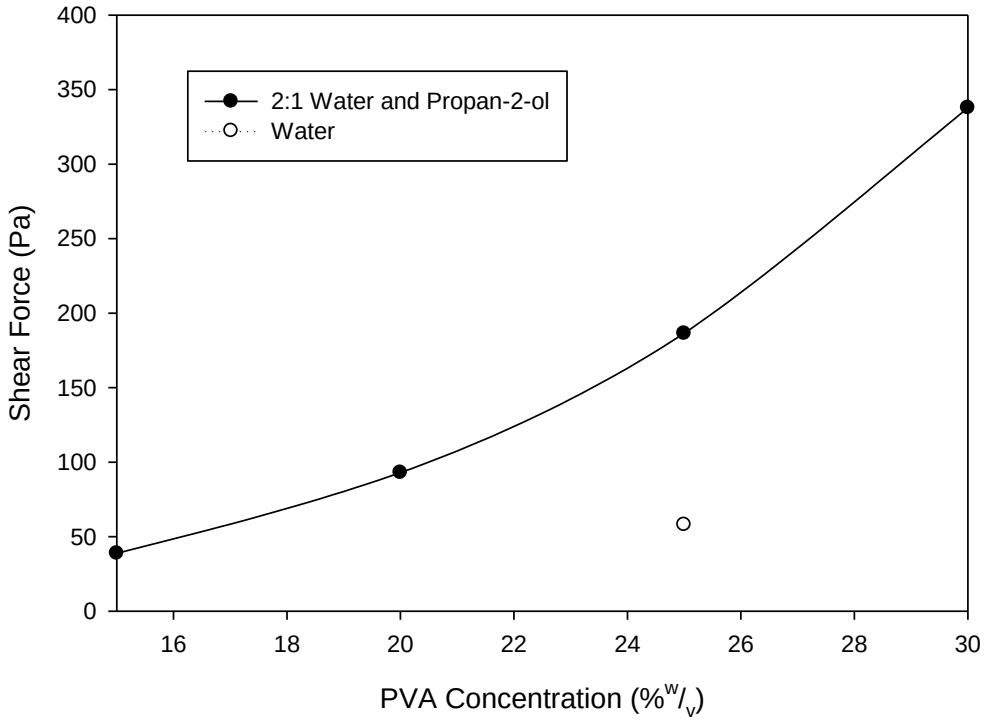


Figure 3.4: Comparison of average shear force for the electrospinning solutions with varying PVA concentrations

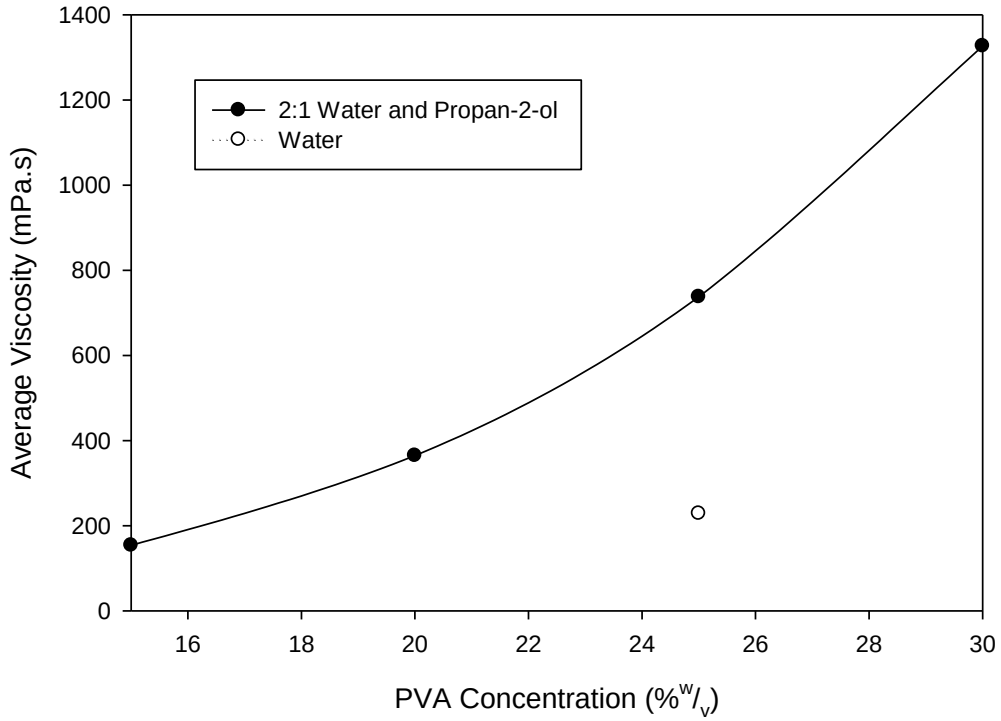


Figure 3.5: Comparison of average viscosity for the electrospinning solutions with varying PVA concentrations

3.3.7. Calibration Curves for UV Spectrophotometric Determination of AZT and DPH

3.3.7.1. AZT in Simulated Saliva (pH 6.75)

The calibration curve for AZT dissolved in simulated saliva (pH 6.75) at λ_{267nm} is displayed in Figure 3.6.

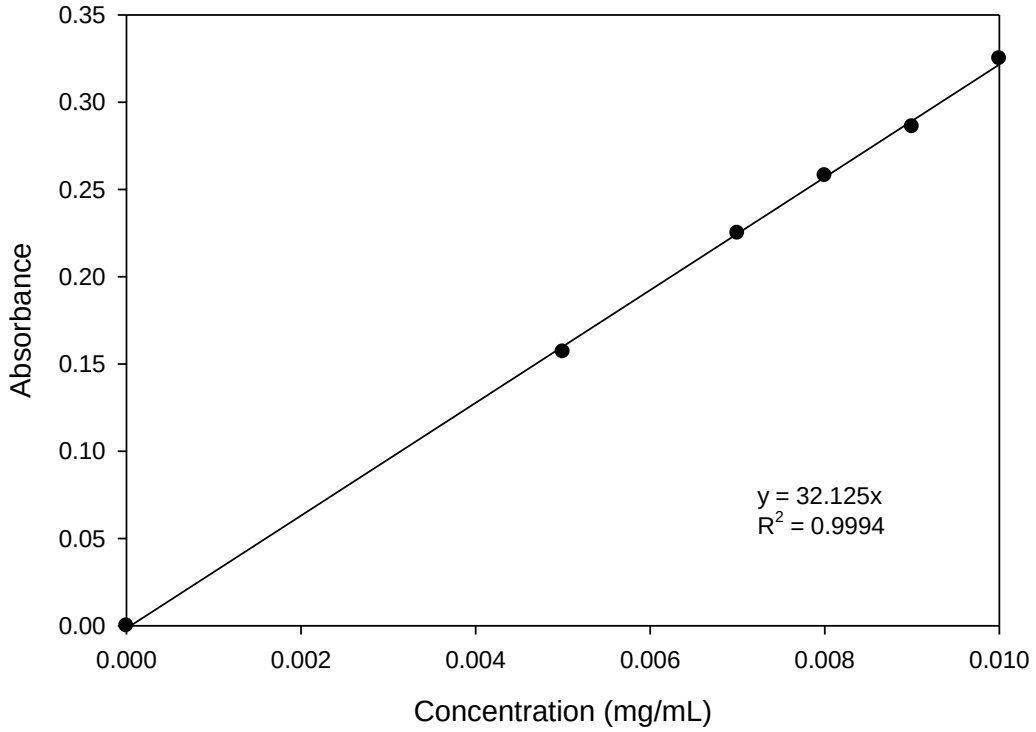


Figure 3.6: Calibration curve for AZT dissolved in simulated saliva (pH 6.75) at λ_{267nm} (in all cases SDs < 0.02, N = 3)

3.3.7.2. AZT in PBS (pH 7.4)

The calibration curve for AZT dissolved in PBS (pH 7.4) at λ_{267nm} is displayed in Figure 3.7.

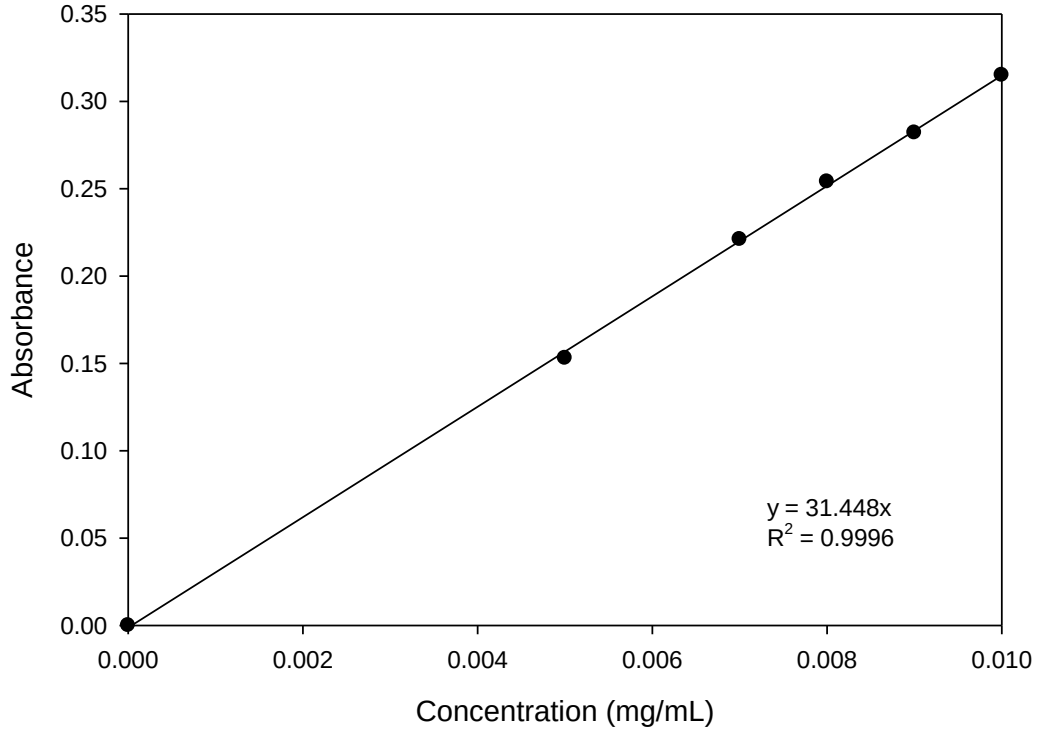


Figure 3.7: Calibration curve for AZT dissolved in PBS (pH 7.4) at λ_{267nm} (in all cases SDs < 0.02, N = 3)

3.3.7.3. DPH in Simulated Saliva (pH 6.75)

The calibration curve for DPH dissolved in simulated saliva (pH 6.75) at λ_{254nm} is depicted in Figure 3.8.

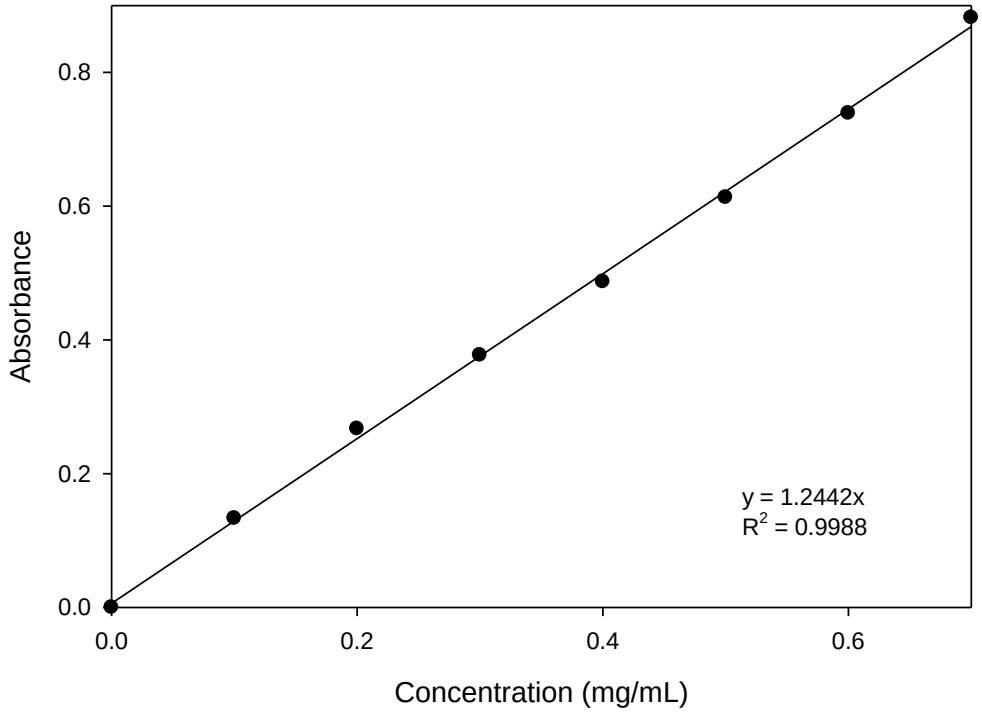


Figure 3.8: Calibration curve for DPH dissolved in simulated saliva (pH 6.75) at λ_{254nm} (in all cases SDs < 0.02, N = 3)

3.3.7.4. DPH in PBS (pH 7.4)

The calibration curve for DPH dissolved in PBS (pH 7.4) at λ_{254nm} is depicted in Figure 3.9.

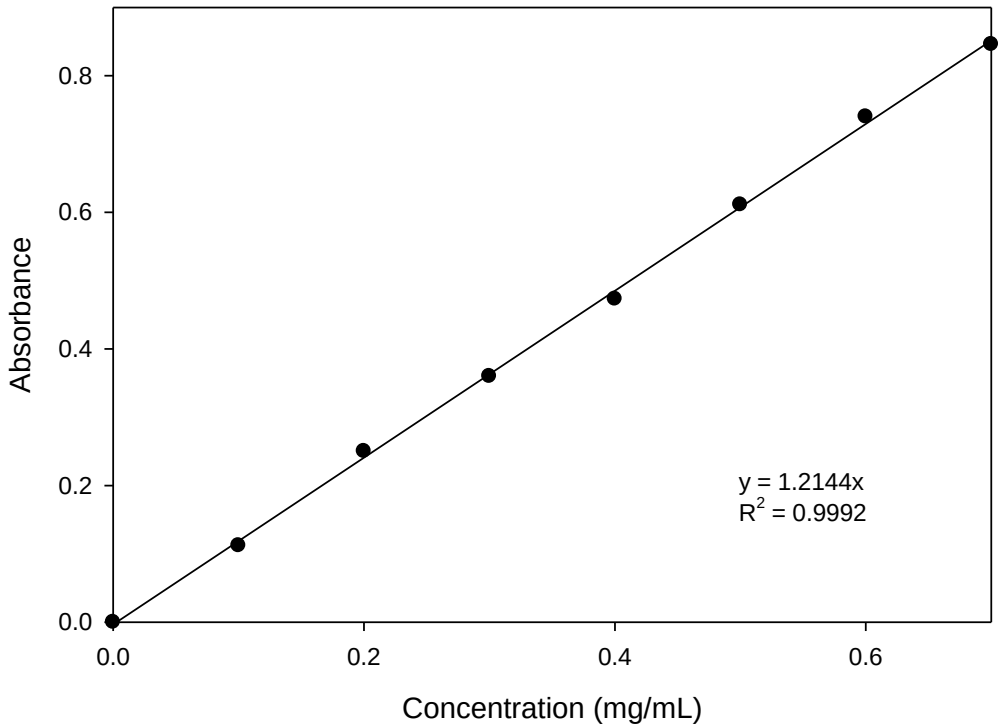


Figure 3.9: Calibration curve for DPH dissolved in PBS (pH 7.4) at λ_{254nm} (in all cases SDs < 0.02, N = 3)

3.3.8. Drug Entrapment

On analysis of the drug entrapment of the electrospun fiber layer, it was found that the average quantity of drug per 1.5cm^2 section varied according to PVA and drug concentrations in the electrospinning solutions and time of electrospinning. When these factors were increased, drug entrapment tended to increase linearly. The average quantity of drug entrapped per section ranged between 0.3-7mg. Drug entrapment and fiber production was observed to be greater at low humidity. Tripatanasuwan and co-workers (2007) found that as the relative humidity was increased, fiber diameter decreased and bead-formation started occurring because solvent evaporation was retarded at higher humidity. It has also been found that small pores form on the surfaces of electrospun fibers at high humidity (Casper et al., 2004), which may also affect the overall fiber morphology and quality. Furthermore, when humidity is high, the charge on the fiber jet may be lost to the moisture in the air (Nieh and Nguyen, 1988; Kalayci et al., 2005; Ramakrishna et al., 2005), resulting in a decrease in fiber production. The technique of electrospinning is therefore sensitive to environmental conditions and, hence, must be conducted in a controlled environment.

3.3.9. Disintegration Time of the PVA Fiber Layer and Backing Film Layer

The average disintegration time of the electrospun PVA fiber layer was 5 seconds, which is desirable for a rapidly disintegrating drug delivery system. The average disintegration time for the backing film layer ranged between 7-60 seconds, depending on constituents, for formulations in the range used as variables for optimization. In order to keep the drug at the surface of absorption and prevent swallowing of the drug, the backing film layer should remain intact for a longer period of time than the fiber layer. However, if the film remains intact for too long, it may result in poor mouth feel and affect patient acceptability.

3.3.10. Drug Permeation by *ex vivo* Studies

The total fraction of permeated drug after 90 minutes for the various formulations that were prepared is outlined in Table 3.1. It is evident in Table 3.1 that the total buccal permeation of AZT was notably low after 90 minutes. Less than 1% of the loaded dose had passed through the buccal mucosal tissue during the testing period, as opposed to 42-82% of DPH. Figure 3.10 depicts the flux profiles of both AZT and DPH, clearly displaying a greater flux for DPH during the period of testing. The poor permeability of AZT, in comparison with DPH, may be a result of the fact that it is sparingly soluble in water (WHO, 2008) and, hence, is not fully dissolved in the relatively small volume of saliva when it comes into contact with the absorptive buccal surface. The addition of permeation enhancers, β-cyclodextrin and chitosan, to the formulations at varying concentrations had little or no effect on the permeation of AZT. In a further endeavor to improve permeation, various oils, such as peppermint oil, spearmint oil, cod liver oil, lemon oil, aniseed oil and oleic acid, were employed in an attempt to solubilize AZT prior to electrospinning. However, the presence of these oils in the electrospinning solutions hindered fiber formation considerably.

Table 3.1: Total percentage of drug permeated after 90 minutes

Film Composition	Drug	Permeation Enhancer	Total Percentage Permeated
PVA + HPMC	Zidovudine	None	0.72
PVA	Zidovudine	None	0.73
PVA	Zidovudine	β-cyclodextrin (1%)	0.74
PVA	Zidovudine	β-cyclodextrin (25%)	0.43
PVA	Zidovudine	Chitosan (1%)	0.59
PVA	Zidovudine	Chitosan (3%)	0.60
PVA + HPMC	Diphenhydramine	None	42
PVA	Diphenhydramine	None	82

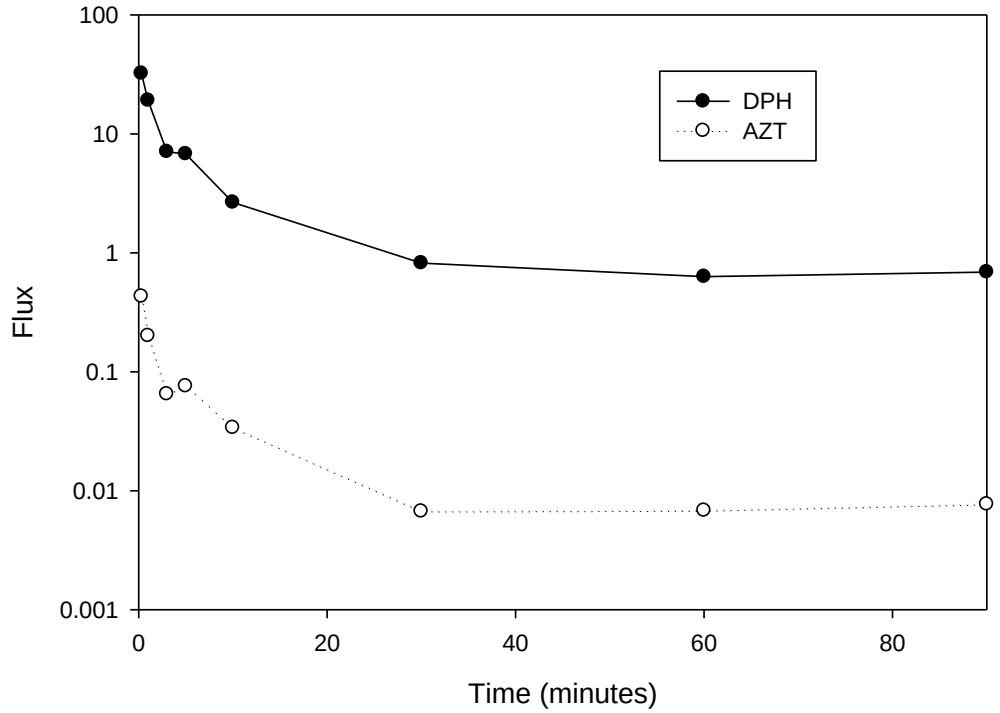


Figure 3.10: Flux profiles of diphenhydramine (DPH) and zidovudine (AZT) (in all cases SDs < 0.02, N = 3)

3.4. Concluding Remarks

A preliminary polymeric backing film layer, containing PVA, HPMC and glycerol, was developed and variables for an experimental design were obtained. A PVA concentration of 1%$^{w}/_{v}$, fill volume of 40-100mL, HPMC concentration of 0-0.5%$^{w}/_{v}$ and glycerol concentration of 10-15%$^{w}/_{w}$ (of total polymer mass) were deemed acceptable for film production and these variables were employed in an experimental design. Various polymers were investigated in order to develop a drug-loaded electrospun fiber layer for application in the FMS. PVA was identified as the most suitable polymer and further studies were therefore undertaken on formulation design using this polymer. On execution of permeation studies, it was discovered that less than 1% of the loaded dose of model drug, AZT, permeated during the testing period. DPH was therefore adopted as the model drug for the purposes of further studies as it exhibited 42-82% permeation during the testing period. The ideal PVA concentration for the electrospinning solution was determined to be 25%$^{w}/_{v}$, the DPH concentration was 10%$^{w}/_{v}$ and the excipients were citric acid and glycerol at 2%$^{w}/_{v}$ and 5%$^{v}/_{v}$, respectively. This ideal formulation was employed in the optimization and further investigations in the design of the FMS.

CHAPTER 4

PREPARATION, CHARACTERIZATION AND OPTIMIZATION OF AN ELECTROSPUN FIBROUS MATRIX SYSTEM FOR RAPID ORAMUCOSAL DRUG DELIVERY

4.1. Introduction

Electrospinning has gleaned considerable interest in the field of drug delivery due to its proficiency in producing fibers with eminently small diameters (Sill and von Recum, 2008). The process of electrospinning involves applying an electrical potential to a polymer solution in order to produce very fine fibers in the nano- and micrometer size range (Liang et al., 2007). When a drop of polymer solution at the end of a capillary tube is subjected to an electrical potential, the drop elongates, becoming conical in shape (Doshi and Reneker, 1995; Sill and von Recum, 2008) and, once the electrical field exceeds surface tension, a fiber jet is ejected from the tip of the cone (Liang et al., 2007; Sill and von Recum, 2008). As the fiber jet travels through the atmosphere, the solvent evaporates and solid polymer fibers are deposited on a grounded collector (Sill and von Recum, 2008), closing the gap between the capillary and collector, and hence completing the circuit (Deitzel et al., 2001). If the polymer concentration, and hence viscosity and chain entanglements, is too low, the jet will break up into droplets before reaching the collector (McKee et al., 2004; Shenoy et al., 2005). However, as the concentration is increased, the viscosity will increase and chain entanglements will become sufficient for fiber formation, resulting in a whipping motion of the jet and stretching and thinning of the fiber on application of a potential (McKee et al., 2004; Shenoy et al., 2005).

Electrospun fibers display a small diameter and extremely high surface area to mass ratio (Frenot and Chronakis, 2003; Reneker and Yarin, 2008). This is advantageous in drug delivery as it results in an increase in the total drug release from drug-loaded fibers when compared to cast-films of the same composition, which have a considerably smaller surface area (Zong et al., 2002; Agarwal et al., 2008). Furthermore, a large exposed surface area can greatly improve the dissolution rate, and hence bioavailability, of a drug (Bruner and Tolloczko, 1901; Sjökvist and Nyström, 1991; Verreck et al., 2003b; Dokoumetzidis and Macheras, 2006).

In order for adequate drug absorption to occur via the buccal mucosa, it is necessary for the drug concentration within the oral cavity to be high (Ponchel, 1994). Accelerated disintegration of an orally dissolving drug delivery system results in a high concentration of drug at the surface of absorption and therefore rapid and extensive absorption (Ponchel, 1994; Rossi et al., 2005). Furthermore, rapid absorption leads to expeditious blood levels (Rathbone et al., 1994) and hence a prompt onset of action (Abrams, 1983; Simpson et al., 2007; Scholz et al., 2008). It has been demonstrated that the *in vivo* availability of a drug administered via the oramucosal route is greatly dependent on the disintegration rate of the drug delivery system (Ponchel, 1994).

Due to the relatively short residence time of an oramucosally administered drug delivery system at the site of absorption, mucoadhesion is often required (Ponchel, 1994). Mucoadhesive drug delivery systems are advantageous in that the entire system is rendered immobile, an intimate contact between the system and buccal mucosa is created (Andrews et al., 2009) and a high drug concentration at the absorption surface is achieved (Ponchel, 1994). This results in a reduction in the required drug concentration as well as an improved bioavailability (Andrews et al., 2009). Thin, mucoadhesive films are favorable for oramucosal drug delivery due to the flexible nature and high contact surface area of such films (Ponchel, 1994; Perioli et al., 2004).

Statistical optimization, by experimental design, employs mathematical and statistical analysis in order to characterize and assess the effects of independent variables on measured responses. In contrast to traditional approaches to formulation optimization, where one variable is assessed at a time, statistical optimization utilizes fewer experimental runs, is less time consuming and provides a true optimized formulation by a systematic approach (Singh et al., 2004).

Therefore the aim of the studies outlined in this chapter was to statistically optimize the polymeric backing film layer of the porous, fibrous matrix system (FMS), for oramucosal drug delivery, developed in Chapter 3. In order to do this, drug-loaded fibers were electrospun directly onto polymeric backing films, produced according to a Box-Behnken experimental design. Polyvinylalcohol (PVA) fibers were produced, according to a formula determined by preliminary experimentation, and loaded with model drug, diphenhydramine, in order to assess drug release and permeation characteristics. The effect of varying polymeric constituents on drug release, drug permeation, mucoadhesion and disintegration was investigated in order to produce an optimized drug delivery system.

4.2. Materials and Methods

4.2.1. Materials

Polyvinylalcohol (PVA) (87-89% hydrolyzed, M_w 13,000-23,000g/mol) and diphenhydramine (DPH) were purchased from Sigma-Aldrich (St. Louis, Missouri, USA). Propan-2-ol, glycerol and citric acid were purchased from Rochelle Chemicals (Johannesburg, South Africa). Hydroxypropylmethylcellulose (HPMC) was purchased from Colorcon Limited (London, England).

4.2.2. Preparation of polymeric backing films by film-casting

Films intended as backing and mucoadhesive layers for electrospun fibers were prepared according to a Box-Behnken experimental design. Polymer solutions were prepared by dissolving glycerol, PVA and HPMC in a 4:1 mixture of deionized water and propan-2-ol. The concentrations and volumes used were as outlined in Table 4.1. Solutions were syringed into rectangular flat-bottomed moulds and left under an extractor at 21°C for 48 hours in order that complete solvent evaporation and film-formation could occur.

Table 4.1: Polymer concentrations and volumes used in film preparation according to the Box-Behnken design

Formulation number	Fill Volume (mL)	HPMC (%$^{w}/_{v}$)	Glycerol (%$^{w}/_{w}$ of PVA + HPMC)
F1	40	0.50	12.5
F2	100	0.25	15.0
F3	40	0.25	15.0
F4	70	0.25	12.5
F5	70	0.50	10.0
F6	100	0.50	12.5
F7	40	0.25	10.0
F8	70	0.25	12.5
F9	70	0.00	10.0
F10	100	0.00	12.5
F11	70	0.00	15.0
F12	70	0.25	12.5
F13	70	0.50	15.0
F14	40	0.00	12.5
F15	100	0.25	10.0

4.2.3. Experimental Design

A 3-factor Box-Behnken experimental design was generated by Minitab®, V15 (Minitab® Inc, Pennsylvania, USA) in order to statistically optimize the polymeric film layer and analyze the effect of formulation variables on system disintegration, drug release from the electrospun fiber layer, by dissolution and permeation, and mucoadhesiveness. The Box-Behnken design is a rotatable, or nearly rotatable, response surface design, which, for three factors, can be visualized by a cube with points in the center and the middle of each edge (Ferreira et al., 2007), as depicted in Figure 4.1. All points on the edges are therefore equidistant from the central point (Box and Behnken, 1960). This type of design was expressly selected for the purposes of this study as it is favored over the Central Composite Design due to the fact that it is considered to be more efficient (Ferreira et al., 2007) and it requires fewer experimental runs (Chopra et al., 2007), which makes the formulation process less expensive. The independent variables, X_1, X_2 and X_3, were selected based on preliminary studies in Chapter 3, and are outlined in Table 4.2. Y_1 through to Y_5, the dependent variables, were disintegration time, work of adhesion (WA), maximum detachment force (MDF), dissolution area under the curve (AUC) at 1 minute (AUC_D) and permeation AUC at 3 minutes (AUC_P), respectively.

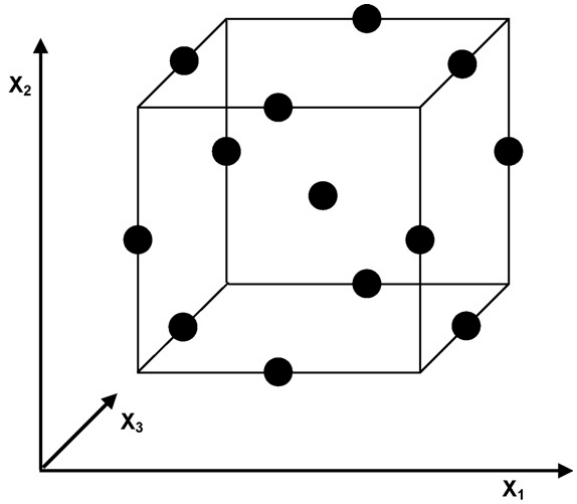


Figure 4.1: Visualization of a Box-Behnken cube with points on the middle of each edge and in the center. X_1, X_2 and X_3 represent the independent variables in the design (Adapted from Ferreira et al., 2007)

Table 4.2: Variables employed in the Box-Behnken design

Variable	**Levels**	
	Low (-1)	**High (1)**
X_1 – Fill Volume (mL)	40	100
X_2 – HPMC concentration ($\%^{w}/_{v}$)	0.00	0.50
X_3 – Glycerol concentration ($\%^{w}/_{w}$ of PVA + HPMC)	10.0	15.0

4.2.4. Preparation of fibers by electrospinning

A drug-loaded solution for electrospinning was produced by dissolving PVA, citric acid, DPH and glycerol in a 2:1 mixture of deionized water and propan-2-ol at concentrations of $25\%^{w}/_{v}$, $2\%^{w}/_{v}$, $10\%^{w}/_{v}$ and $0.5\%^{v}/_{v}$, respectively. These quantities were based on optimal fiber production, reproducibility and drug-loading proficiencies, determined in Chapter 3. The solution was placed in a 5mL pipette, which was fitted into the adjustable supporting bracket of an electrospinning device. Electrospinning of the solutions was performed at 20kV with a tip-to-collector distance of 11cm, using a custom-built electrospinning device (RGC Engineering, Johannesburg, South Africa) equipped with a voltmeter and MJ Series High Voltage Power Supply (Glassman High Voltage Inc., New Jersey, USA). Fibers were collected on polymeric backing films secured on aluminum foil-lined board. Samples were cut into sections.

4.2.5. Morphological and Surface Structure Analysis of the Drug-loaded Fiber Layer

The surface structure of the electrospun fibers was analyzed by images produced by scanning electron microscopy (SEM), using a Phenom Microscope (FEI Company, Hillsboro, Oregon, USA). Samples were mounted on stubs and sputter-coated with gold prior to examination.

4.2.6. Drug Entrapment of Experimental Design Formulations

Individual drug-loaded FMS samples were cut into 1.5cm^2 sections, dissolved in simulated saliva (pH 6.75) and the drug content of each section was analyzed by UV spectrophotometry.

4.2.7. Disintegration Time of Experimental Design Formulations

The *in vitro* disintegration time of individual FMS samples was determined according to a modified method based on the United States Pharmacopoeia (USP) method for tablet disintegration testing using a Type PTZ 1 basket-rack assembly disintegration apparatus (Pharma Test, Hainburg, Germany). According to the USP 32, disintegration is considered to have occurred when there is no longer any solid residue left on the mesh of the basket-rack assembly apparatus (USP 32, 2009). The disintegration medium was 150mL simulated saliva (pH 6.75) in a glass jar placed in a water bath maintained at 37˚C. FMS samples were cut into 1.5cm^2 sections and placed on the mesh of the basket rack assembly, with a mesh disc placed on top. The basket rack assembly was raised and lowered through a distance of 55mm and at a frequency of 25 cycles per minute and the time taken for sample disintegration to occur was determined by observation and recorded.

4.2.8. *In vitro* Drug Release

Standard USP tests and apparatuses for *in vitro* dissolution and drug release testing require large volumes of fluid, which do not accurately reflect the *in vivo* conditions within the oral cavity, where there is only a small volume of fluid available for the dissolution of a drug delivery system (Azarmi et al., 2007). A modified drug release testing method was therefore developed for the purposes of this study. *In vitro* drug release was tested using a 10mm-long magnet in a 35mm diameter petri-dish, placed on a temperature-controlled magnetic stirrer. Simulated saliva (pH 6.75) (2mL) was placed in the petri-dish, maintained at 37˚C and stirred at a constant rate to ensure circulation of buffer. FMS samples were cut into sections and placed in the buffer. 1mL

samples were drawn at 5, 15, 30 seconds, 1, 3, 5, 10 and 15 minutes, analyzed by UV spectrophotometry and replaced by fresh buffer.

4.2.9. *Ex vivo* Drug Permeation Studies

Ex vivo drug permeation testing and tissue preparation were performed as outlined in Chapter 3. Samples were drawn from the acceptor compartment at 20 seconds, 1, 2, 3, 5, 10, 15 and 30 minutes and analyzed by UV spectrophotometry, and the removed volume replaced with fresh PBS. The apparent permeability coefficient (P_{app}) and steady-state flux (J_{ss}) values were calculated using Equations 4.1 and 4.2, respectively.

$$P_{app} = \frac{Q}{A \times c \times t} \qquad \text{(Equation 4.1)}$$

$$J_{ss} = \frac{\Delta M}{A \times \Delta t} \qquad \text{(Equation 4.2)}$$

Where Q is the total amount of drug permeated during the testing time (µg), A is the diffusional area (cm^2), c is the initial drug concentration in the donor compartment (µg/mL), t is the total time that the experiment was run for (seconds) and ΔM is the amount of drug that had permeated through the mucosal tissue during time Δt.

4.2.10. Mucoadhesion of Experimental Design Formulations

Mucoadhesion testing was performed on FMS sections using a *TA.XTplus* Texture Analyser (Stable Micro Systems, England) fitted with a cylindrical probe. Porcine buccal mucosal tissue was attached to the probe, using rubber bands, and exposed to simulated saliva (pH 6.75). The FMS samples were attached to the stage directly below the probe. Mucoadhesion was tested by measuring the maximum detachment force (MDF) and the work of adhesion (WA) (AUC_{FD}) between the buccal mucosa and the fibrous membranes. The pre-test, test and post-test speeds were 2, 2, and 10mm/s, respectively. An applied force of 50g, a trigger force of 5g and contact time of 5 seconds were used for the test.

4.3. Results and Discussion

The films produced were even, thin, transparent or cloudy and pliable. The fibers formed a white layer on the films.

4.3.1. Morphological and Surface Structure Analysis of the Drug-loaded Fiber Layer

On SEM analysis, it was observed that the fibers produced were randomly arranged and had uniform diameters on average. The fiber diameter was approximately 0.36µm, as depicted in Figure 4.2.

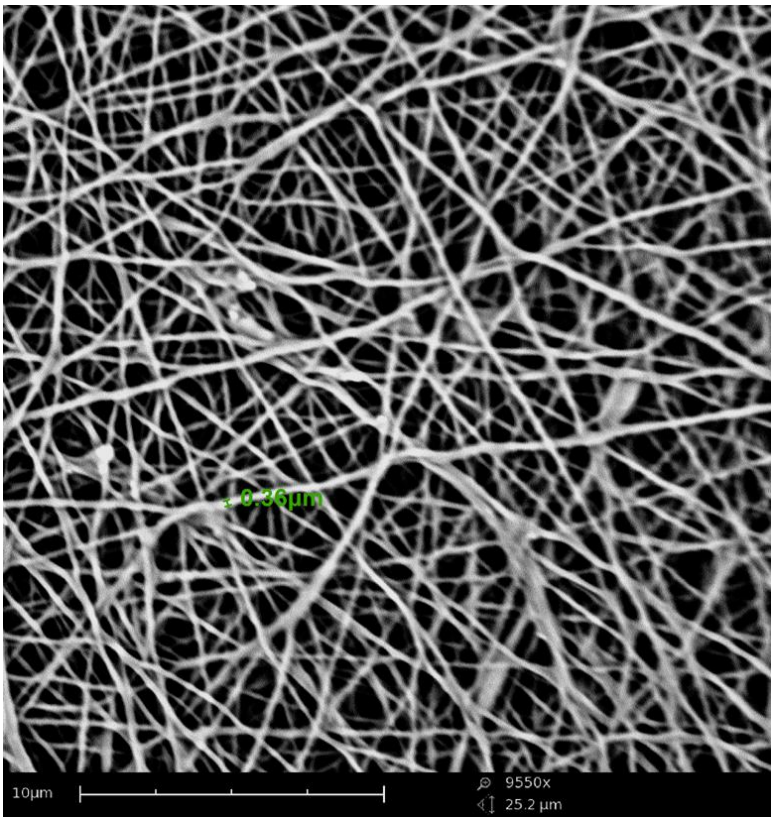


Figure 4.2: SEM image of electrospun PVA fibers loaded with DPH

4.3.1. Drug Entrapment of Experimental Design Formulations

The average drug entrapment and standard deviations for sections of each formulation was as outlined in Table 4.3. Samples were analyzed in triplicate. Inter-sample and inter-formulation variation was high due to uneven deposition of drug-loaded fibers during the electrospinning process.

Table 4.3: Drug entrapment per 1.5cm^2 section of electrospun fibrous membrane system (FMS)

Formulation	Drug Entrapment (mg) ± SD
F1	3.2 ± 2.4
F2	1.5 ± 0.19
F3	1.9 ± 0.56
F4	2.0 ± 0.21
F5	2.3 ± 0.73
F6	2.1 ± 1.2
F7	2.0 ± 0.98
F8	1.8 ± 0.23
F9	3.4 ± 1.6
F10	3.7 ± 2.2
F11	4.3 ± 1.1
F12	1.9 ± 0.22
F13	4.7 ± 1.9
F14	4.1 ± 1.6
F15	2.6 ± 0.46

4.3.2. Disintegration Time of Experimental Design Formulations

The average disintegration time for each formulation was as depicted in Figure 4.3. Formulations 5 and 6 exhibited the longest disintegration times, whereas formulations 1, 9, 14 and 15 took the shortest time for disintegration. Figure 4.4 is a contour plot displaying the relationship between the disintegration time and HPMC concentration and fill volume. It was observed that the time for disintegration was greater for formulations with a higher HPMC content. This can be attributed to the relatively slow rate of disintegration of HPMC (Rodriguez et al., 2000; Nafee et al., 2003). Formulations with both a high HPMC content and a large fill volume exhibited an exceedingly longer disintegration time. The anomalous results, where formulations with a larger HPMC concentration displayed a similar disintegration time to those with lower concentrations, may be rationalized by the idiosyncrasies involved in the subjective observation of perceived formulation disintegration (Chandrasekhar et al., 2009).

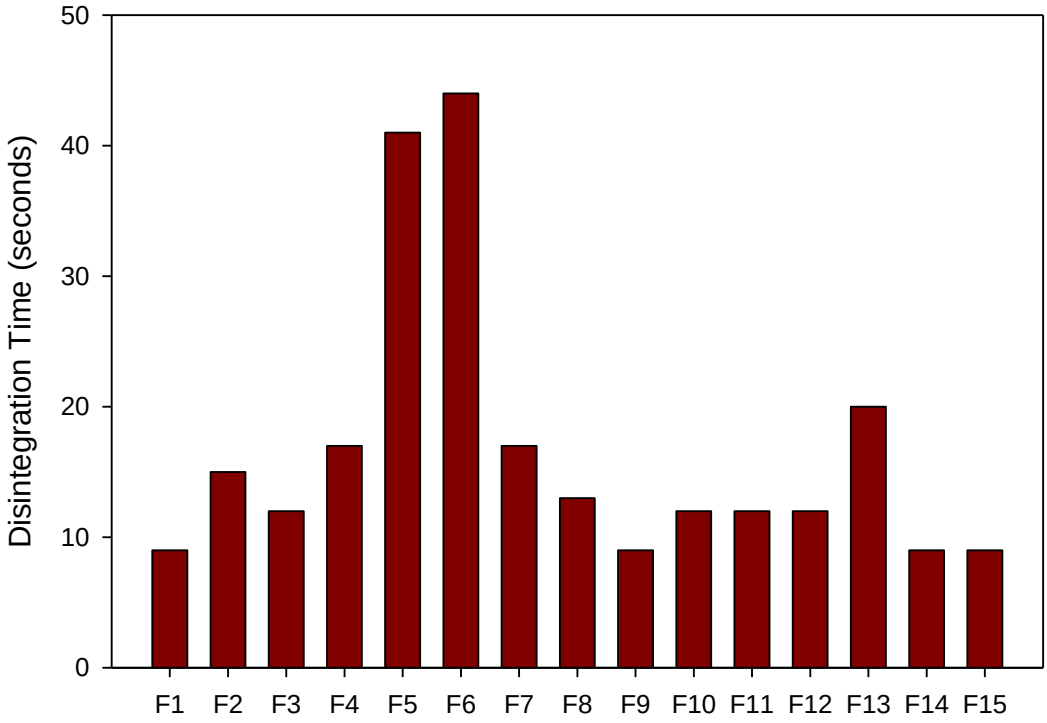


Figure 4.3: Vertical bar chart depicting the average disintegration times of the experimental design formulations (in all cases SDs < 0.02, N = 3)

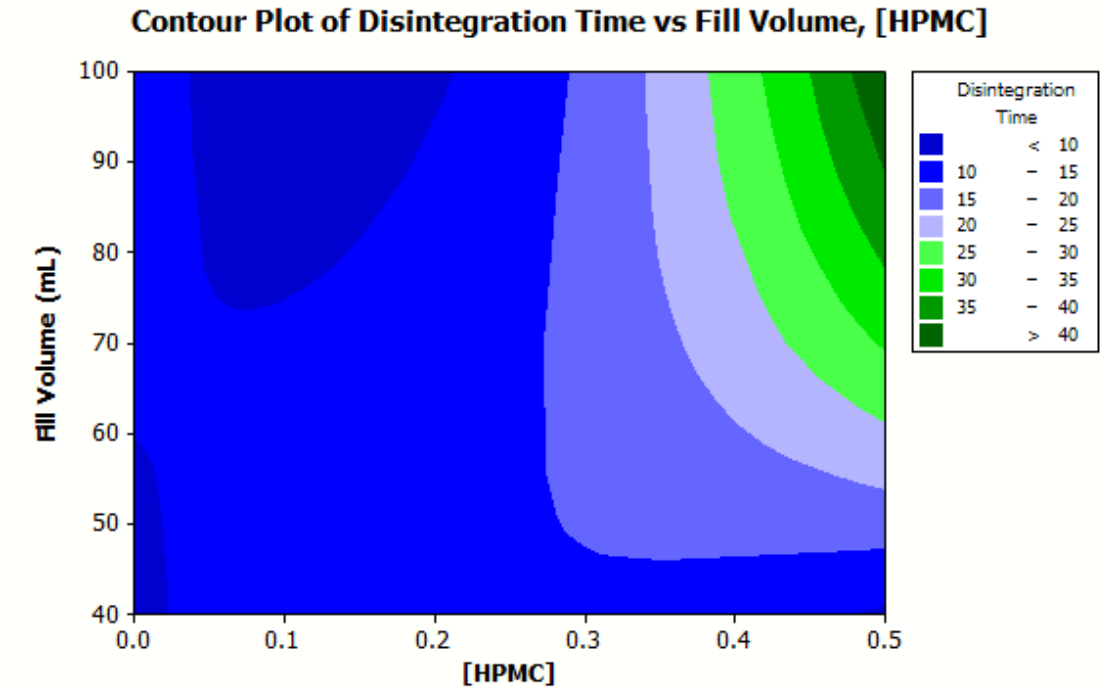
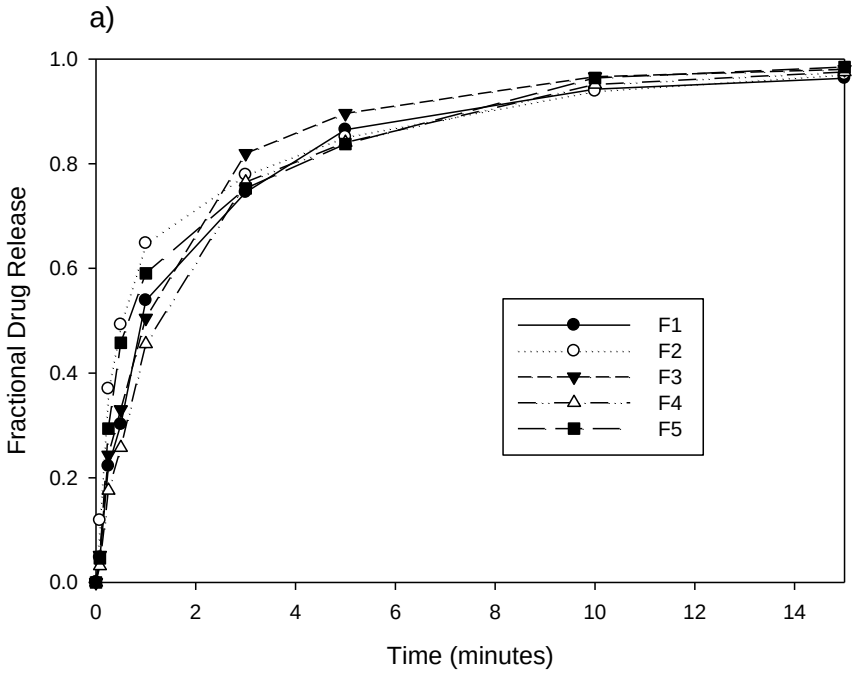


Figure 4.4: Contour plot depicting the relationship between the disintegration time, HPMC concentration and fill volume

4.3.3. *In vitro* Drug Release by Dissolution

The DPH-loaded experimental design FMS samples displayed rapid drug release, with 24-65% of the loaded dose releasing after 1 minute, depending on the formulation. Figure 4.5a, b and c depicts the drug release profiles of formulations 1-5, 6-10 and 11-15, respectively. No significant differences were noted between the drug release profiles of the first five formulations (Figure 4.5a). Formulation 2 exhibited the largest fractional drug release after the first minute and formulation 4 the smallest. Formulations 6-10 (Figure 4.5b) displayed slightly more variance than the first five formulations, with formulation 9 exhibiting the slowest drug release and formulation 7 the most rapid. On analysis of the drug release profiles of the last five formulations (Figure 4.5c), it was noted that formulation 14 exhibited significantly slower drug release than the other five formulations.



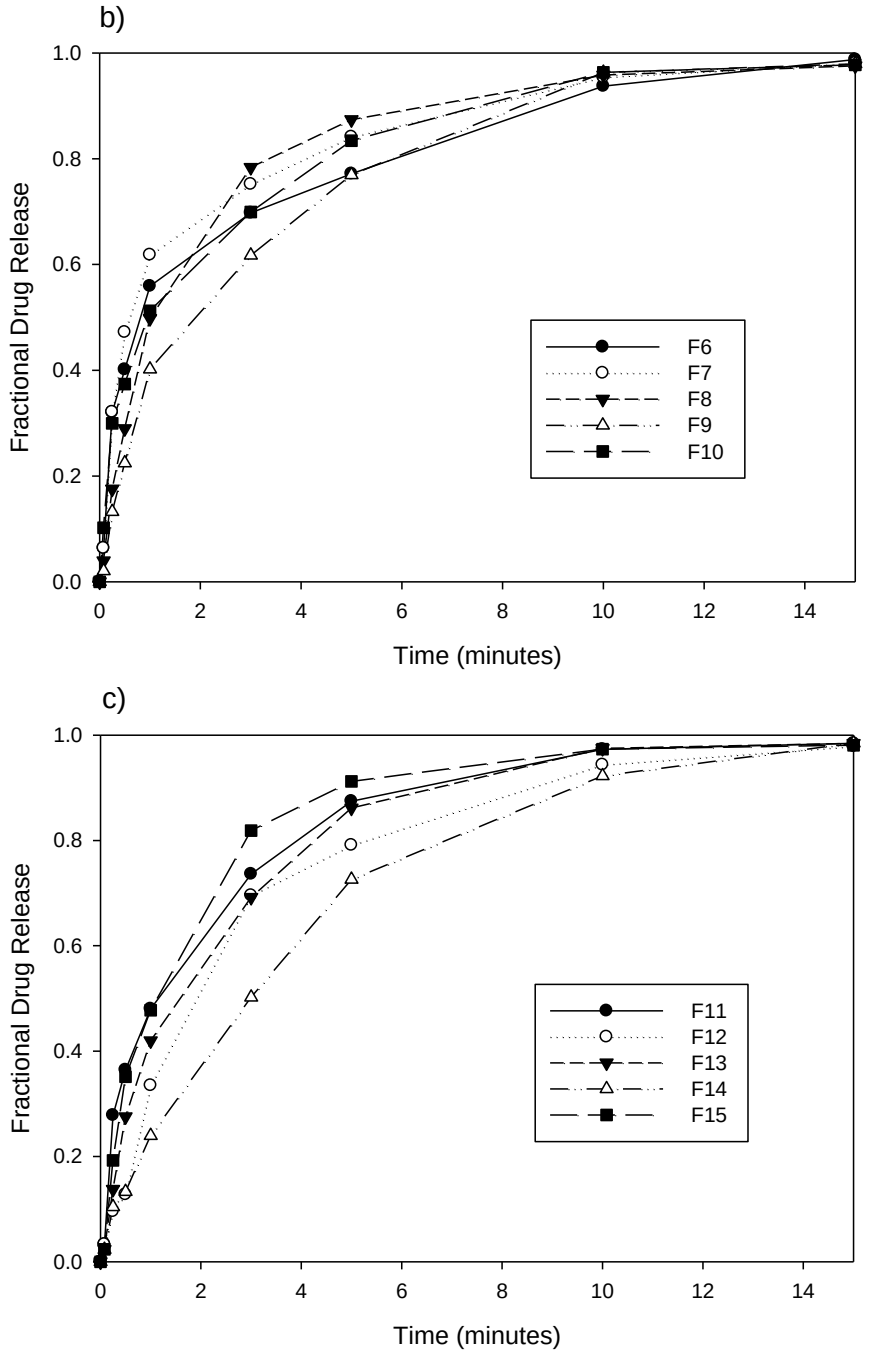


Figure 4.5: Drug release profiles of formulations (a) 1-5, (b) 6-10 and (c) 11-15 (in all cases SDs < 0.02, N = 3)

AUC_D at 1 minute was calculated for all formulations and was plotted as in Figure 4.6. Formulation 2 had the largest AUC_D at 1 minute and, hence, the most rapid drug release, whereas formulation 14 had the smallest AUC_D and, as a deduction, the slowest drug release. This is in agreement with the observations noted on analysis of the drug release profiles. During dissolution testing, it was observed that films consisting of smaller quantities of polymers disintegrated rapidly and often left fragmented clumps of the drug-loaded fiber layer, which tended to dissolve and release drug slower than

fibers on films that remained intact for a longer period of time. Films that took significantly longer to disintegrate hindered dissolution only slightly when compared to films with an intermediate disintegration time. Figure 4.7 displays a contour plot depicting the relationship between HPMC concentration, fill volume and AUC_D at 1 minute. Formulations with both a large fill volume and HPMC concentration displayed a large AUC_D, whereas formulations with a small fill volume revealed an increase in AUC_D with increasing fill volume.

The dissolution testing method that was adopted for the purposes of this study was deemed to be reproducible and indicative of *in vivo* conditions within the oral cavity.

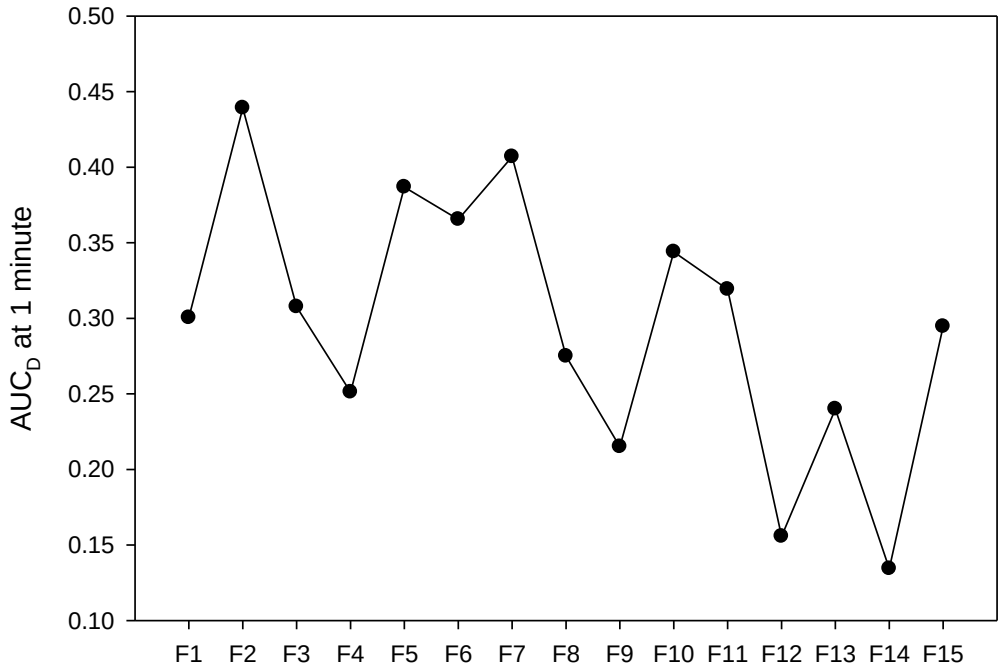


Figure 4.6: Scatter plot depicting AUC of dissolution (AUC_D) at 1 minute for the 15 experimental design formulations

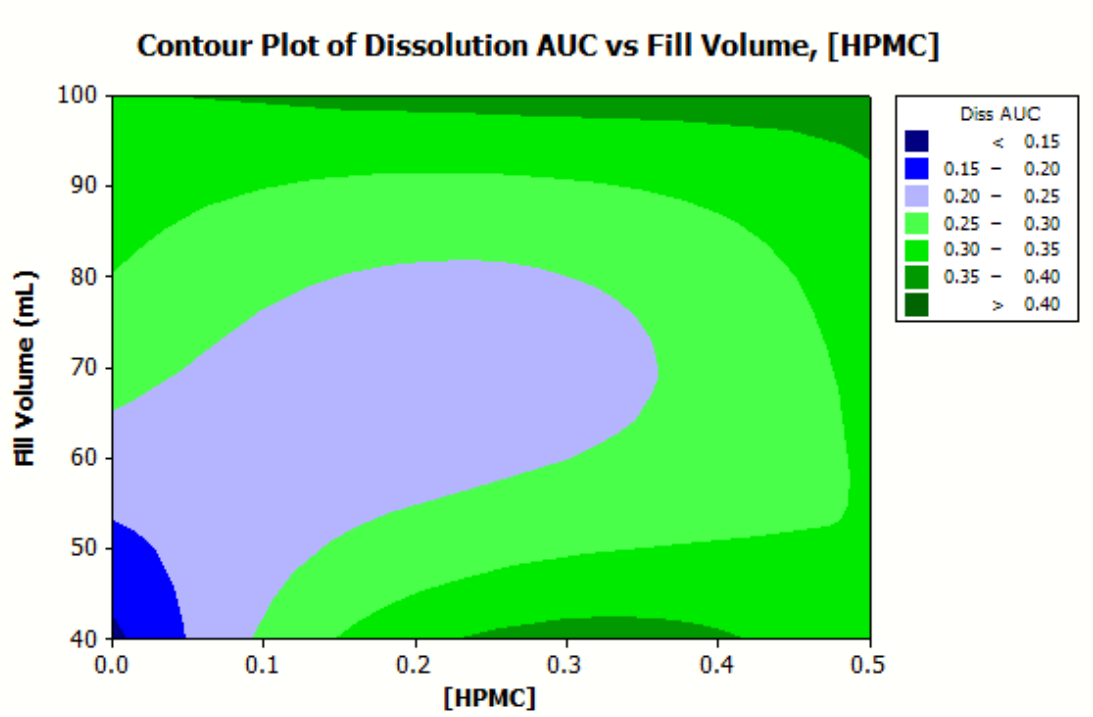


Figure 4.7: Contour plot depicting the relationship between the HPMC concentration in film formulations, fill volume and AUC_D at 1 minute

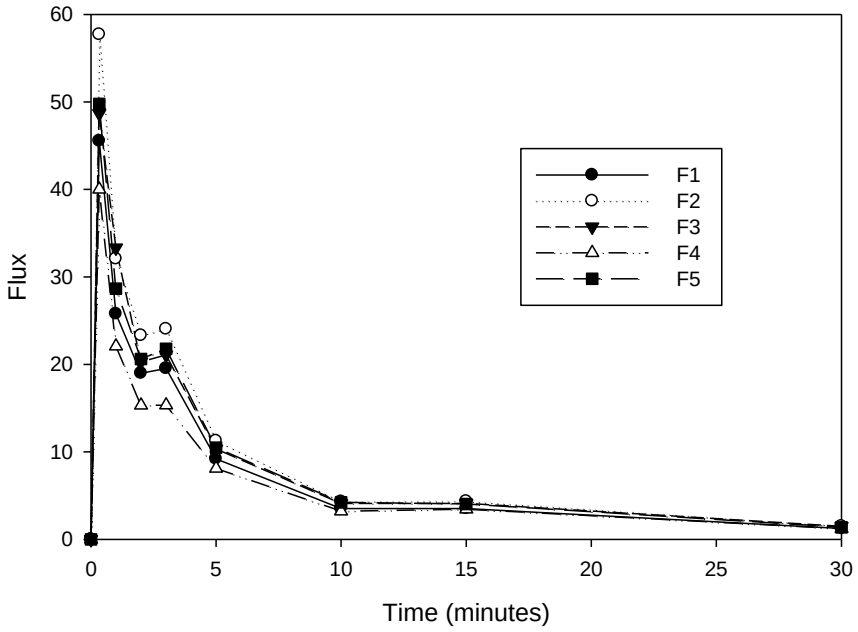
4.3.4. Drug Permeation by *ex vivo* Studies

Ex vivo drug permeation, where conditions are as similar as possible to *in vivo* circumstances (Figueiras et al., 2009), is a valuable study to conduct in order to determine the expediency of employing a particular drug or drug delivery system for buccal administration (Sudhakar et al., 2006).

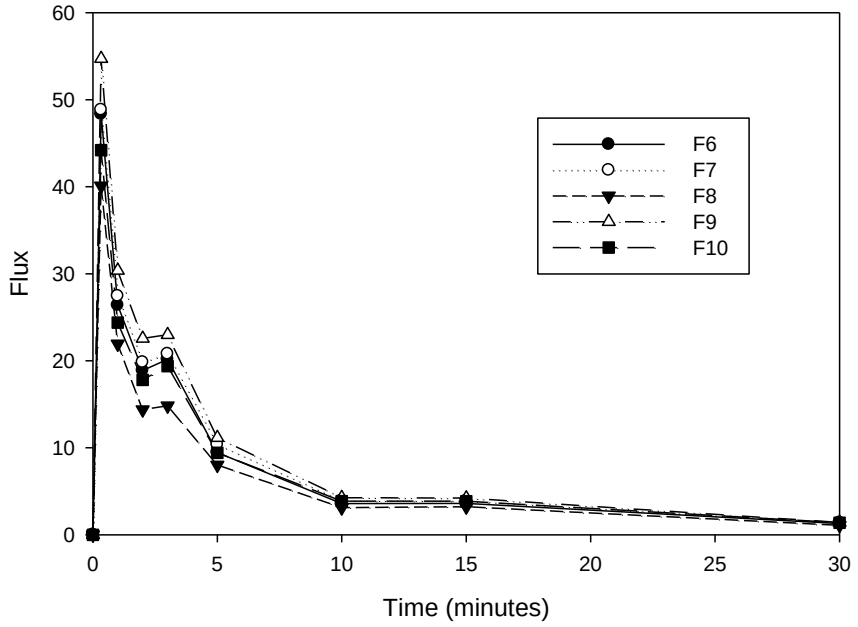
The flux at each time point was calculated and was plotted against time as depicted in Figure 4.8. Formulations 4, 8 and 14 exhibited the lowest flux values in the three groups and formulations 2, 9 and 15 the greatest. Flux was greatest between 20 seconds and 5 minutes, after which it was considerably reduced. AUC_P at 3 minutes was calculated from permeation data for each formulation and the values were plotted, as depicted in Figure 4.9. Formulations 2, 7 and 15 exhibited the greatest AUC_P and, hence, the most rapid rate of permeation, whereas formulation 14 had the lowest AUC_P and the slowest permeation. This is in agreement with the *in vitro* dissolution data, where formulation 2 displayed the most rapid drug release, formulations 7 and 15 also showed relatively rapid dissolution rates, and formulation 14 had the smallest AUC_D at 1 minute. The apparent permeability coefficient (P_{app}) and steady-state flux (J_{ss}) values were calculated for the 15 experimental design formulations and are outlined in Table 4.4. These values are somewhat anomalous, possibly due, in part, to the disparities in drug-loading for the

experimental design formulations, as well as the variations between individual buccal mucosal specimens.

a)



b)



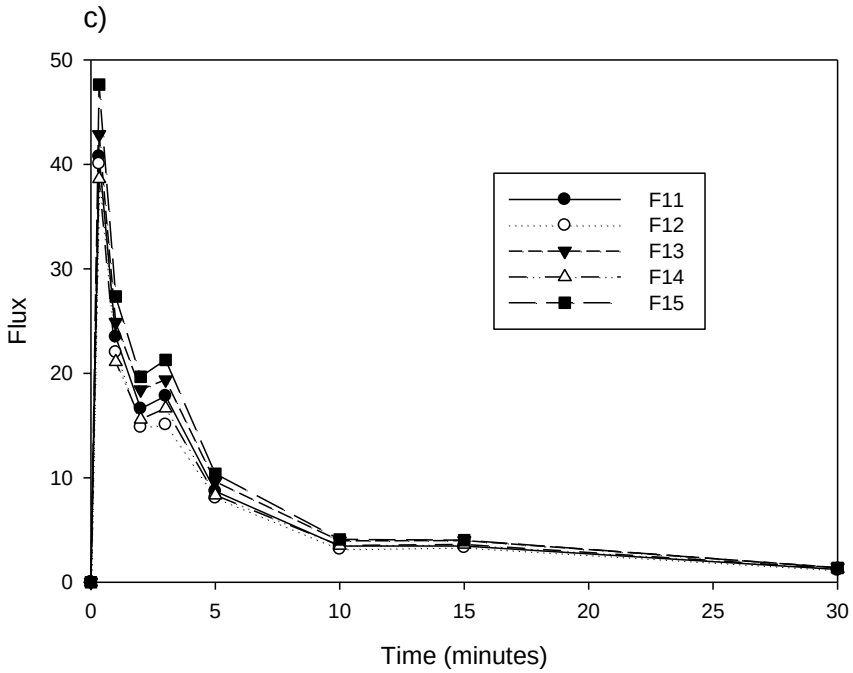


Figure 4.8: Flux profiles displaying the flux over time of formulations (a) 1-5, (b) 6-10 and (c) 11-15

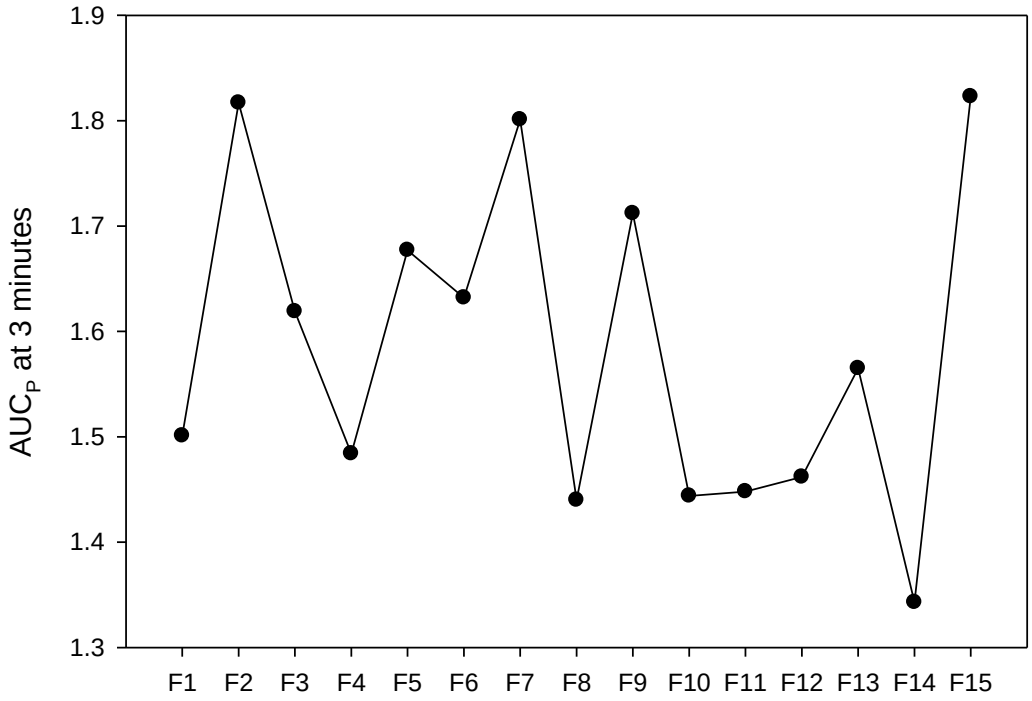


Figure 4.9: Scatter plot depicting AUC of permeation (AUC_P) at 3 minutes for the 15 experimental design formulations

Table 4.4: Calculated apparent permeability coefficient (P_{app}) and steady-state flux values (J_{ss}) for the 15 experimental design formulations.

Formulation	P_{app}	J_{ss}
F1	4.34×10^{-4}	4.17
F2	5.34×10^{-4}	2.40
F3	4.68×10^{-4}	2.67
F4	4.02×10^{-4}	2.41
F5	4.84×10^{-4}	3.34
F6	4.48×10^{-4}	2.82
F7	4.62×10^{-4}	2.77
F8	3.56×10^{-4}	1.92
F9	5.11×10^{-4}	5.21
F10	4.31×10^{-4}	4.78
F11	3.96×10^{-4}	5.11
F12	3.58×10^{-4}	2.04
F13	4.67×10^{-4}	6.58
F14	4.32×10^{-4}	5.32
F15	4.73×10^{-4}	3.69

4.3.5. Mucoadhesion of Experimental Design Formulations

The affixment of a polymer to a mucosal surface, such as the buccal mucosa, is termed mucoadhesion. Mucoadhesiveness is an eminent factor to consider in oramucosal drug delivery because the retention of a drug delivery system at a specific site influences drug absorption at that site (Andrews et al., 2009). The average work of adhesion (WA) and maximum detachment force (MDF) for the 15 experimental design formulations were calculated from textural profiles, an example of which is depicted in Figure 4.10. The calculated values were as depicted in Figures 4.11 and 4.12, respectively. The largest WA and MDF values were exhibited by formulations 9, 14 and 15 and the smallest values by formulations 1, 5 and 6.

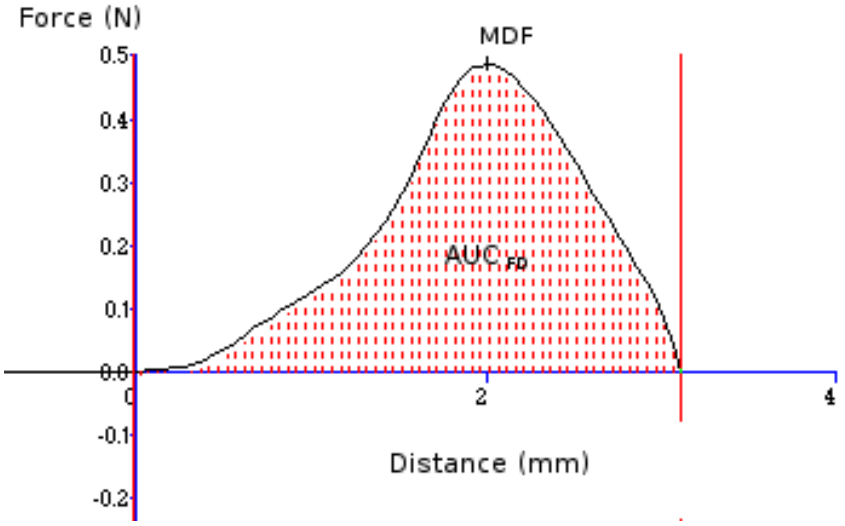


Figure 4.10: Typical textural profile showing the peak force (MDF) (N) and work of adhesion (AUC_{FD}) (mJ) used to determine mucoadhesive properties of the experimental design formulations

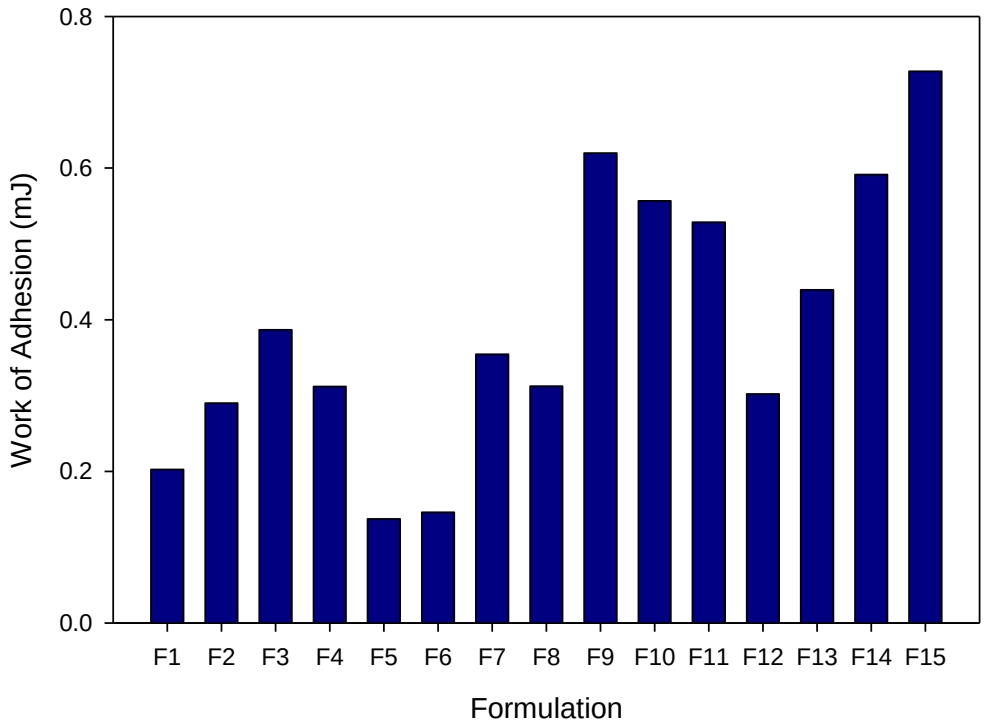


Figure 4.11: Vertical bar chart depicting the average work of adhesion (WA)

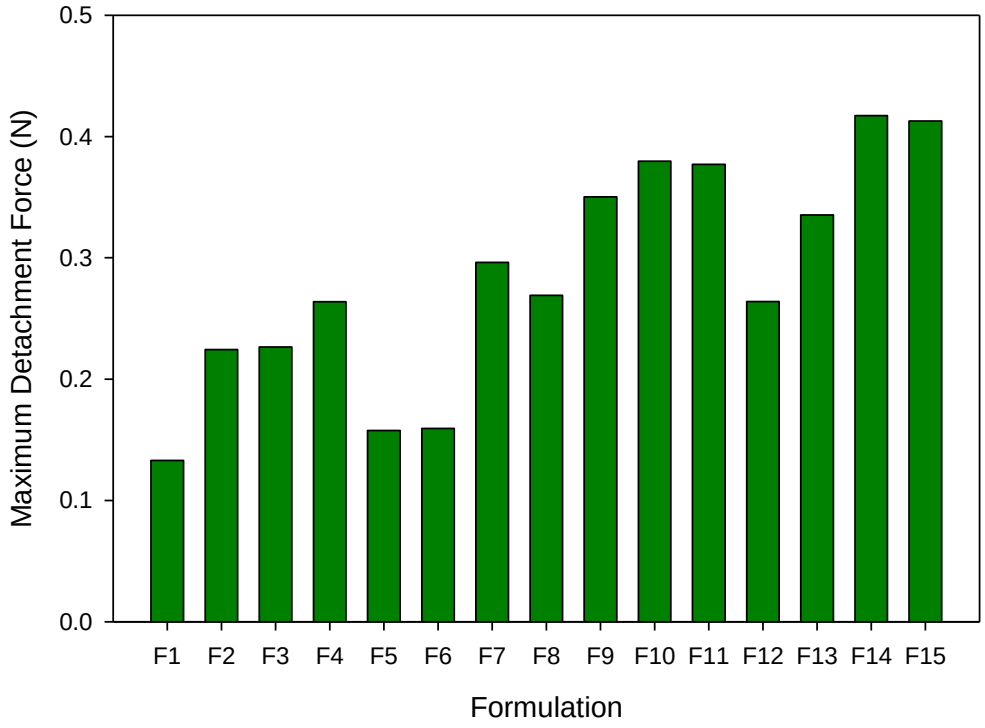


Figure 4.12: Vertical bar chart depicting the average maximum detachment force (MDF)

Figure 4.13 depicts the relationship between WA, HPMC concentration and fill volume. As HPMC concentration in the formulations increased, the average WA decreased. The process of mucoadhesion occurs largely through interpenetration and hydrogen bonding between the polymeric system and the mucosal surface. In order for interpenetration to occur between these two surfaces, the polymer chains are required to be flexible (Andrews et al., 2009). HPMC is able to form weak hydrogen bonds with mucosal surfaces and an adherent gel upon hydration, which both make it a strongly mucoadhesive polymer in theory. Notwithstanding this, it has a high glass transition temperature (>200˚C), which results in poor chain flexibility and therefore poor experimental mucoadhesion (Karavas et al., 2006). This elucidates the observed decrease in WA with an increase in HPMC concentration.

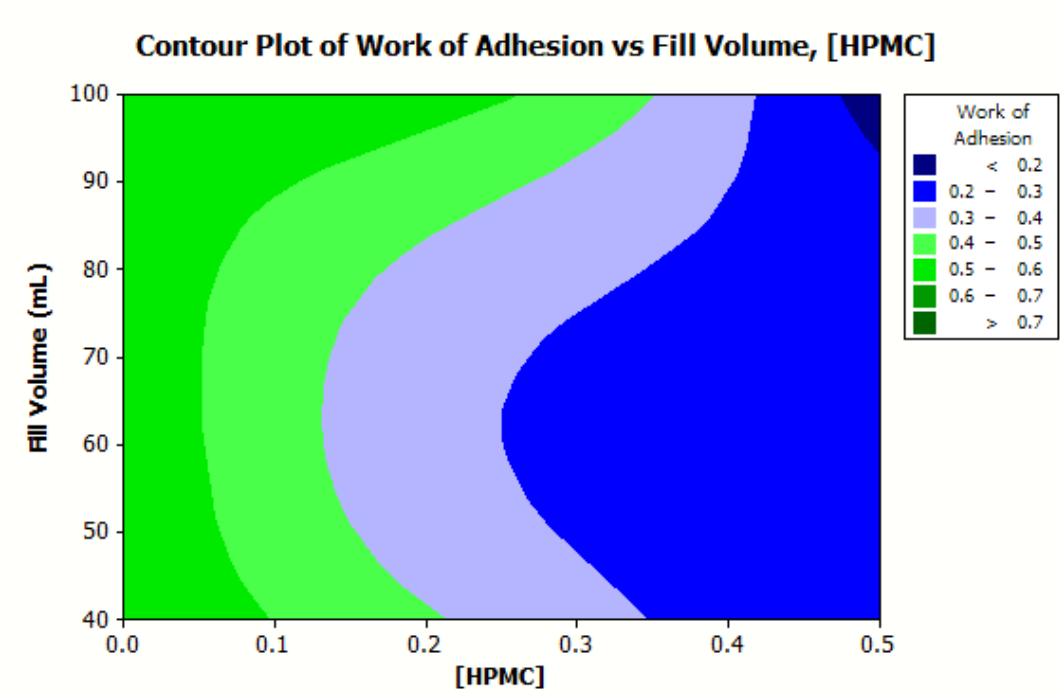


Figure 4.13: Contour plot depicting the relationship between the HPMC concentration in film formulations, fill volume and work of adhesion

Figure 4.14 depicts the relationship between WA, HPMC concentration and glycerol concentration. As can be seen in Figure 4.14, an aberrant trend occurred with varying glycerol concentration. For formulations containing HPMC at 0.25%$^{w}/_{v}$ or less, the average WA decreased with increasing glycerol concentration. However, formulations containing 0.5%$^{w}/_{v}$ HPMC displayed an increase in WA with an increase in glycerol concentration. At HPMC concentration of 0.25%$^{w}/_{v}$ or less (where the fraction of PVA was greater), the disintegration time was relatively short compared to that at 0.5%$^{w}/_{v}$, thus suggesting that PVA has a faster rate of disintegration than HPMC. With a disintegration rate that is already elevated, the addition of increasing concentrations of glycerol to formulations with a large proportion of PVA enhances the rate of disintegration even further (McCarron et al., 2005). When a formulation disintegrates rapidly, there may be less of it available in its original form at the point in time when mucoadhesive strength is measured and hence the decreasing WA with increasing glycerol concentration may be accounted for. At the higher HPMC concentration, the increase in WA with increasing glycerol concentration may be attributed to the pliability of poorly-flexible HPMC chains being enhanced, hence resulting in an increased WA as the glycerol concentration was increased (Llabot et al., 2007).

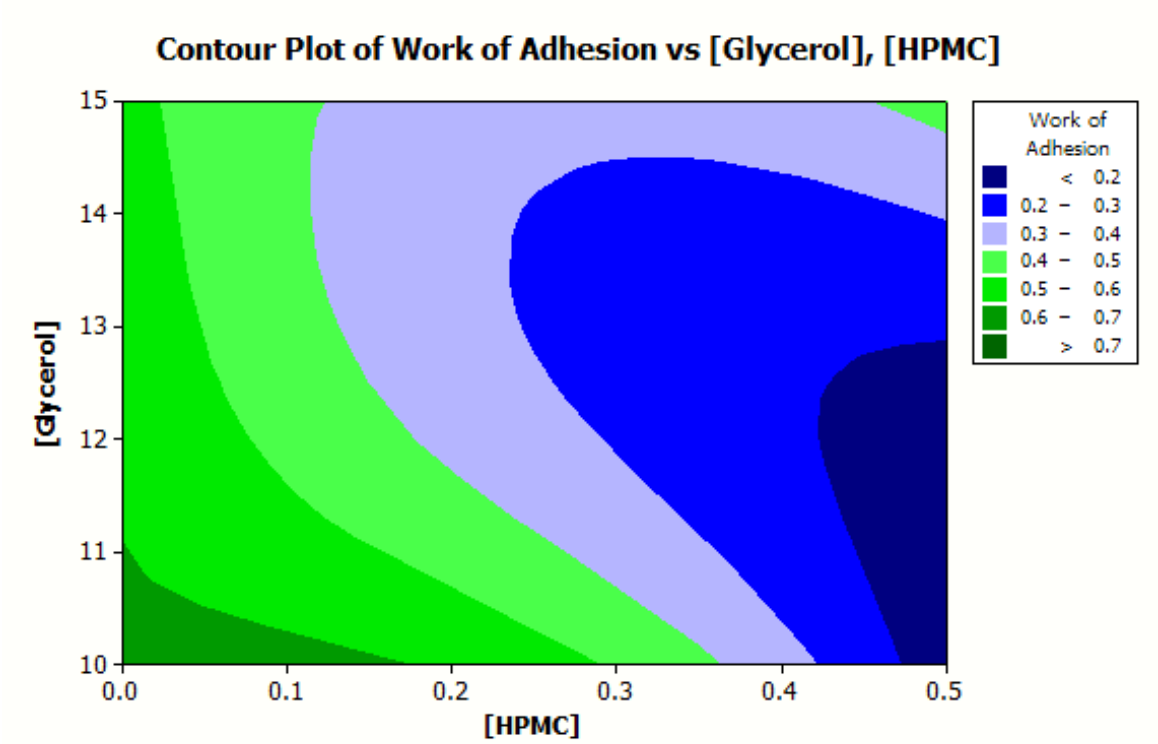


Figure 4.14: Contour plot depicting the relationship between HPMC concentration, glycerol concentration and work of adhesion

4.3.6. Analysis of Main Effects and Interaction Effects on Responses

4.3.6.1. Disintegration Time

The main effects plot for disintegration time (Figure 4.15a) showed that both fill volume and HPMC concentration had positive effects on disintegration time, i.e. increasing the values of these two variables resulted in an increase in disintegration time. Glycerol concentration imparted a negative effect on the disintegration time, decreasing the response for an increase in concentration. HPMC concentration imparted the most significant effect on disintegration time ($p = 0.015$). The interactions plot (Figure 4.15b) suggested that interactions occurred between variables, observed where the lines were not parallel. From this, it was deduced that the effect of HPMC concentration on disintegration time was dependent on fill volume. The effect of glycerol concentration on disintegration time was presumed to be dependent on fill volume at a high fill volume, but there was little interaction between these two variables at fill volumes of 70mL or below. The effect of glycerol concentration on disintegration rate appeared to be dependent on HPMC concentration when HPMC concentration was high; however, little interaction was observed at HPMC concentration of 0.25%$^{w}/_{v}$ or less.

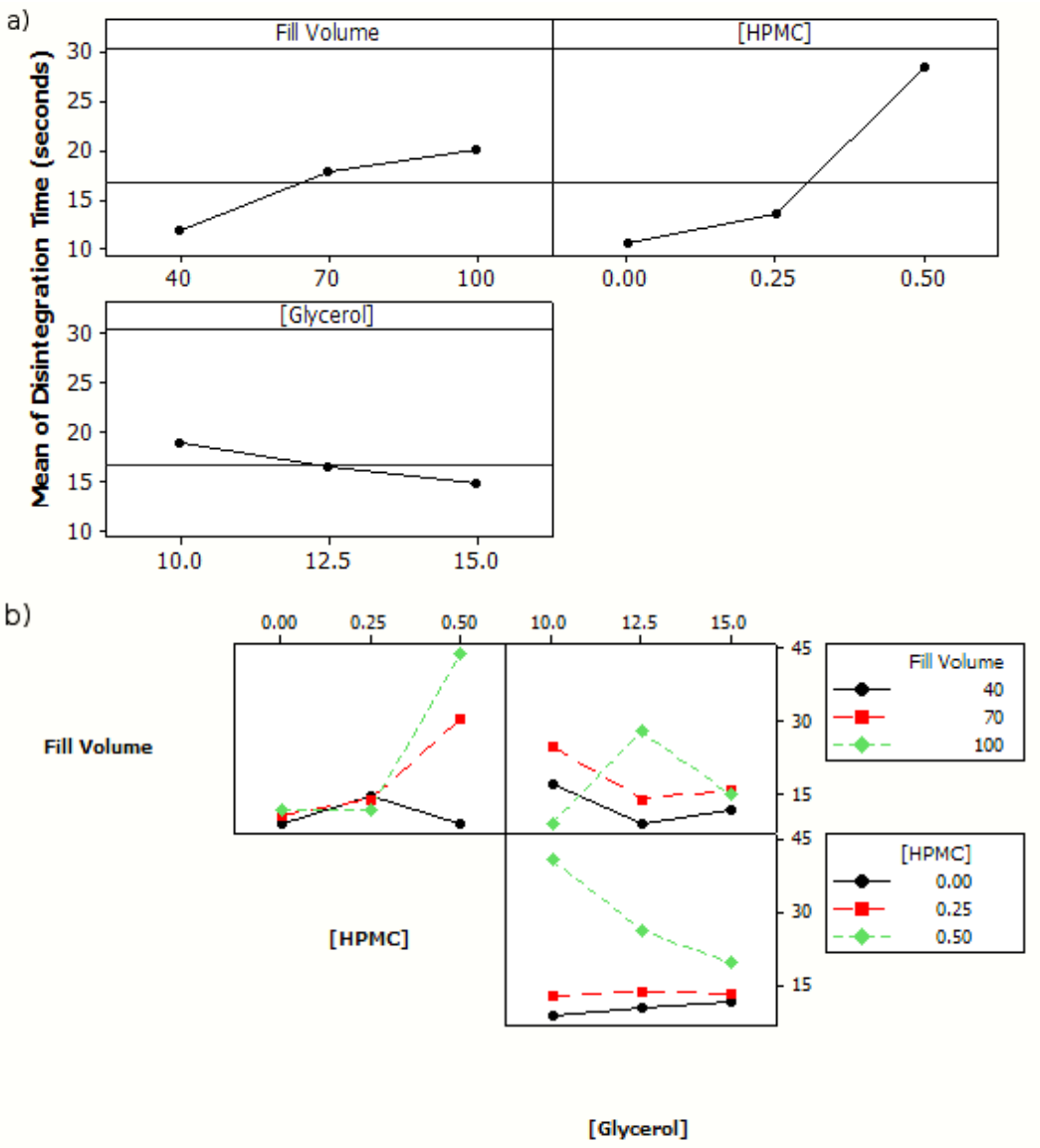


Figure 4.15: Diagnostic plots of the design showing (a) main effects plot and (b) interactions plot for disintegration time

4.3.6.2. Work of Adhesion

Analysis of the main effects plot for WA (Figure 4.16a) revealed that WA increased with increasing fill volume, decreasing HPMC concentration and glycerol concentration above and below 12.5%$^{w}/_{w}$; however, it decreased at glycerol concentration of 12.5%$^{w}/_{w}$. The most significant effect on WA was from HPMC concentration ($p = 0.004$). The interactions plot (Figure 4.16b) suggested that the effect of all three individual variables on WA depended on the other independent variables.

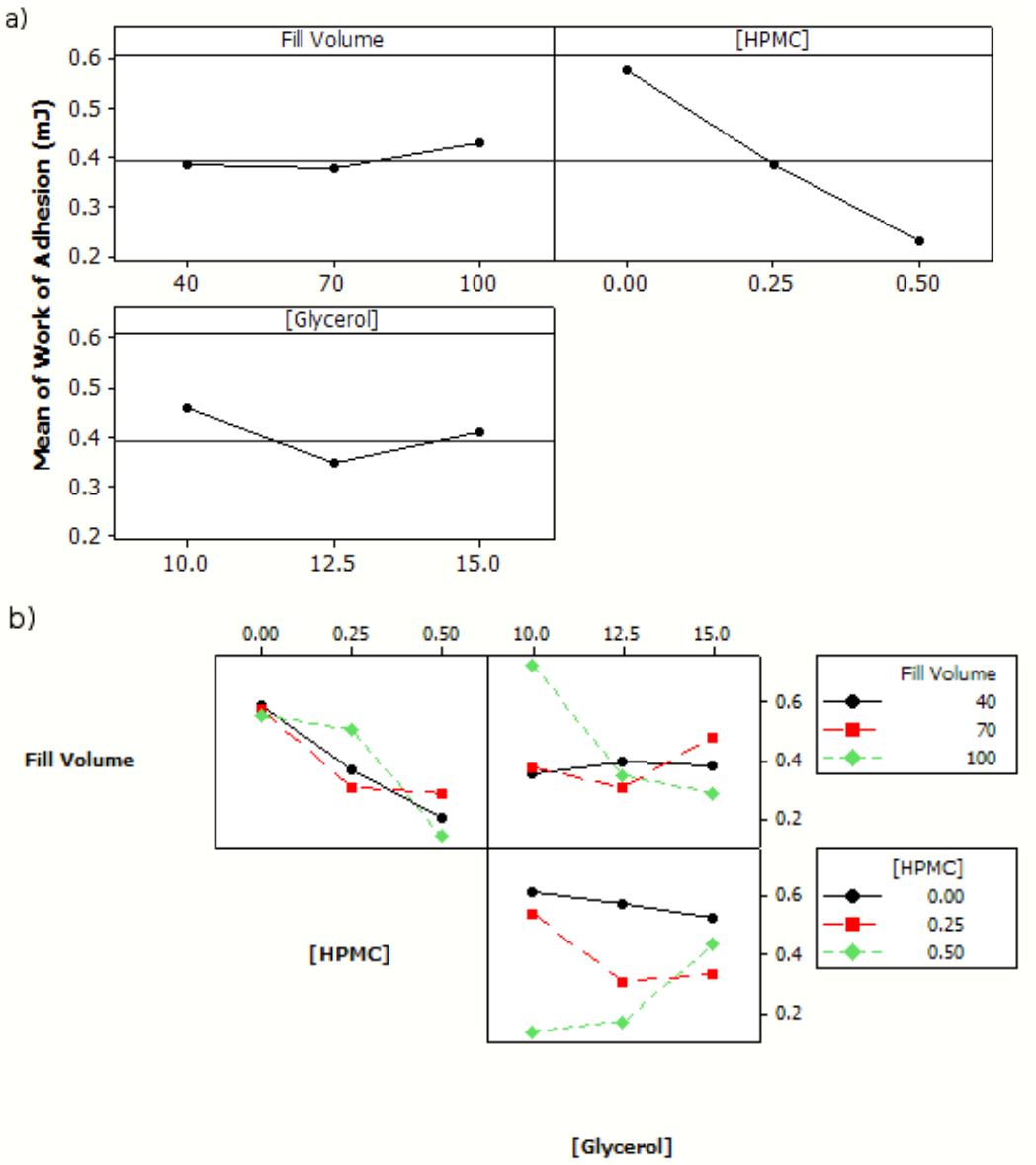


Figure 4.16: Diagnostic plots of the design showing (a) main effects plot and (b) interactions plot for work of adhesion

4.3.6.3. Maximum Detachment Force

The main effects (Figure 4.17a) and interactions (Figure 4.17b) plots for MDF displayed similar trends to that of WA regarding the effects of the three variables on the response and on each other's effects on the response (refer to Figure 4.16 and the discussion on WA). The most significant effect on MDF was from HPMC concentration ($p = 0.003$).

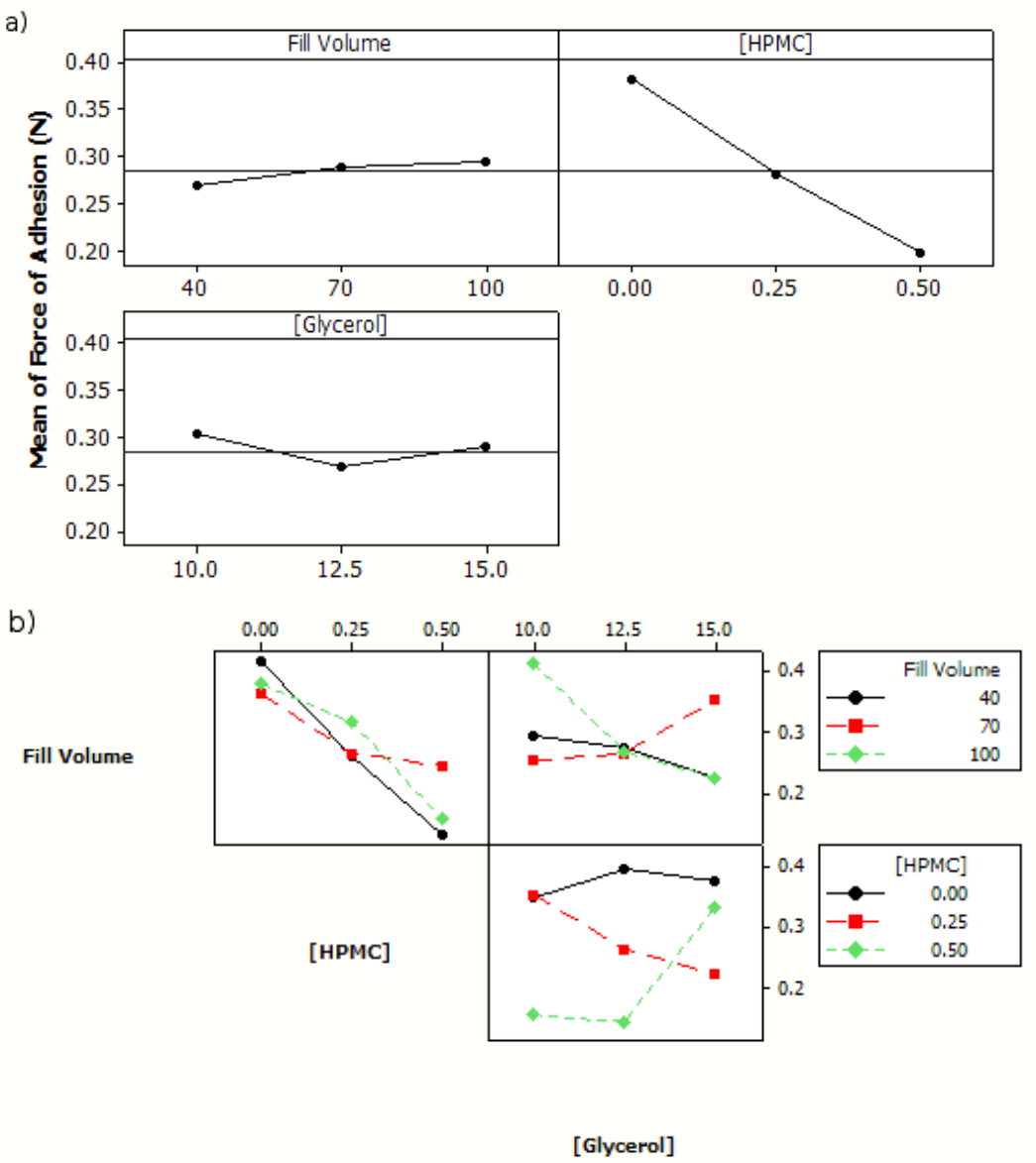


Figure 4.17: Diagnostic plots of the design showing (a) main effects plot and (b) interactions plot for maximum detachment force

4.3.6.4. AUC_D at 1 minute

On analysis of the main effects plot (Figure 4.18a) of AUC_D at 1 minute, it was observed that AUC_D was appreciably high for large fill volumes, high HPMC concentration and glycerol concentration above and below 12.5%$^{w}/_{w}$. AUC_D was affected significantly by fill volume ($p = 0.265$). The interactions plot (Figure 4.18b) suggested that the effect of all three individual variables on AUC_D depended on the other independent variables.

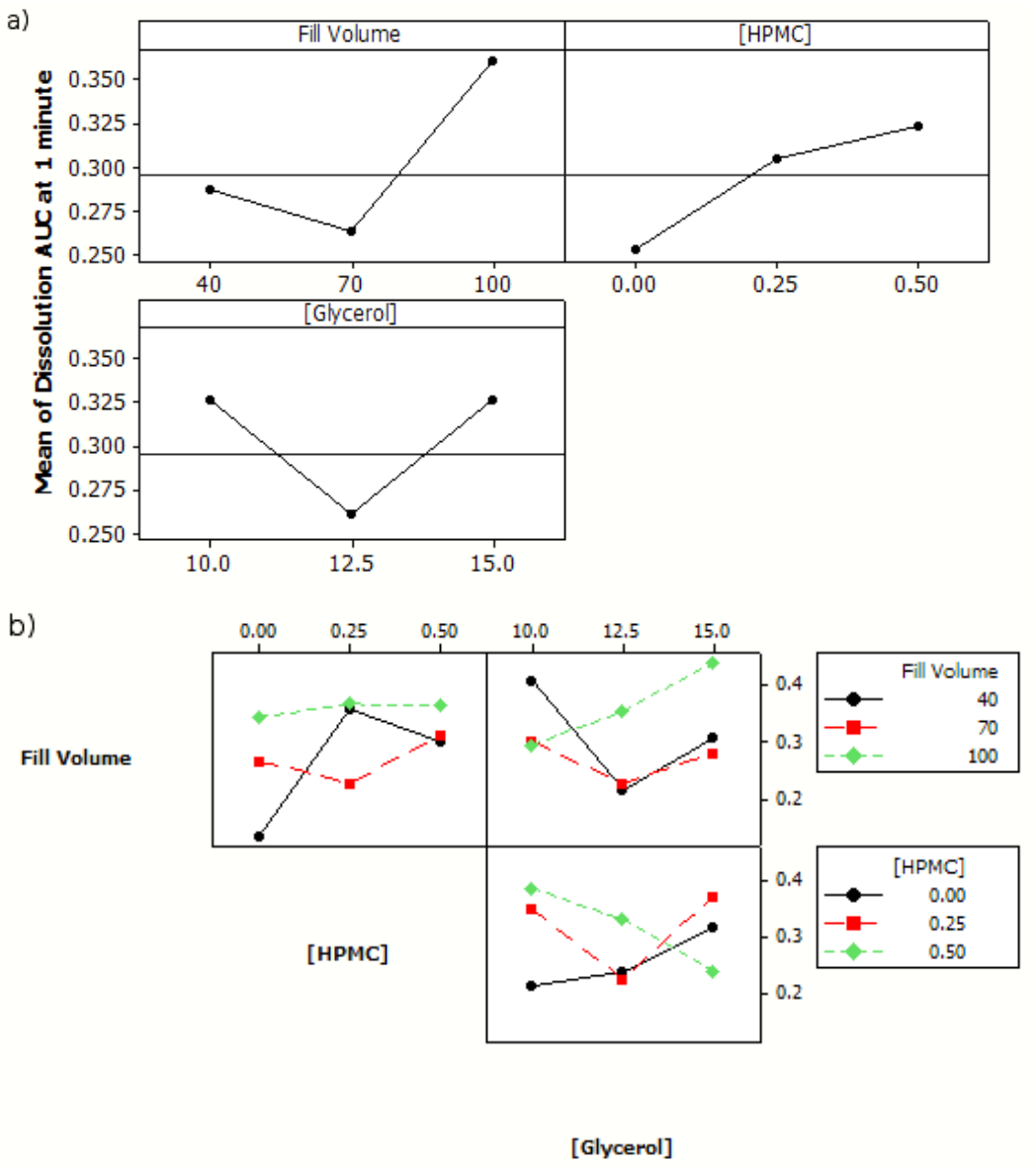


Figure 4.18: Diagnostic plots of the design showing (a) main effects plot and (b) interactions plot for AUC_D at 1 minute

4.3.6.5. AUC_P at 3 minutes

The main effects plot for AUC_P at 3 minutes (Figure 4.19a) revealed that AUC_P was greatest at low fill volumes, high glycerol concentration and an HPMC concentration of 0.25%$^{w}/_{v}$. Fill volume had the most significant effect on AUC_P ($p = 0.585$). The interactions plot (Figure 4.19b) suggested that the effect of all three individual variables on AUC_P depended on the other independent variables.

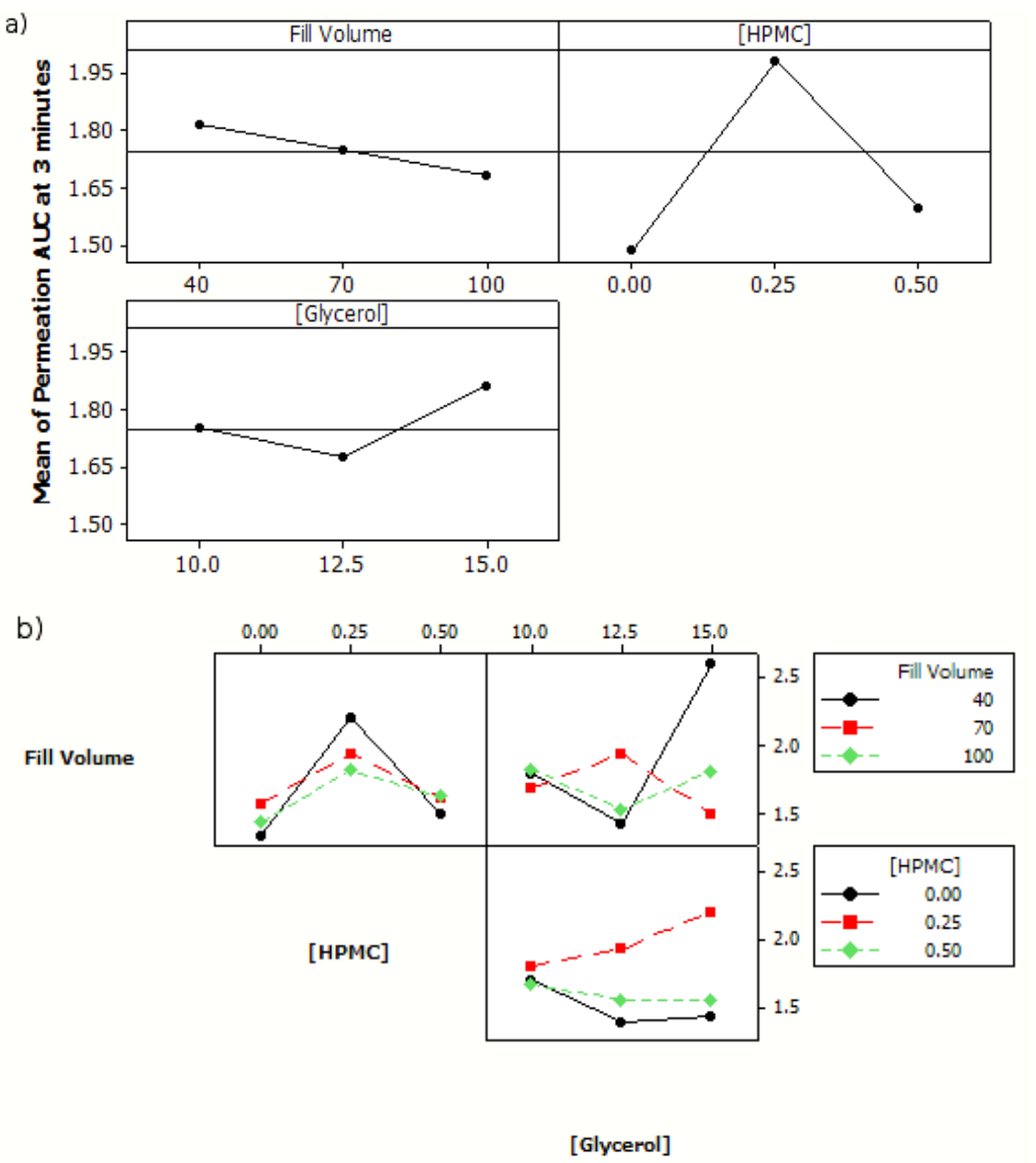


Figure 4.19: Diagnostic plots of the design showing (a) main effects plot and (b) interactions plot for AUC_P at 3 minutes

4.3.7. Analysis of the Box-Behnken Experimental Design

Residuals are useful for the fitting of data to regression models and residual plots can be employed to analyze the fit of such models (Deschepper et al., 2006) in a Box-Behnken experimental design. Residual plots are plots of the differences between observed values and predictions for a particular response (Stewardson and Whitfield, 2004). The residual plots for the responses analyzed using the Box-Behnken experimental design are depicted in Figures 4.20, 4.21, 4.22, 4.23 and 4.24.

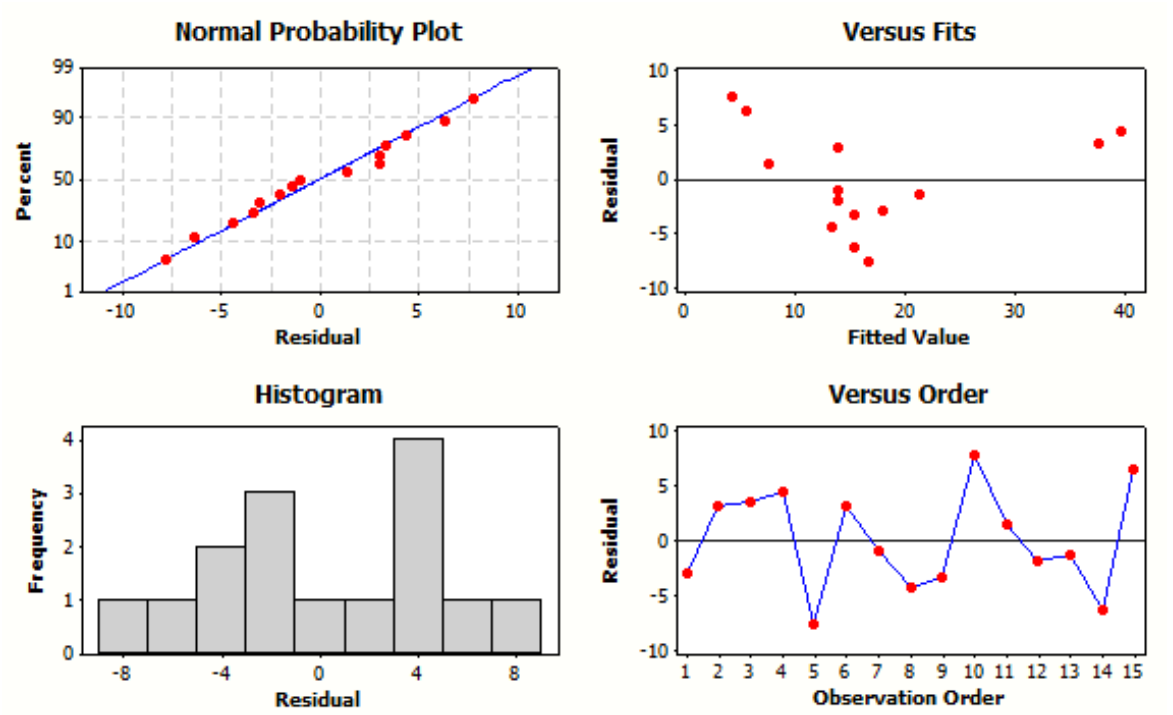


Figure 4.20: Diagnostic plots of the design showing residual plots for disintegration time

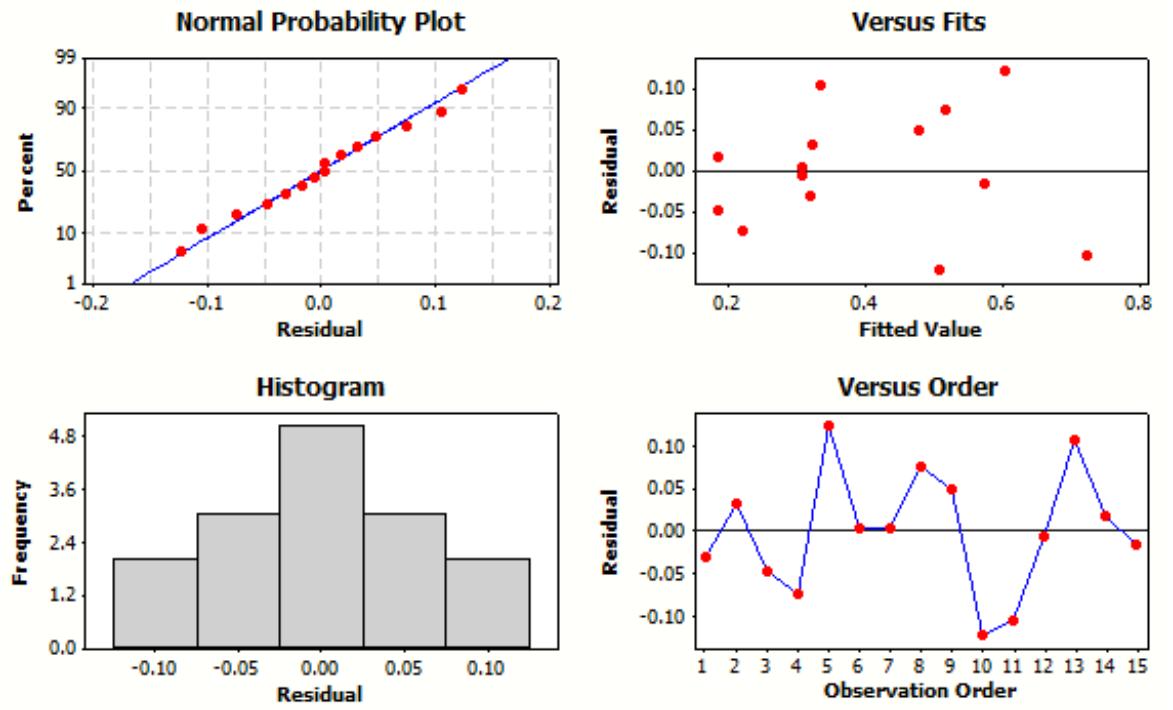


Figure 4.21: Diagnostic plots of the design showing residual plots for work of adhesion

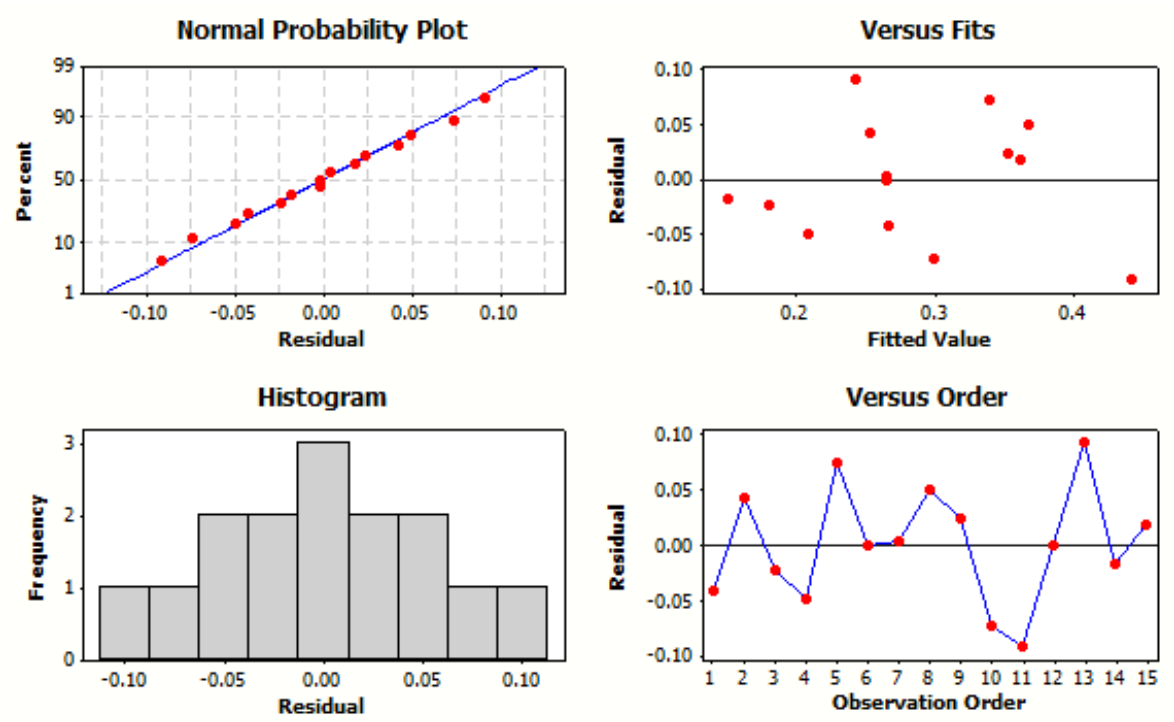


Figure 4.22: Diagnostic plots of the design showing residual plots for maximum detachment force

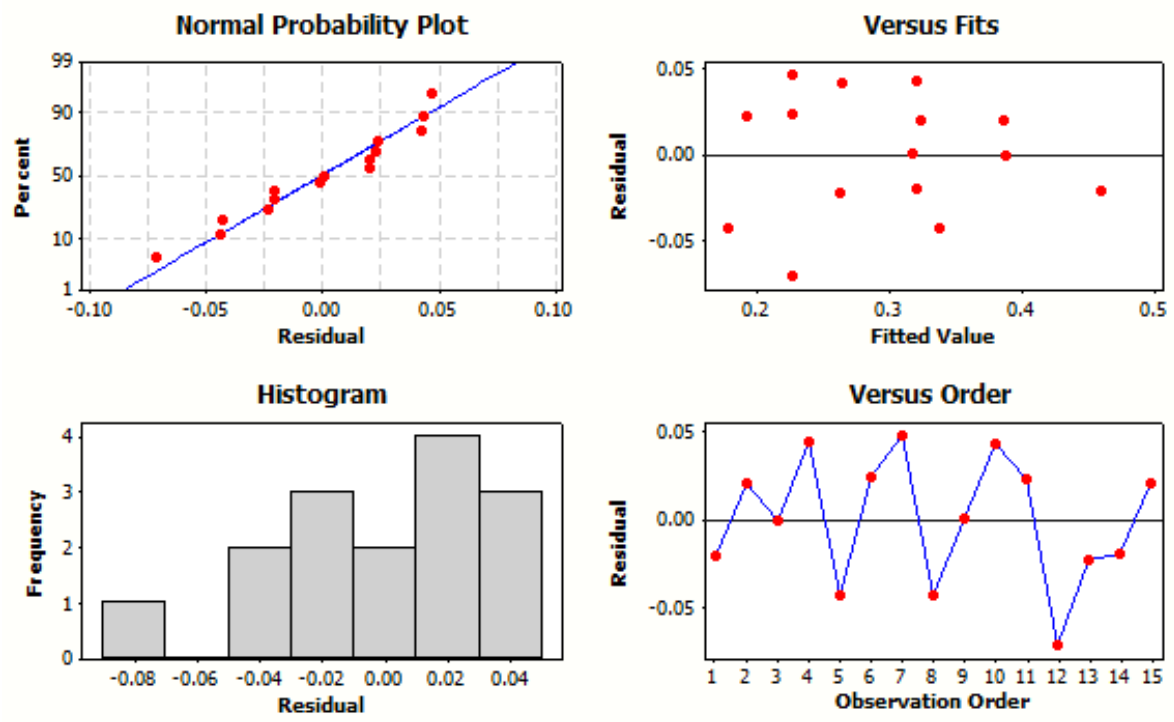


Figure 4.23: Diagnostic plots of the design showing residual plots for AUC_D at 1 minute

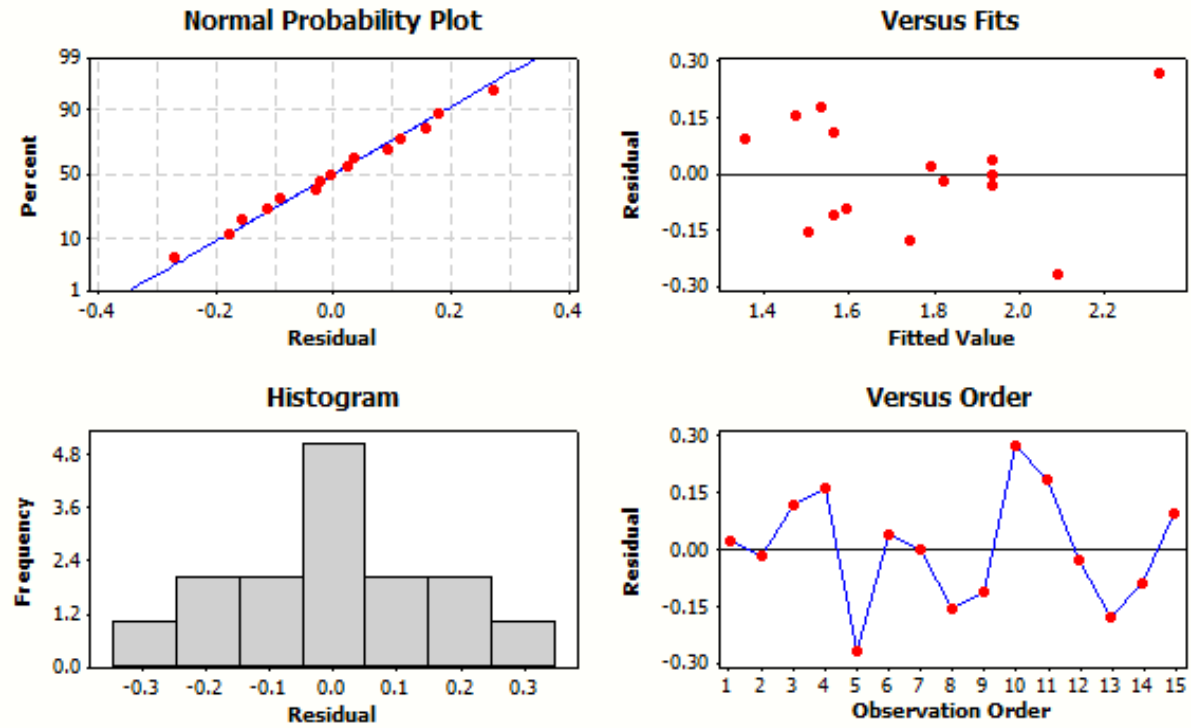


Figure 4.24: Diagnostic plots of the design showing residual plots for AUC_P at 3 minutes

Table 4.5: ANOVA analysis for the measured responses investigated in the Box-Behnken experimental design

Term	p-value				
	DT	**WA**	**MDF**	**AUC_D**	**AUC_P**
FV	0.699	0.340	0.615	0.054	0.285
[HPMC]	0.724	0.102	0.245	0.055	0.376
[Glycerol]	0.840	0.272	0.601	0.062	0.736
FV*FV	0.746	0.578	0.929	0.092	0.859
[HPMC]*[HPMC]	0.204	0.666	0.820	0.843	0.020
[Glycerol]*[Glycerol]	0.883	0.190	0.556	0.078	0.490
FV*[HPMC]	0.093	0.931	0.728	0.285	0.954
FV*[Glycerol]	0.508	0.106	0.526	0.099	0.163
[HPMC]*[Glycerol]	0.181	0.160	0.426	0.092	0.772

Where DT = disintegration time, WA = work of adhesion, MDF = maximum detachment force, AUC_D = AUC_D at 1 minute, AUC_P = AUC_P at 3 minutes and FV = fill volume.

On residual analysis of disintegration time (Figure 4.20), WA (Figure 4.21), MDF (Figure 4.22), AUC_D at 1 minute (Figure 4.23) and AUC_P at 3 minutes (Figure 4.24), it was observed that there was a random distribution of data. The normal probability plots for all responses exhibited a linear curve, indicating normality. The residuals versus fitted values plots demonstrated a random arrangement of data points, signifying an

acceptable and normal fit with a linear regression model. The residual histograms exhibited bell-shaped or nearly bell-shaped curves, suggesting that the data is normally distributed. The residual versus observation order plots displayed a random fluctuation about the center line, suggesting that the error terms are not correlated with one another. An ANOVA analysis with the p-values for the various responses is outlined in Table 4.5.

The regression equations that were generated for five responses are outlined below:

Disintegration time = 40.764 – 0.374(FV) + 34.333[HPMC] – 3.517[glycerol] – $0.0015(FV^2)$ + $94.000[HPMC]^2$ + $0.100[glycerol]^2$ + 1.067(FV)[HPMC] + 0.0367(FV)[glycerol] – 9.600[HPMC][glycerol] (Equation 4.3)

Work of adhesion = 2.235 + 0.0148(FV) -2.828[HPMC] – 0.315[glycerol] + $0.00004(FV^2)$ + $0.455[HPMC]^2$ + $0.0150[glycerol]^2$ – 0.00072(FV)[HPMC] – 0.00157(FV)[glycerol] + 0.157[HPMC][glycerol] (Equation 4.4)

Maximum detachment force = 0.943 + 0.00550(FV) – 1.360[HPMC] – 0.104[glycerol] – $0.000(FV^2)$ + $0.174[HPMC]^2$ + $0.00457[glycerol]^2$ + 0.00213(FV)[HPMC] – 0.00040(FV)[glycerol] + 0.0604[HPMC][glycerol] (Equation 4.5)

AUC_D = 2.504 – 0.0179(FV) + 1.785[HPMC] – 0.310[glycerol] + $0.00007(FV^2)$ – $0.105[HPMC]^2$ + $0.0111[glycerol]^2$ – 0.00482(FV)[HPMC] + 0.00081(FV)[glycerol] – 0.100[HPMC][glycerol] (Equation 4.6)

AUC_P = 1.460 +0.0351(FV) + 2.868[HPMC] – 0.190[glycerol] – $0.00003(FV^2)$ – $6.967[HPMC]^2$ + $0.0154[glycerol]^2$ + 0.00100(FV)[HPMC] – 0.00270(FV)[glycerol] + 0.0608[HPMC][glycerol] (Equation 4.7)

4.3.8. Response Optimization

Response optimization was performed using Minitab®, V15 (Minitab® Inc, Pennsylvania, USA). The film formulation was optimized according to the measured responses of disintegration time, WA, MDF, AUC_D at 1 minute and AUC_P at 3 minutes, which were targeted as outlined in Table 4.6. Maximizing and minimizing responses, where appropriate, resulted in a low desirability for the optimized formulation and the values were therefore targeted within the limits of acceptability. Figure 4.25 displays the final optimization plot, revealing a composite desirability of 95.23%.

Table 4.6: Targeted response values employed in formulation optimization

Response	Lower	Target	Upper
Disintegration time (seconds)	12	13	20
Work of Adhesion (mJ)	0.3	0.4	0.7
Maximum Detachment Force (N)	0.2	0.3	0.45
AUC_D at 1 minute	0.3	0.35	0.45
AUC_P at 3 minutes	1.6	1.9	2

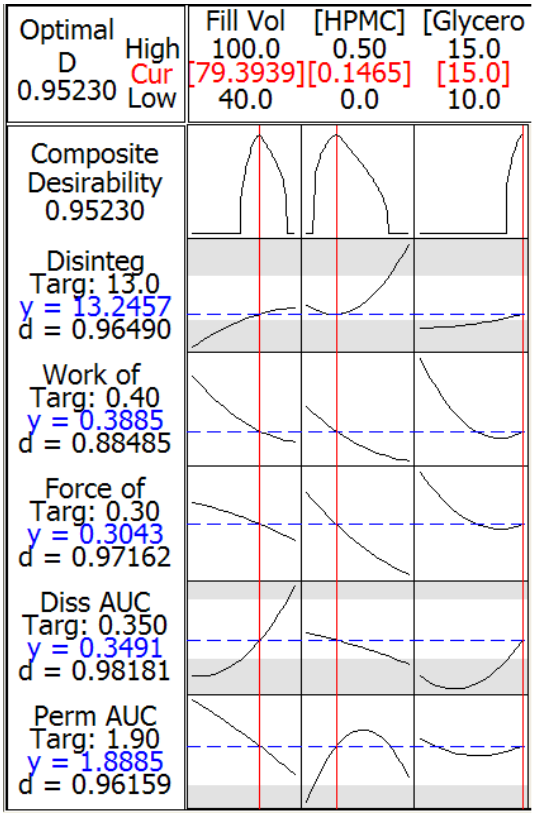


Figure 4.25: Final optimization plot for the response optimization of the polymeric film formulation

Table 4.7 displays the predicted values acquired from formulation optimization with the observed experimental values for the various responses.

Table 4.7: Predicted and experimental values for optimization of the responses

Response	Predicted Value	Experimental Value	Desirability
Disintegration time (seconds)	13.2457	12.8	96.6%
Work of Adhesion (mJ)	0.3885	0.335	86.2%
Maximum Detachment Force (N)	0.3043	0.2705	88.9%
AUC_D at 1 minute	0.3491	0.4179	83.5%
AUC_P at 3 minutes	1.8885	2.0860	90.5%

4.4. Concluding Remarks

Mucoadhesive, drug-loaded electrospun fibers were incorporated directly onto polymeric backing films that were prepared and optimized according to a 3-level, 3-factor Box-Behnken experimental design. The effects of the independent variables on the dependent response variables were analyzed and an optimized formulation was mathematically produced. The optimized formulation was found to have a desirable disintegration time, mucoadhesiveness and rapid drug release and permeation. The rapid drug release may be attributed to the exceedingly large surface area of the electrospun fibers. However, drug-loading was somewhat irregular due to asymmetrical fiber deposition and it would therefore be necessary to conduct further studies in order to temper the regularity of the fiber layer. Notwithstanding the uneven drug-loading, the FMS displays a favorable propensity to be employed as a rapidly releasing, mucoadhesive buccal drug delivery system.

CHAPTER 5

PHYSICOCHEMICAL AND PHYSICOMECHANICAL INVESTIGATION OF AN OPTIMIZED FIBROUS MATRIX SYSTEM FOR RAPID ORAMUCOSAL DRUG DELIVERY

5.1. Introduction

During electrospinning, the polymer chain orientation that occurs during fiber formation has a significant effect on the physicomechanical properties of the fibrous matrix that is formed (Baji et al., 2010). The fiber diameter has been found to affect the mechanical properties of electrospun materials (Tan and Lim, 2006), where fibers with smaller diameters displayed a greater strength, but were less pliable than larger fibers (Tan et al., 2005). The physicomechanical properties of a material have a significant effect on drug release (Coviello et al., 2005), patient acceptability (Malone et al., 2003) and residence time at the site of absorption (Zaman et al., 2008; Andrews et al., 2009) and it is thus necessary to investigate the physicomechanical properties of a drug delivery system.

In the work outlined in this chapter, drug-loaded fibers were electrospun directly onto an optimized polymeric backing film in order to form a porous, rapidly disintegrating fibrous matrix system (FMS) for oramucosal drug delivery. Polyvinylalcohol (PVA) fibers were produced and loaded with model drug, diphenhydramine (DPH). The polymeric backing film was produced according to an optimized formula determined by a Box-Behnken experimental design, in Chapter 4. Drug-loaded films, serving as a comparison, were produced according to the same formula as the backing film and using the same constituents as the electrospinning solution. This chapter details the investigation into drug release, *ex vivo* permeation, mucoadhesion, micro-environmental pH variation and mechanical properties of the optimized FMS.

5.2. Materials and Methods

5.2.1. Materials

The materials used in this phase of the study were the same as in Chapter 4.

5.2.2. Preparation of Polymeric Backing Films by Film-Casting

A film intended as a backing and mucoadhesive layer for electrospun fibers was prepared according to an optimized formula using a Box-Behnken experimental design in as described in Chapter 4. Polymer solutions were prepared by dissolving 136.5mg of glycerol, 794mg of polyvinylalcohol (PVA) and 116mg of hydroxypropylmethylcellulose (HPMC) in 79.39mL of a 4:1 mixture of deionized water and propan-2-ol. The solution was syringed into a rectangular flat-bottomed mould and left in a fume hood for 48 hours in order that complete solvent evaporation and film-formation could occur. For comparative purposes, a DPH-loaded film (F_D) containing the same polymeric and plasticizer constituents was prepared.

5.2.3. Preparation of Fibers by Electrospinning

A drug-loaded solution for electrospinning was produced by dissolving PVA, citric acid, DPH and glycerol in a 2:1 deionized water:propan-2-ol mixture at concentrations of 25%$^{w}/_{v}$, 2% $^{w}/_{v}$, 10% $^{w}/_{v}$ and 0.5%$^{v}/_{v}$, respectively. These quantities were based on optimal fiber production, reproducibility and drug-loading efficiency. The solution was placed in a 5mL pipette, which was fitted into the adjustable supporting bracket of an electrospinning device. Electrospinning of the solution was performed as outlined in Chapter 4. Fibers were collected on the polymeric backing film secured on aluminum foil-lined board. Samples were cut into 1.5cm^2 sections. For comparative purposes, a film (F_E) was prepared with the same drug/polymer ratio as the electrospinning solution.

5.2.4. Morphological and Surface Structure Analysis of the Drug-loaded Fiber Layer

The surface structure of the electrospun fibers was analyzed by images produced by scanning electron microscopy (SEM), using a Phenom Microscope (FEI Company, Hillsboro, Oregon, USA). Samples were mounted on stubs and sputter-coated with gold prior to examination.

5.2.5. Drug Entrapment of the Optimized FMS and Drug-Loaded Films

Samples of the FMS and the two drug-loaded films (F_D and F_E) were cut into sections, dissolved in simulated saliva (pH 6.75) and the drug content of each section was analyzed by UV spectrophotometry.

5.2.6. Disintegration Time of the Optimized FMS and Drug-Loaded Films

The *in vitro* disintegration time of FMS samples and drug-loaded films (F_D and F_E) was determined as outlined in Chapter 4.

5.2.7. *In vitro* Drug Release by Dissolution Testing

In vitro drug release was tested according to the method outlined in Chapter 4. As a branded product comparison, the *in vitro* dissolution testing of Sleepeze-PM® tablets was performed using a USP rotating paddle apparatus (Model 7ST, Caleva, Frankfurt, Germany) and employing 900mL phosphate buffered saline (PBS) (pH 6.8, 37°C). 5mL samples were drawn at 1, 3, 5, 10, 15, 30, 60 and 90 minutes and analyzed by UV spectrophotometry.

5.2.8. Drug Permeation by *ex vivo* Studies

Ex vivo drug permeation testing was performed according to the method outlined in Chapter 4. After equilibration, the PBS in the donor compartment was removed and was replaced with an FMS, F_D, or F_E sample in simulated saliva (pH 6.75). A 2mg/mL DPH in simulated saliva solution was also tested for comparative purposes.

5.2.9. Mucoadhesion of the Optimized FMS and Drug-Loaded Films

Mucoadhesion testing was performed according to the method outlined in Chapter 4.

5.2.10. Determination of Micro-Environmental Surface pH Variation within the FMS

Extreme changes in pH on the surface of the matrix can cause irritation to mucous membranes within the oral cavity (Patel et al., 2007). Measurement of the surface pH is therefore essential. Matrices were allowed to swell in contact with 1mL of simulated saliva (pH 6.75). The surface pH was measured by glass micro-electrode (Mettler Instruments, Giessen, Germany). Measurements were taken after the matrices had been hydrated for 20 seconds and at 1, 3, 5, 10 and 15 minutes thereafter.

5.2.11. Determination of FMS Toughness and Bi-Axial Extensibility

Bi-axial extensibility was determined from Force-Distance profiles generated using a TA.XT*plus* Texture Analyser (Stable Micro Systems, London, England) fitted with a 2mm flat cylindrical probe and a 5kg loadcell. The method of testing the extensibility was based on work by Sibeko and co-workers (2009). The sample was secured onto a ring assembly with a central hole (5mm diameter), which was attached to a supportive, hollow, raised platform. The setup was placed such that the cylindrical probe of the textural analyzer was centralized over the hole. The probe was lowered and penetrated into the sample according to the test parameters outlined in Table 5.1.

Table 5.1: Test parameters employed in bi-axial extensibility testing

Parameter	Setting
Test mode	Compression
Pre-test speed	1mm/s
Test speed	1mm/s
Post-test speed	1mm/s
Target mode	Distance
Distance	10mm
Trigger force	0.5N

5.2.12. Determination of Tensile Properties of the Optimized FMS and Drug-Loaded Films

The tensile properties of samples were measured using a nanoTensile^{TM} 5000 (Hysitron Incorporated, Minneapolis, Minnesota, USA). Samples were cut into thin 1 × 22mm (approximately) strips and mounted, with cyanoacrylate-based adhesive, onto specially designed mounting brackets held together with rigid strips of cardboard. Once the sample had cured completely, the width, length and thickness were measured with digital calipers. The sample and sample bracket were secured in the upper sample gripper on the nanotensile (NT) Head and the mass was measured. The NT Head was lowered and the axes were aligned in order to secure the bottom of the sample bracket in the sample stage (lower) sample gripper. The mounting brackets were moved apart at a constant rate of displacement and the tensile properties of the sample were measured and recorded.

5.2.13. Analysis of the Stress-Strain Rheological Parameters of the Components of the FMS

The rheological properties of polymer solutions and hydrated FMS, F_D and F_E samples were determined with the use of a Haake Modular Advanced Rheometer System (ThermoFisher Scientific, Karlsruhe, Germany). The stress-strain rheological parameters of the polymer solution have an influence on drug release, electrospinning, palatability and effect on saliva, and are important factors when considering the desired characteristics of the system. Samples were analyzed by placing the polymer solution or FMS/film sample, hydrated in 1mL simulated saliva (pH 6.75), on the sample stage and immersing the spindle in the fluid. The shear rate was ramped from 0 to 500/s and the shear forces and viscosities of the samples were measured at 37°C for the FMS and film samples and at 25°C for the electrospinning solution. The thixotropy of the 25%$^{w}/_{v}$ PVA electrospinning solution was determined by ramping the shear rate from 0 to 50/s

over 60 seconds, holding for 60 seconds and then decreasing back to 0/s over 60 seconds. Oscillation studies were carried out by subjecting samples to oscillating stresses or strains. Oscillation measurements were used to determine the storage modulus, G', and the loss modulus, G", as a function of angular frequency, ω. Oscillation tests provide information on sample elasticity and viscosity related to the applied frequency.

5.2.14. Vibrational Chemical Structure Analysis

Fourier Transform Infrared (FTIR) Spectroscopy was performed in order to assess structural changes that may have occurred in the polymeric backbone due to interactions of excipients, drugs or polymers during film or fiber formation. A Spectrum 100 FT-IR Spectrometer (PerkinElmer Inc., Waltham, Massachusetts, USA) was used to assess vibration characteristics of chemical functional groups.

5.3. Results and Discussion

5.3.1. Physical Dimensions of the Films and Fiber Layer

The films produced were even, thin, transparent and pliable. The fibers formed a white layer on the films. The FMS backing layer film was 80µm thick, while the complete FMS was 460µm thick, and hence the fiber layer was 380µm thick. The F_E film was 110µm thick and the F_D film was approximately 90µm thick, but was somewhat uneven in places.

5.3.2. Morphological and Surface Structure Analysis of the Electrospun Fiber Layer

On SEM analysis, it was observed that the fibers produced were randomly arranged and had uniform diameters on average. The fiber diameter was approximately 0.36µm and the average visible pore size ranged between approximately 0.69 and 1.91µm, as depicted in Figure 5.1.

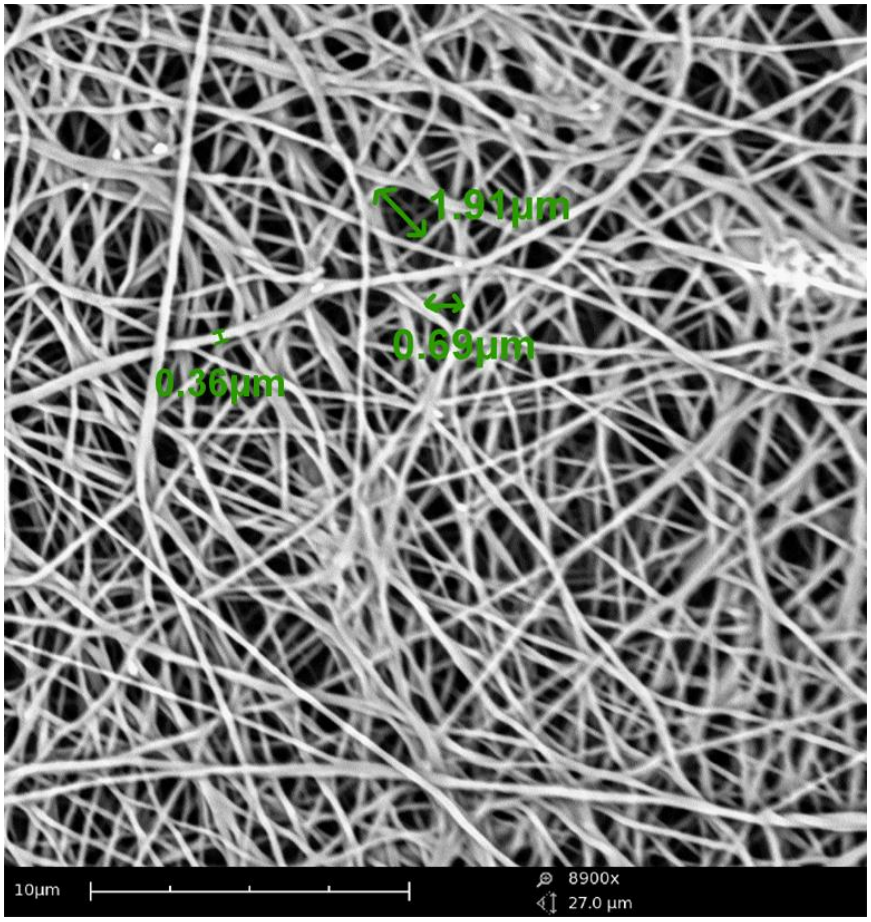


Figure 5.1: SEM image of the electrospun fiber layer, showing average fiber diameter of 0.36µm and visible pore size of 0.69-1.91µm

5.3.3. Drug Entrapment of the Optimized FMS and Drug-Loaded Films

The average drug entrapment of the FMS and the F_D and F_E films was determined along with standard deviation, and is outlined in Table 5.2.

Table 5.2: Drug entrapment per 1.5cm^2 section of fibrous matrix system (FMS), drug-loaded optimized film (F_D) and film produced from ratios in electrospinning solution (F_E)

Formulation	Drug Entrapment (mg) ± SD
FMS	2.3 ± 0.44
F_D	8.8 ± 0.11
F_E	5.5 ± 0.48

5.3.4. Disintegration Time of the Optimized FMS and Drug-Loaded Films

The time taken for the FMS and the F_D and F_E films to disintegrate was 12.8 seconds, 15.8 seconds and 52.6 seconds, respectively, and is depicted in Figure 5.2. The DPH-loaded fiber layer of the FMS took an average of 3.6 seconds to disintegrate, which is considerably shorter than the time taken for the drug-loaded films to disintegrate.

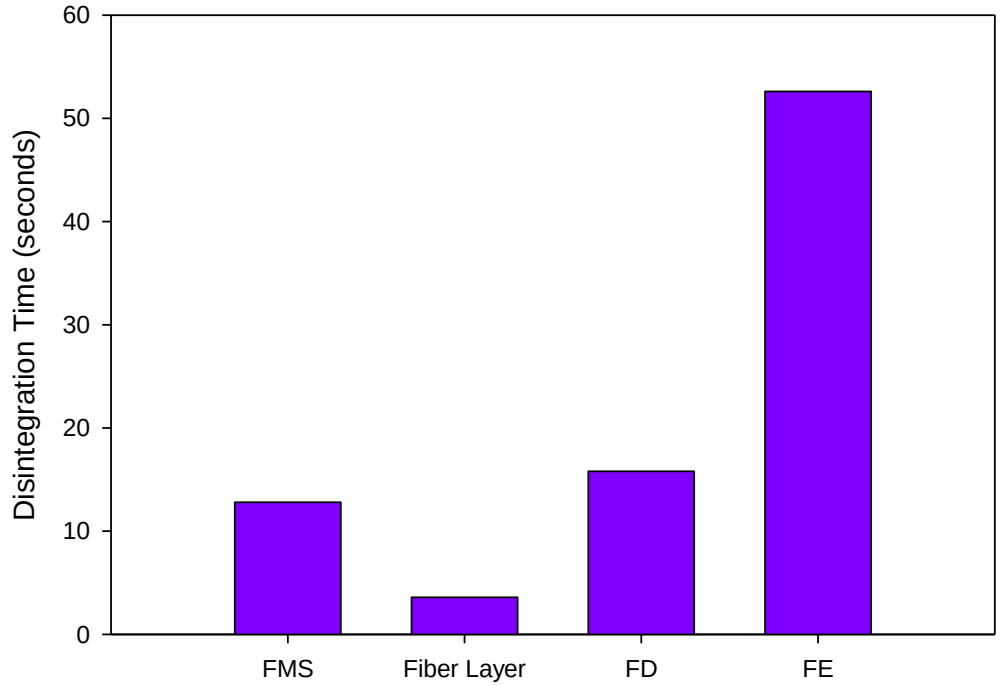


Figure 5.2: Vertical bar chart depicting the disintegration times of the fibrous matrix system (FMS), fiber layer of the FMS, drug-loaded optimized film (F_D) and film formed from the same components as the electrospinning solution (F_E) (in all cases SDs < 0.02, N = 3)

5.3.5. *In vitro* Drug Release by Dissolution

The optimized FMS exhibited a rapid dissolution rate, with an average of 63% of the loaded dose releasing after 1 minute and 86% after 3 minutes. In comparison, the F_D and F_E films released 27% and 17% of the loaded dose after 1 minute and 48% and 46% at 3 minutes, respectively. Drug release profiles are depicted in Figure 5.3. It is apparent that the dissolution rate of the FMS is significantly more rapid than that of either of the drug-loaded films, owing to the extremely high surface area of the fibrous layer in comparison to films (Agarwal et al., 2008; Reneker and Yarin, 2008), which enhances the rate of disintegration and dissolution (Dokoumetzidis and Macheras, 2006). Figure 5.4 displays the drug release profiles of the FMS and the branded comparator product. The branded comparator product, Sleepeze-PM®, displayed a relatively rapid drug release, with 31% and 55% of the loaded dose releasing after 1 and 3 minutes, respectively. However, the optimized FMS exhibited a superior drug release profile in a considerably smaller volume of buffer, which makes it preferable to the conventional system on the market in terms of its rapid action.

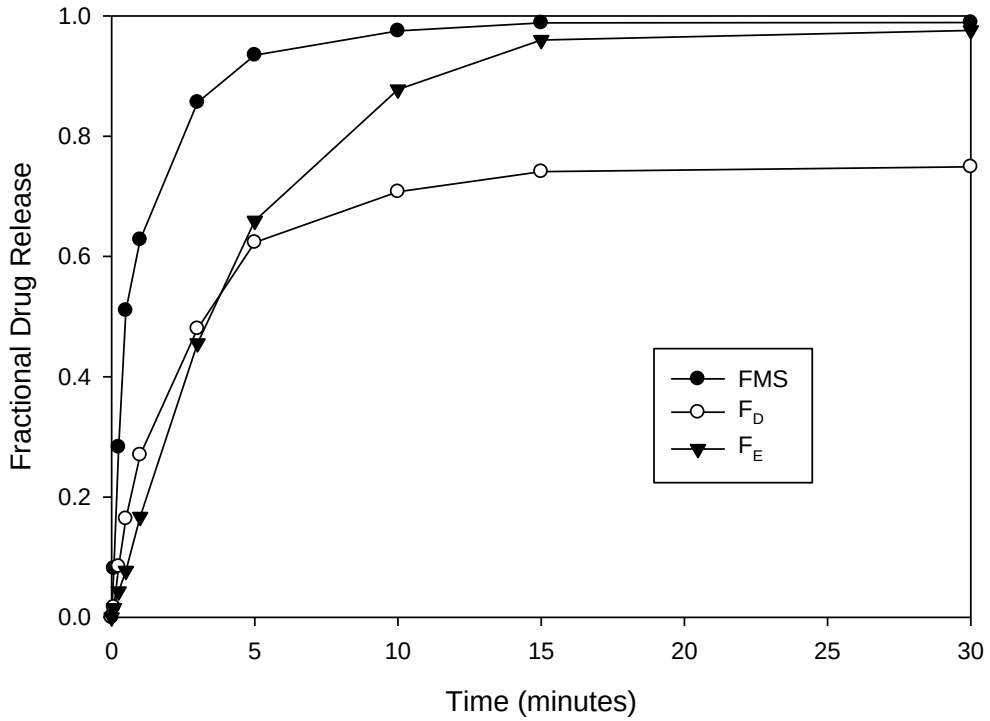


Figure 5.3: Drug release profiles of the fibrous matrix system (FMS), DPH-loaded film formulation (F_D) and film formed from the same components as the electrospinning solution (F_E) (in all cases SDs < 0.02, N = 3)

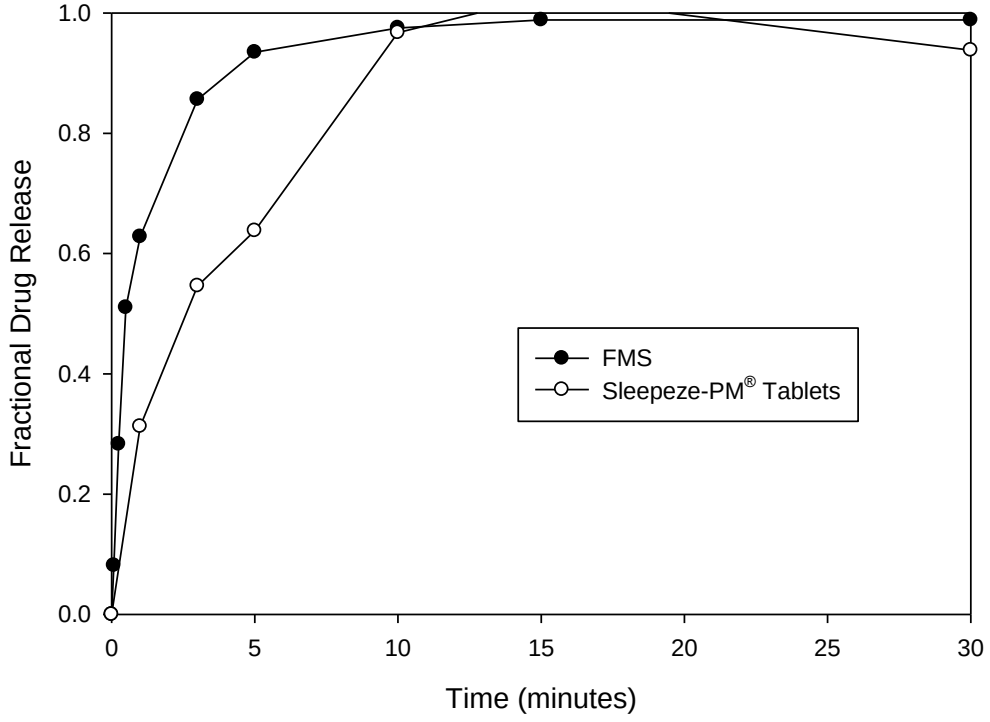


Figure 5.4: Drug release profiles of the fibrous matrix system (FMS) and Sleepeze-PM® tablets (in all cases SDs < 0.02, N = 3)

The area under the curve (AUC_D) at 1 minute was calculated for the FMS, F_D and F_E films and Sleepeze-PM® tablets, and is illustrated as a bar chart in Figure 5.5. The AUC_D of the FMS is nearly 3 times greater than that of the F_D film and Sleepeze-PM® tablets, and approximately 5 times greater than the AUC_D of the F_E film. Hence it can be deduced that drug release from the FMS occurs more rapidly than from any of the comparison test formulations.

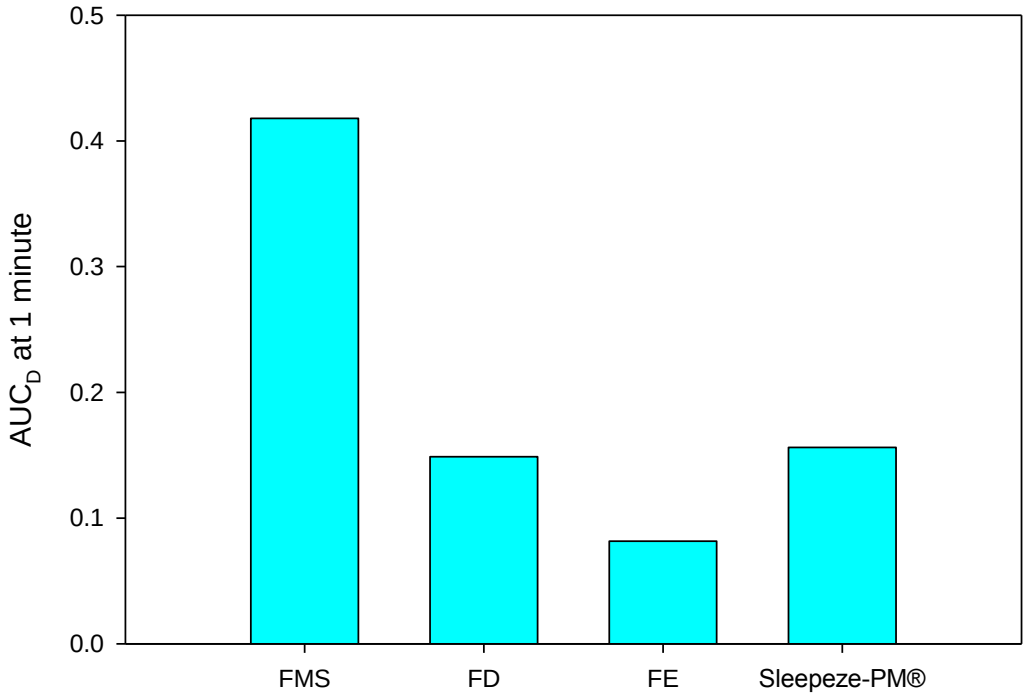


Figure 5.5: Dissolution AUC (AUC_D) comparison between the FMS, comparator DPH-loaded film formulations (F_D and F_E) and Sleepeze-PM® tablets (in all cases SDs < 0.02, N = 3)

5.3.6. Drug Permeation by *ex vivo* Studies

Figure 5.6 depicts the flux profiles of the FMS, a 2mg/mL DPH solution and the drug-loaded films, F_D and F_E. The DPH solution exhibited a slightly greater flux than the FMS, with 79% and 78% of the loaded dose permeated at 3 minutes, respectively. The F_D and F_E films displayed a lower flux than the FMS, where 74% and 55% of the loaded dose had permeated after 3 minutes, respectively. This is in agreement with the *in vitro* dissolution data. Permeation AUC (AUC_P) at 3 minutes was calculated for the tested formulations and plotted as in Figure 5.7. AUC_P of the 2mg/mL DPH solution was slightly greater than that for the FMS, suggesting that the rate of permeation of drug from solution was only marginally faster than from the FMS. The F_E film exhibited the smallest AUC_P value and the value for the F_D film was between that of the FMS and F_E

film. The rate of drug permeation from the DPH-loaded films was somewhat slower than from the FMS or the drug solution.

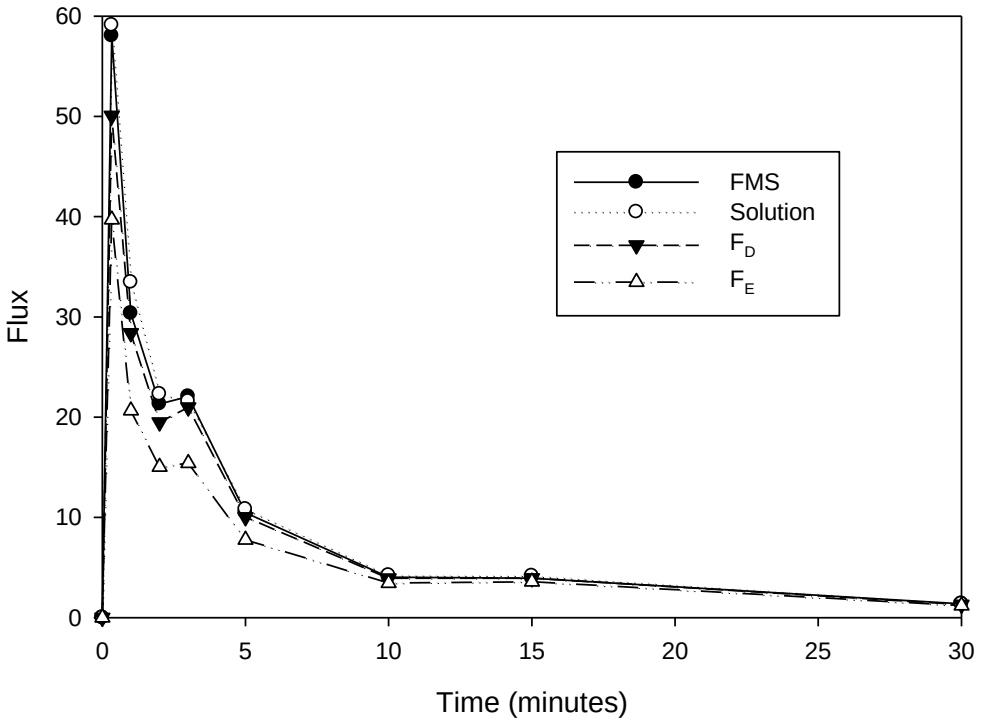


Figure 5.6: Flux profiles of the fibrous matrix system (FMS), DPH solution, DPH-loaded film formulation (F_D) and film formed from the same components as the electrospinning solution (F_E)

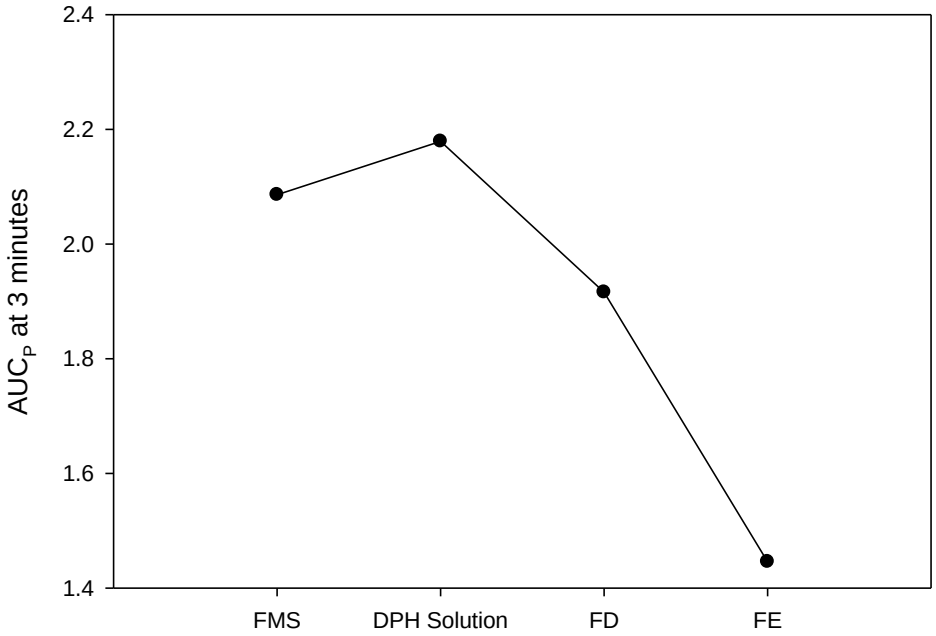


Figure 5.7: Scatter plot depicting AUC_P at 3 minutes for the fibrous matrix system (FMS), DPH solution, DPH-loaded film formulation (F_D) and film formed from the same components as the electrospinning solution (F_E)

The apparent permeability coefficient (P_{app}) and steady-state flux (J_{ss}) values were calculated for the tested formulations and are outlined in Table 5.3. These values were in accordance with those for AUC_P of the various formulations, with the F_E film exhibiting the smallest P_{app} and J_{ss} values and the DPH solution having the largest P_{app} and J_{ss} values.

Table 5.3: Calculated apparent permeability coefficient (P_{app}) and steady-state flux (J_{ss}) values for the FMS, DPH solution, F_D and F_E

Formulation	P_{app}	J_{ss}
FMS	4.9×10^{-4}	5.88
DPH Solution	5.0×10^{-4}	5.95
F_D	4.7×10^{-4}	5.60
F_E	3.4×10^{-4}	4.11

5.3.7. Mucoadhesion of the Optimized FMS and Drug-Loaded Films

The average maximum detachment force (MDF) and work of adhesion (WA) were determined from the peak and AUC, respectively, of the Force-Distance profiles (Figure 5.8) generated by textural profiling. Table 5.4 outlines the values of MDF and WA for the FMS film, fibrous layer and the drug-loaded films (F_D and F_E). The backing film of the FMS exhibited an adequate MDF and WA. The fibrous layer was observed to be apparently more mucoadhesive than the film; however, due to the rapid disintegration rate of the fibers, the backing film is required to hold the system in place and ensure that the released drug is detained at the buccal mucosa until absorption occurs. The F_E film was found to have a considerably larger MDF than the fibrous layer of the FMS. This may be attributed to the rapid disintegration rate of the fibers. In comparison to the FMS film layer, the F_D film displayed an exceedingly smaller MDF and WA. From this, it can be deduced that the addition of drug to the film formulation resulted in a reduction in mucoadhesiveness. The disparity between the MDF and WA values of the FMS backing film and the F_E film may be due to the presence of HPMC in the FMS film formulation. As discussed in Chapter 4, HPMC has poorly flexible chains due to a high glass transition temperature and is therefore poorly mucoadhesive (Karavas et al., 2006), and hence the addition of HPMC to the film formulation will decrease the mucoadhesive strength of the resulting film.

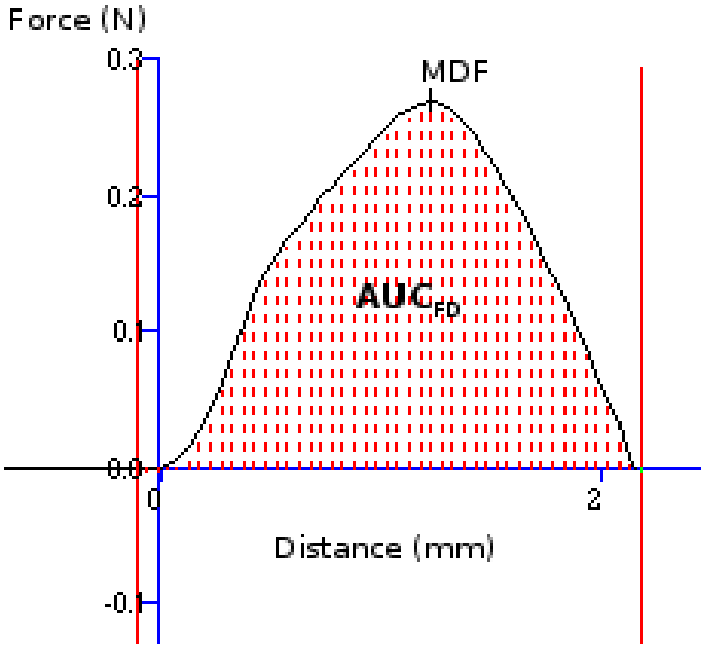


Figure 5.8: Typical textural profile used to determine MDF (peak) and WA (AUC_{FD}) for assessing mucoadhesion

Table 5.4: Maximum detachment force (MDF) and work of adhesion (WA) for the FMS film, fiber layer of the FMS and the drug-loaded films, F_E and F_D

Formulation	MDF (N)	WA (mJ)
FMS Film	0.2705	0.335
FMS Fibrous Layer	0.2982	0.601
F_D	0.0468	0.041
F_E	0.3867	0.599

5.3.8. Micro-Environmental Surface pH Variation within the FMS

It has been observed that extreme changes in surface pH may cause damage to mucosal surfaces (Bottenberg et al., 1991). The evaluation of surface pH variation is therefore an important factor to consider (Munasur et al., 2006). The surface pH values ranged between 6.63 and 6.75 over the 15 minutes in which measurements were taken (Figure 5.9). There was an initial drop in pH to 6.63 at the 20 second time point, possibly due to dissolution and subsequent solubilization of citric acid, which was employed as a taste-masking component. At the 3 minute time point, the pH had increased to 6.73, which may be due to the buffering effect of the simulated saliva or the dissolving of the polymeric components of the formulation. The variation of pH was less than 0.5 units and considered acceptable for an oramucosally administered drug delivery system as it can be deduced that minimal irritation to the buccal mucosa would occur.

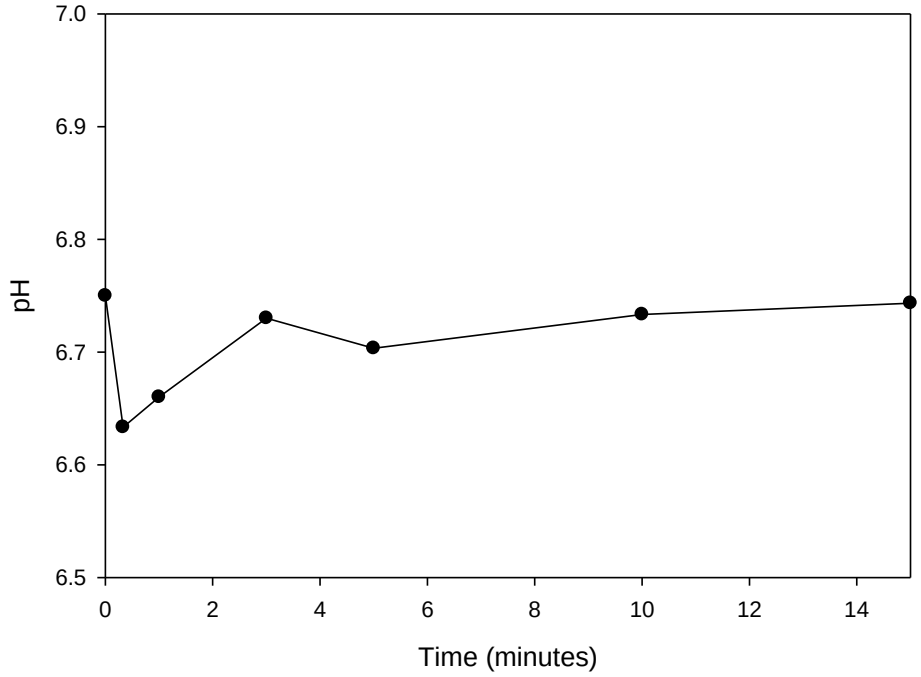


Figure 5.9: Average pH variation over time for the FMS hydrated in simulated saliva (pH 6.75)

5.3.9. FMS Toughness and Bi-Axial Extensibility

Extensibility is the degree of extension or stretching that a material can withstand before fracture occurs and polymer linkages have a substantial effect on the physicomechanical strength of materials (Sibeko et al., 2009). Figure 5.10 is a typical textural profile obtained during extensibility testing. The maximum force (F_{max}) and distance (D_{max}) values for the FMS, optimized FMS film, F_D film and F_E film were plotted as a vertical bar chart in Figure 5.11. The complete FMS was found to be slightly stronger than the FMS film (F_{max} = 5.29N and 5.17N, respectively), but also less extensible (D_{max} = 4.435 and 4.957mm, respectively). It can therefore be deduced that the presence of electrospun fibers resulted in a slight increase in film strength and a decrease in extensibility. When electrospun fibers are produced, there is a thinning and extending process that takes place (Kalayci et al., 2005), and this may result in the fibers being less extensible than the film. The presence of drug in the FMS film (F_D) brought about a decrease in both F_{max} and D_{max}. This may also partially explain the reduction in extensibility with the presence of a drug-loaded fiber layer. The F_E film had a significantly larger F_{max} and D_{max} than the FMS, which may be due to the absence of the more rigid polymer, HPMC, and formation by film-casting, which does not result in thinning, of the former.

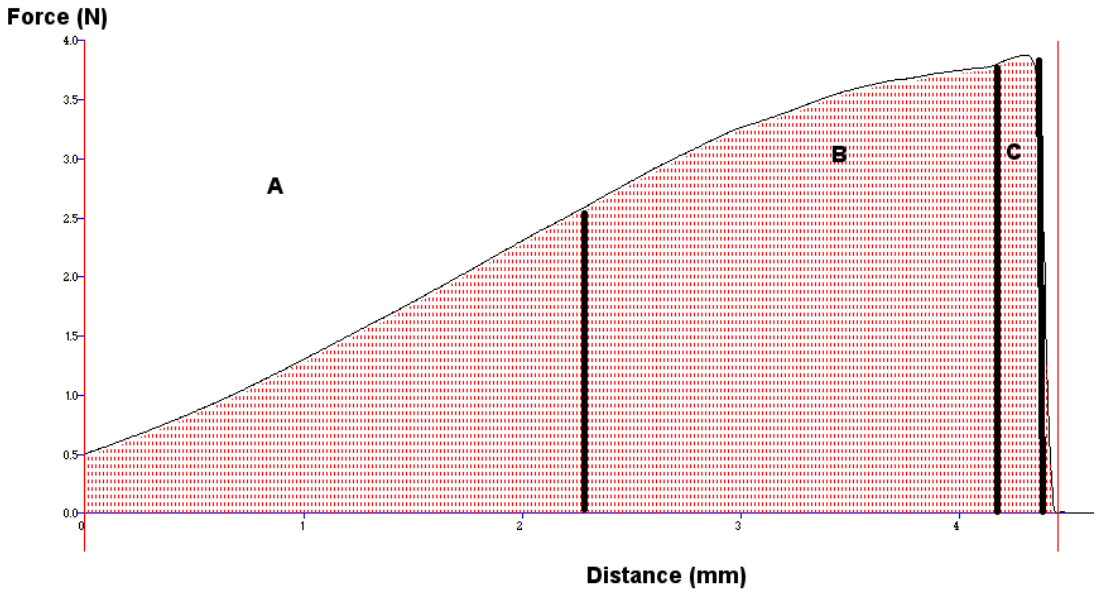


Figure 5.10: Typical textural extensibility profile for the FMS, showing 3 distinct regions: linear extensibility (A), maximum extensibility (B) and fracture point (C)

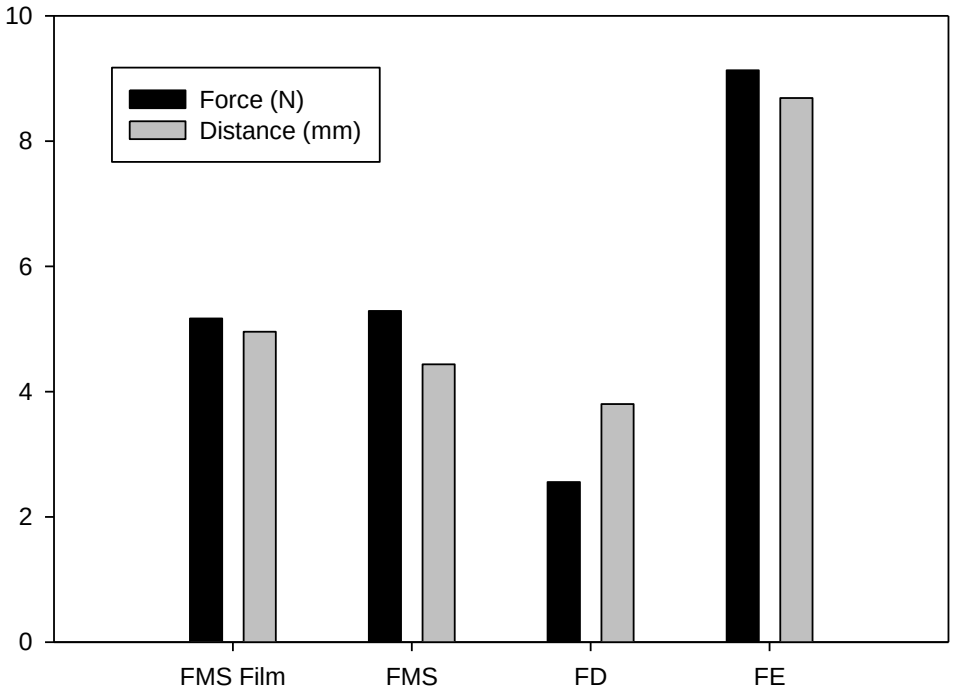


Figure 5.11: Vertical bar chart outlining average maximum force and distance values for the film of the fibrous matrix system (FMS), the complete FMS, drug-loaded FMS film (F_D) and film containing the same components as the electrospinning solution (F_E) (in all cases SDs < 0.02, N = 3)

5.3.10. Determination of Tensile Properties by Nanotensile Testing

The stress-strain relationship of a material is highly dependent on the flexibility of the polymer chains and the strength of the material. When only a small amount of stress is

required to produce a large amount of strain, the material is considered to be flexible and the Young's modulus, which is the slope of the linear portion of the stress-strain curve, will be relatively small (Wu and McGinity, 2000). The average experimental values for Young's modulus (E), yield stress (σ_y), ultimate strength (σ_u), ultimate strain (ε_u) and toughness (u_f) are outlined in Table 5.5. The samples tested were the fiber layer of the FMS (Figure 5.12a), the FMS film (Figure 5.12b), the complete FMS (Figure 5.12c), the F_D film (Figure 5.12d) and the F_E film (Figure 5.12e).

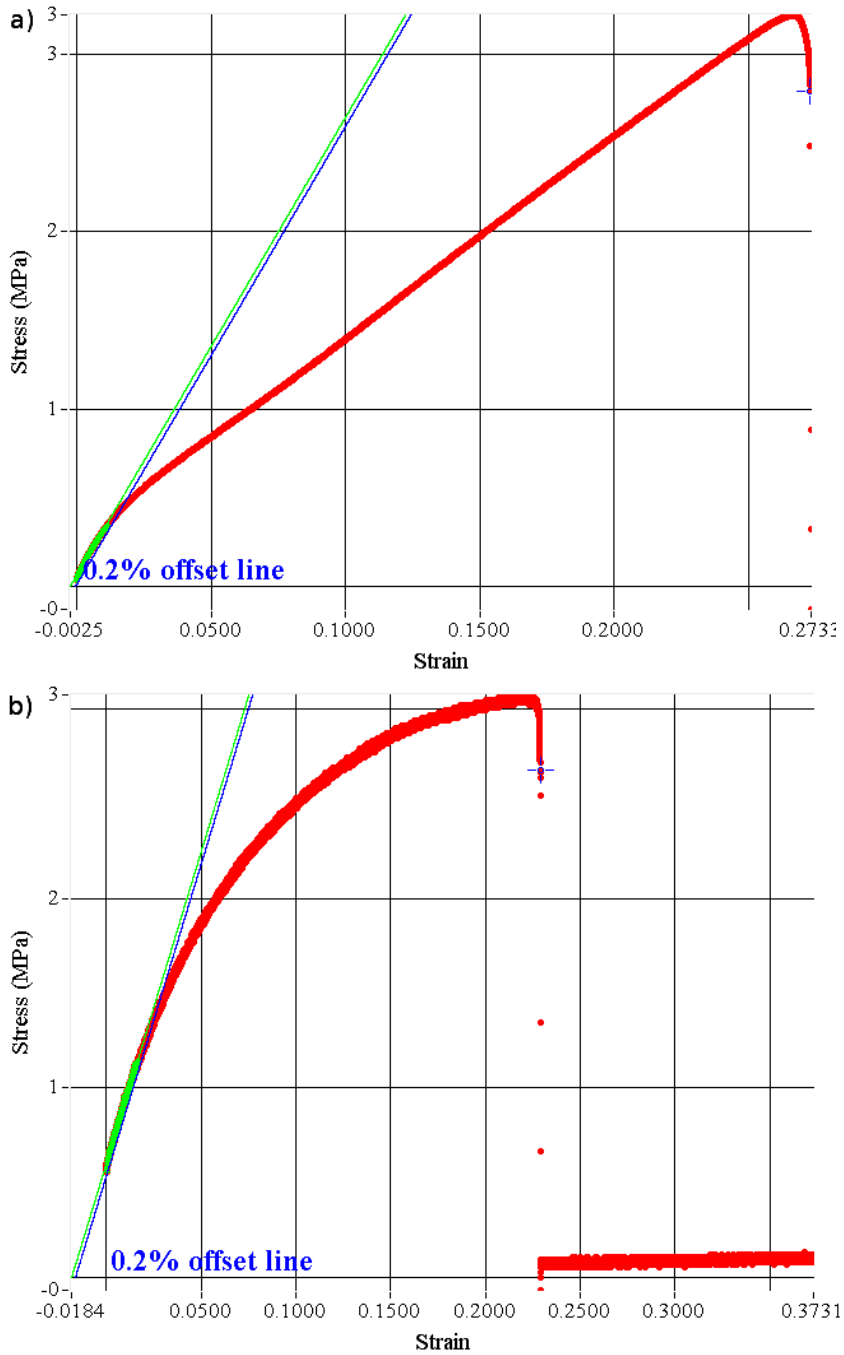
The drug-loaded fiber layer (Figure 5.12a) exhibited the smallest yield stress, ultimate strain and toughness. The Young's modulus of the fiber layer was greater than that of the F_E film (Figure 5.12e) but smaller than the other tested samples, suggesting that it was more flexible than the film onto which it was incorporated but less flexible than the F_E film. When compared to the F_E film, which was prepared using the same components at the same ratios, the fiber layer was found to have a larger Young's modulus and a considerably smaller yield stress, ultimate strength, ultimate strain and toughness, as well as a smaller elastic region (green portion of nanotensile profile), which may be attributed to the elongating forces experienced by polymer chains during electrospinning (Lu et al., 2008; Baji et al., 2010). When a polymer is exposed to greater elongating forces, the fibers that are formed will have smaller diameters, which have also been associated with a larger Young's modulus and hence a greater stiffness (Arinstein et al., 2007). It can therefore be deduced that the differences between the tensile properties of the fiber layer and the F_E film are due to polymer chain stretching during fiber formation.

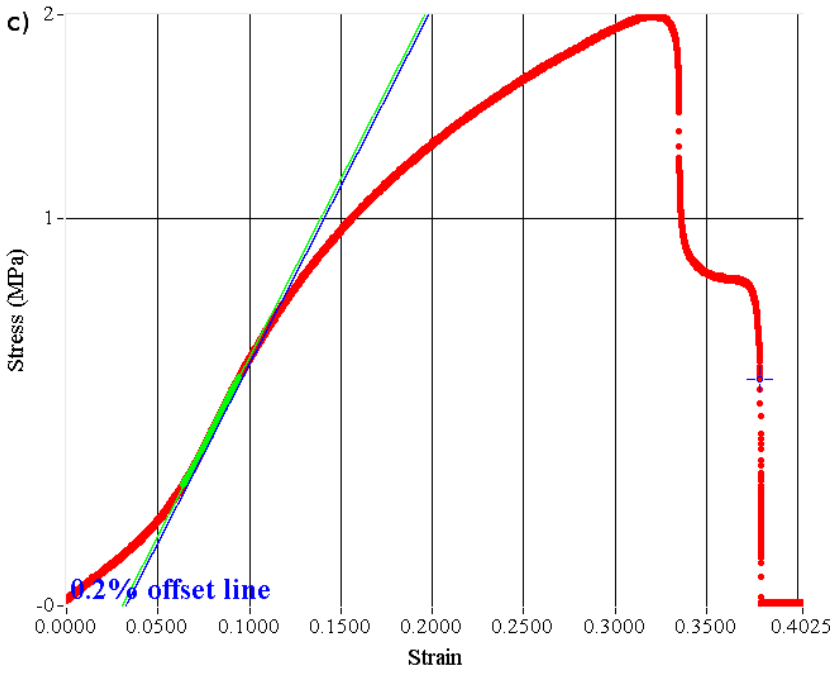
Table 5.5: Experimental values obtained from nanotensile analysis of the FMS and various films

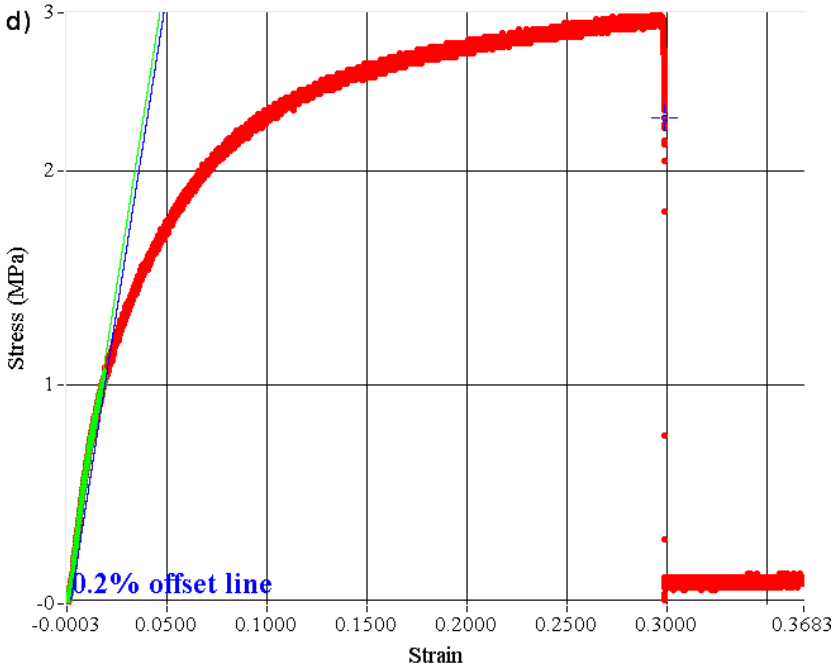
Sample	E (MPa)	σ_y (MPa)	σ_u (MPa)	ε_u	u_f (J/cm^3)
Fiber Layer	26.09	0.49	2.98	0.227	0.38
FMS Film	36.01	1.675	3.33	0.242	0.62
FMS	30.31	1.18	2.79	0.238	0.48
F_D	56.35	1.13	2.73	0.314	0.71
F_E	20.34	1.10	3.52	0.731	2.10

The FMS film (Figure 5.12b) revealed slightly larger values than the fiber layer for the various responses determined during nanotensile testing. This may be due to the presence of the more rigid polymer, HPMC, in the film. The profile for the FMS (Figure 5.12c) revealed two distinct points of fracture – the first one being the point at which the fiber layer fractured and the second where the film layer fractured. The F_D film (Figure

5.12d), which is the DPH-loaded FMS film, featured a substantially larger Young's modulus than the FMS film, suggesting that the presence of DPH in the formulation enhanced the rigidity of the film.




c)
2
1
-0
Stress (MPa)
0.2% offset line
0.0000
0.0500
0.1000
0.1500
0.2000
0.2500
0.3000
0.3500
0.4025
Strain


d)
3
2
1
-0
Stress (MPa)
0.2% offset line
-0.0003
0.0500
0.1000
0.1500
0.2000
0.2500
0.3000
0.3683
Strain

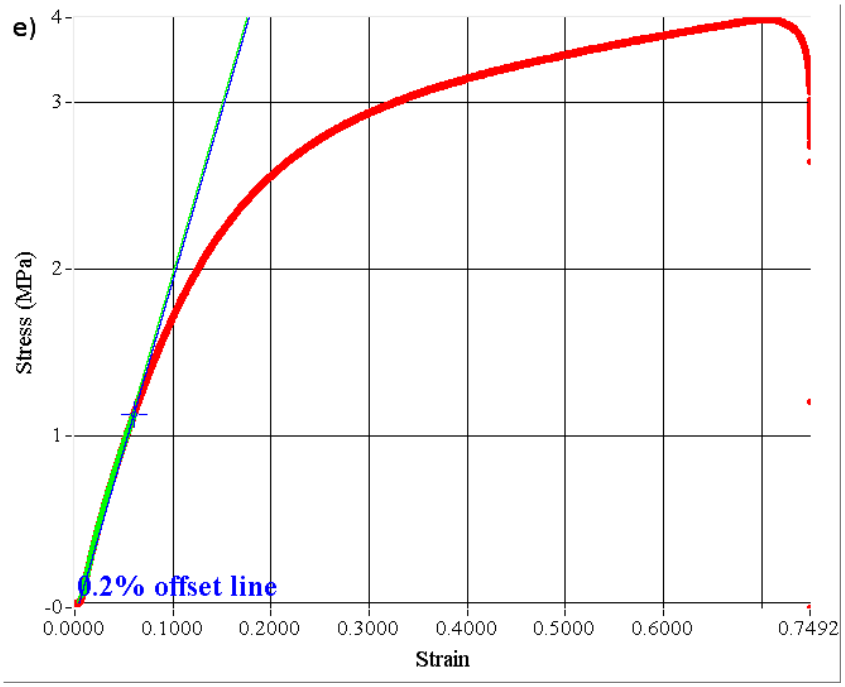


Figure 5.12: Stress-strain nanotensile profiles of the (a) drug-loaded fiber layer, (b) FMS film, (c) FMS, (d) drug-loaded F_D film and (e) drug-loaded F_E film

The results of nanotensile testing were in agreement with the extensibility results in the previous section. However, the two tests were performed disparately and with varying sensitivity. The extensibility test utilized a large sample area, imbedded a probe into the sample until fracture and measured the force-distance relationship. Whereas the nanotensile test employed only a small sample area, pulled the sample apart until fracture and measured the stress-strain relationship, from which various parameters, such as Young's modulus, yield stress and toughness, could be calculated. While both tests are useful, the nanotensile test was more applicable for this particular formulation due to the method of testing, type of results produced and the augmented sensitivity of the test.

5.3.11. Analysis of the Stress-Strain Rheological Parameters of the Components of the FMS

5.3.11.1. Rheological Analysis of the Optimized FMS and Drug-Loaded Film Formulations

The rheological properties of a hydrated sample play an important role in the retention of that sample within the buccal cavity (Eouani et al., 2001; Zaman et al., 2008). The hydrated film and FMS samples were investigated for the effect of an increasing shear rate ($\dot{\gamma}$) on shear force (τ) and viscosity (η). The average values over the shear rate range for these parameters are outlined in Table 5.6. Linear rheological profiles are depicted in Figure 5.13. The F_E film (Figure 5.13c) exhibited an exceedingly larger

average viscosity and shear force than the FMS (Figure 5.13a) and F_D film (Figure 5.13b), which correlates with the greater mucoadhesive properties and slower disintegration rate evinced by this film. However, such a high viscosity may result in an unpleasant mouth-feel *in vivo* (Malone et al., 2003). The large disparity between the parameters of the FMS and F_E film may be due to the more rapid disintegration rate of the former. Nevertheless, the rheological properties of the FMS suggest that it would have an adequate retention time, which is in agreement with the mucoadhesion data.

Table 5.6: Average rheological parameters of the FMS, F_D film and F_E film in 1mL simulated saliva (pH 6.75)

Sample	**Shear Rate (1/s)**	**Shear Force (Pa)**	**Viscosity (mPa.s)**
FMS	254.3	7.44	32.29
F_D	252.3	7.39	30.49
F_E	253.2	82.71	1616.67

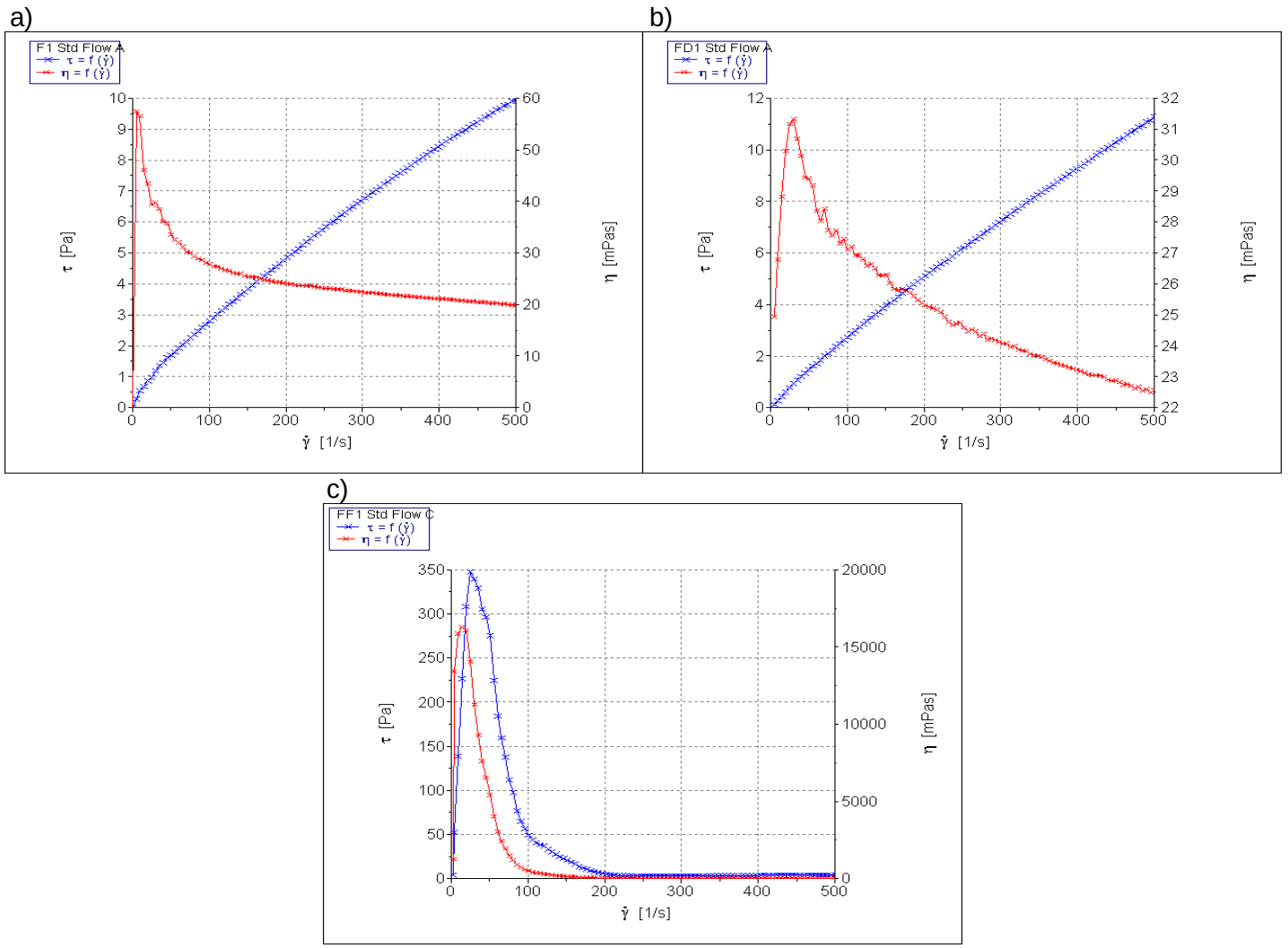


Figure 5.13: Linear rheological profiles of the (a) FMS, (b) F_D film and (c) F_E film

5.3.11.2. Rheological Analysis of the Electrospinning Solution

The rheological properties of a solution employed for electrospinning can have a substantial effect on the process of electrospinning as well as the quality and morphology of fibers that are formed (Tao and Shivkumar, 2007). The degree of polymer chain entanglements, and hence the polymer concentration, has a considerable influence over the viscosity of a solution (Ramakrishna et al., 2005). The actual conformation of individual polymer chains also has a significant influence on solution viscosity, considering that solutions containing coiled chains have a lower viscosity than those with extended chains (Ramakrishna et al., 2005). It is therefore important to investigate the rheological properties of polymeric solutions employed in electrospinning.

The 25%$^{w}/_{v}$ PVA solution that was electrospun to form the fiber layer of the FMS was analyzed for responses to rheological stresses, both linear and oscillating. The average shear force (τ) and viscosity (η) was 186.40Pa and 737.5mPa.s, respectively, for an average shear rate ($\dot{\gamma}$) of 252.3/s. Figure 5.14 displays the rheological profile. The linear rheological properties of the 25%$^{w}/_{v}$ solution were deemed acceptable for electrospinning because adequate fiber formation occurred at that polymer concentration.

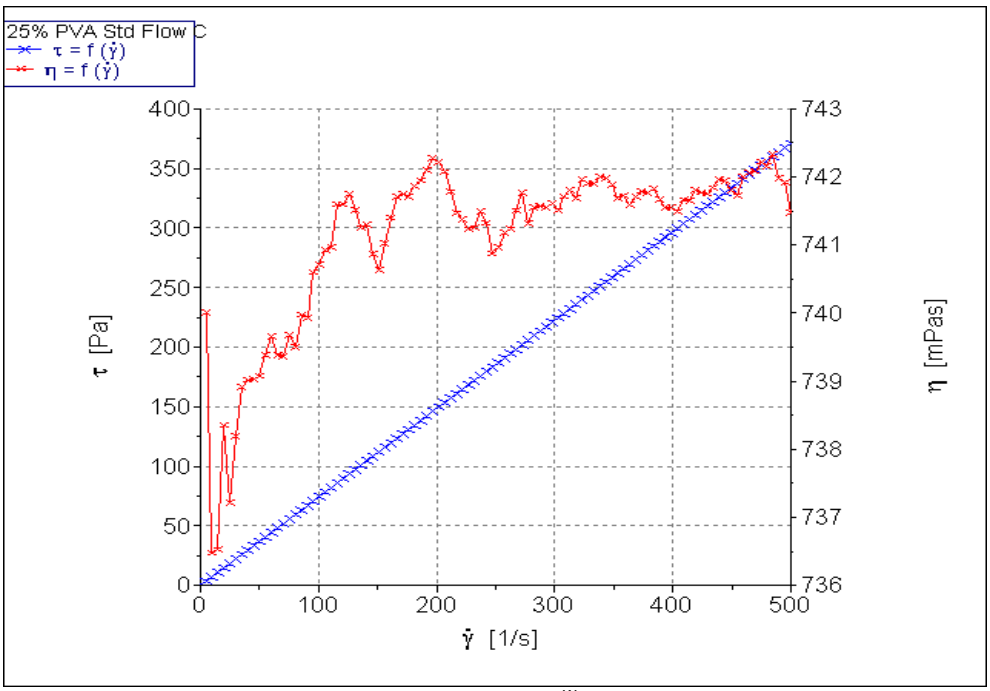


Figure 5.14: Linear rheological profile of the 25%$^{w}/_{v}$ PVA electrospinning solution

Thixotropy is when the viscosity of a material, that was at rest, decreases on exposure to a mechanical stress and consequently increases again upon removal of the stress (Barnes, 1997; Mewis and Wagner, 2009). The thixotropy of the 25%$^{w}/_{v}$ PVA electrospinning solution was determined by calculating the difference between the AUC values of the increasing shear and decreasing shear rate curves and was determined to be -1.229Pa.s^{-1}. This difference is relatively small when compared to the average AUC, which was 757.4Pa.s^{-1} and it was deduced that the electrospinning solution underwent adequate recovery. Figure 5.15 displays the thixotropy curve for the 25% PVA solution. The curves of shear stress as a function of shear rate (blue line) for both increasing and decreasing rates follow an almost identical path and appear as one thick line, suggesting a favorable recovery of the sample.

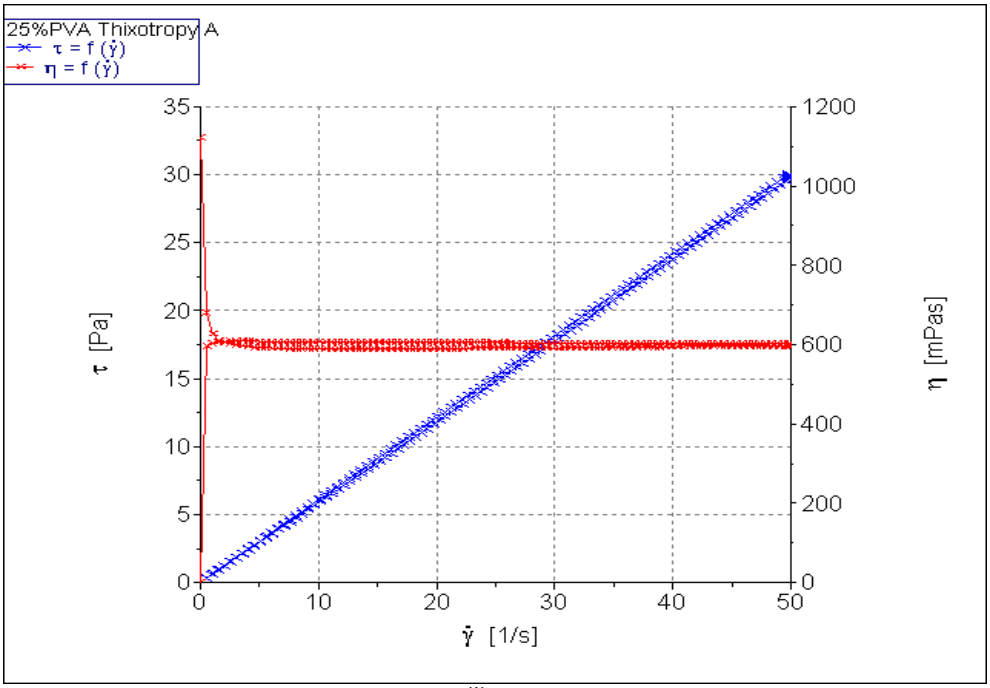


Figure 5.15: Thixotropy curve for the 25%$^{w}/_{v}$ PVA solution used for electrospinning

Viscoelasticity is an important factor to be considered for the electrospinning of a polymer solution as the polymer is required to be stretched in order to produce fibers. It is necessary for the elastic properties of a solution to be great enough so that the fiber jet will not break up before reaching the collector surface (Eggers and Villermaux, 2008). Oscillation rheology testing is a useful tool for assessing the viscoelastic behavior of materials intended for electrospinning. The yield stress (τ_o) was determined for the 25%$^{w}/_{v}$ PVA electrospinning solution at 25°C by measuring the deformation (γ) over a range of controlled stress (τ). The average yield stress was 0.3782Pa and the rheological plot is depicted in Figure 5.16. In order to determine the viscoelastic region of the 25%$^{w}/_{v}$ PVA electrospinning solution, a stress sweep was performed at various

frequencies to ascertain the yield point. The yield point was found to be 6.36Pa at a frequency of 0.1Hz and is depicted graphically in Figure 5.17. A frequency sweep was performed in order to determine the stability of the 25%$^{w}/_{v}$ PVA solution. The frequency of oscillations was ranged from 8 to 0.008Hz at a constant stress. The resulting plot is depicted in Figure 5.18.

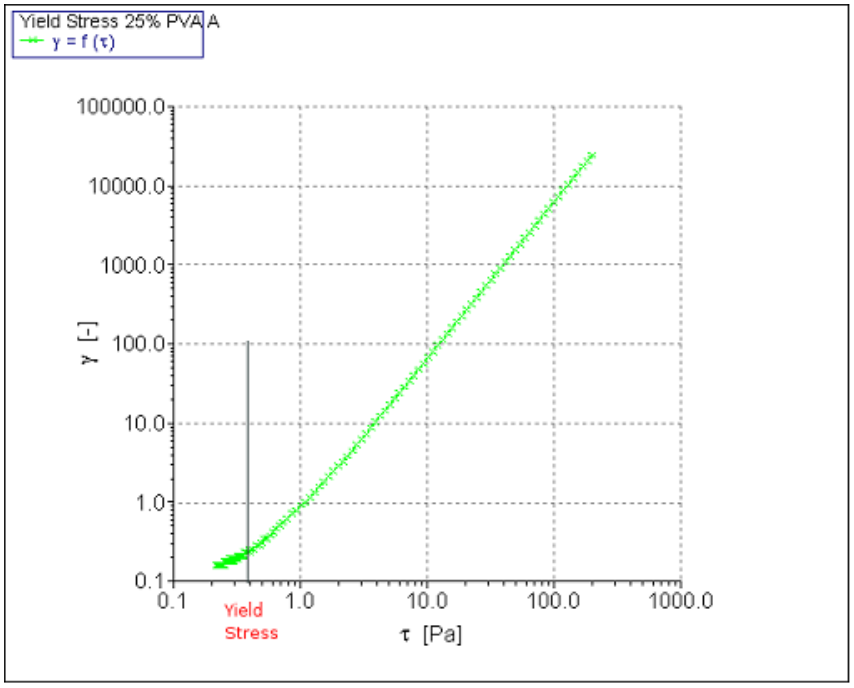


Figure 5.16: Rheology plot depicting the yield stress (at 0.3782Pa) of a 25%$^{w}/_{v}$ PVA solution intended for electrospinning

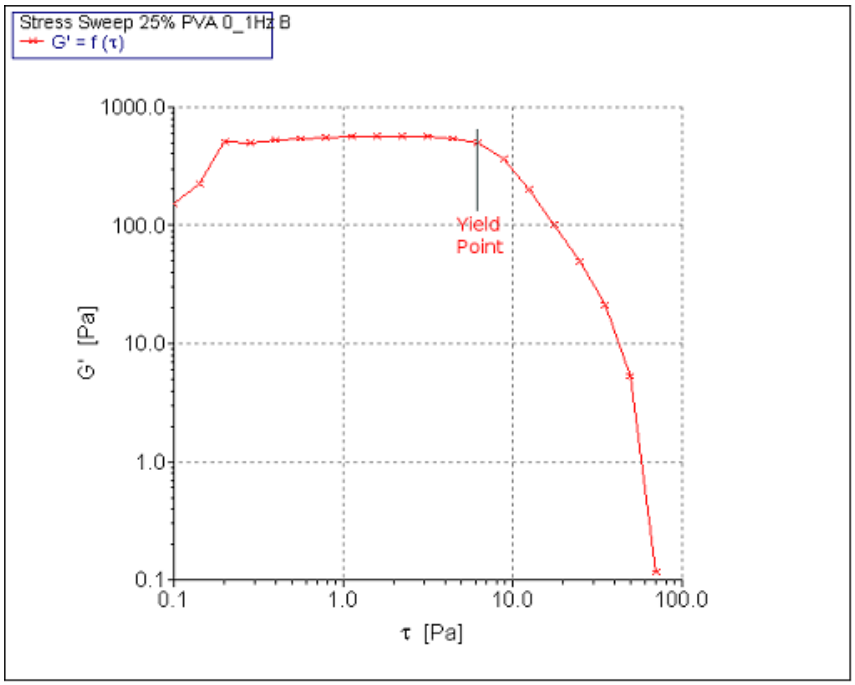


Figure 5.17: Rheological plot depicting the yield point in a stress sweep of a 25%$^{w}/_{v}$ PVA solution

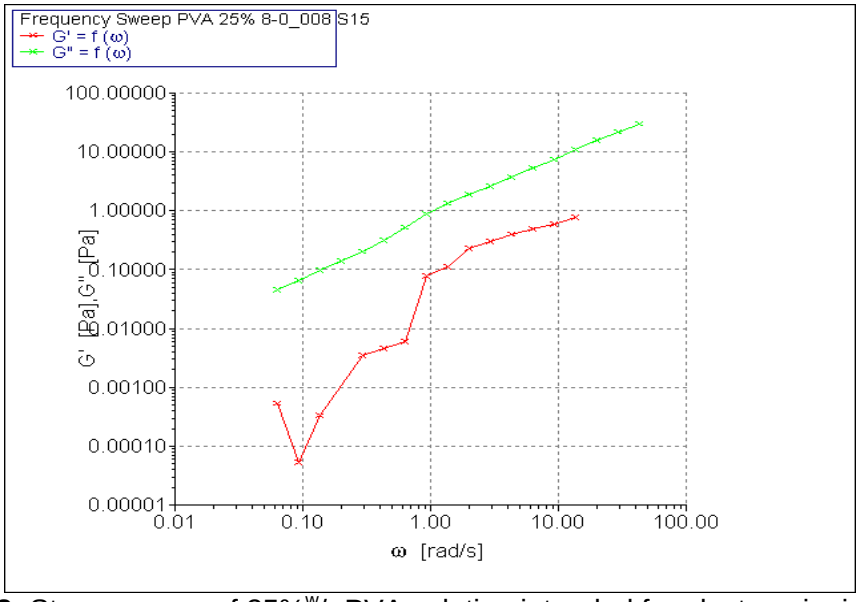


Figure 5.18: Stress sweep of 25%$^{w}/_{v}$ PVA solution intended for electrospinning

5.3.12. Vibrational Chemical Structure Analysis

FTIR spectroscopy is a propitious tool for determining whether two or more components exist together as a mixture or if there is a chemical interaction (Bourtoom and Chinnan, 2008). FTIR is the analysis of the infrared spectrum, which is formed by measuring the absorption of electromagnetic radiation over a range of frequencies. The radiation is absorbed by molecules at the frequencies of the vibrations of the chemical bonds within (Coates, 2000). FTIR analysis was performed in order to determine whether any chemical changes occurred to the drug and/or polymer during the process of electrospinning.

The molecular structures of DPH and PVA are depicted in Figure 5.19. The FTIR spectra for the DPH-loaded fiber layer (DF), DPH and non-drug-loaded PVA placebo fibers (PF) are depicted in Figure 5.20. The broad O-H stretching vibration of PVA (Figure 5.19b) can clearly be seen for both DF and PF at 3295cm^{-1}. DPH and DF both show a small peak at 3033cm^{-1}, characteristic of the phenyl groups present in the DPH molecule (Figure 5.19a). The phenyl groups are also identified by the presence of large peaks at 755cm^{-1} and 702cm^{-1} in both profiles where DPH was present. The peak associated with the stretching vibration of the alkoxy substituent in the DPH molecule at 2955cm^{-1} is obscured by the slightly broader band of the alkyl group of the PVA molecule at 2913cm^{-1} in the DF spectrum, which can also be seen in the PF spectrum. The broad peaks at 2594cm^{-1}, 2524cm^{-1} and 2487cm^{-1} in the DPH spectrum, representative of the tertiary amine group, are also visible in the DF spectrum, but not in

the PF spectrum. The peak at 1598cm^{-1}, indicating the absorption from the phenyl groups, is visible in both the DPH and DF spectra. From the FTIR data, it can be concluded that no significant chemical changes occurred to the drug during solution preparation and electrospinning.

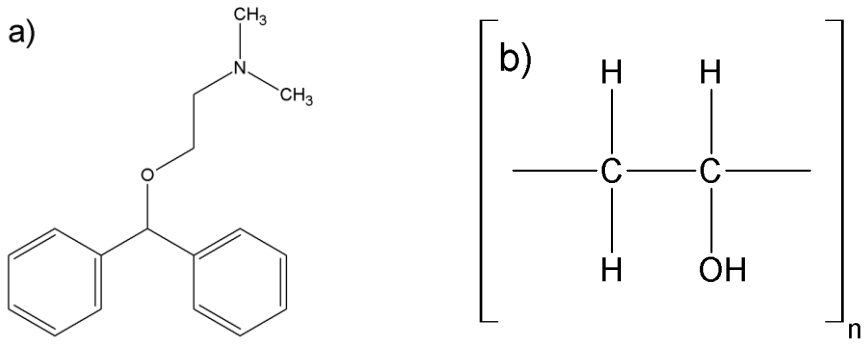


Figure 5.19: Molecular structures of (a) DPH and (b) PVA

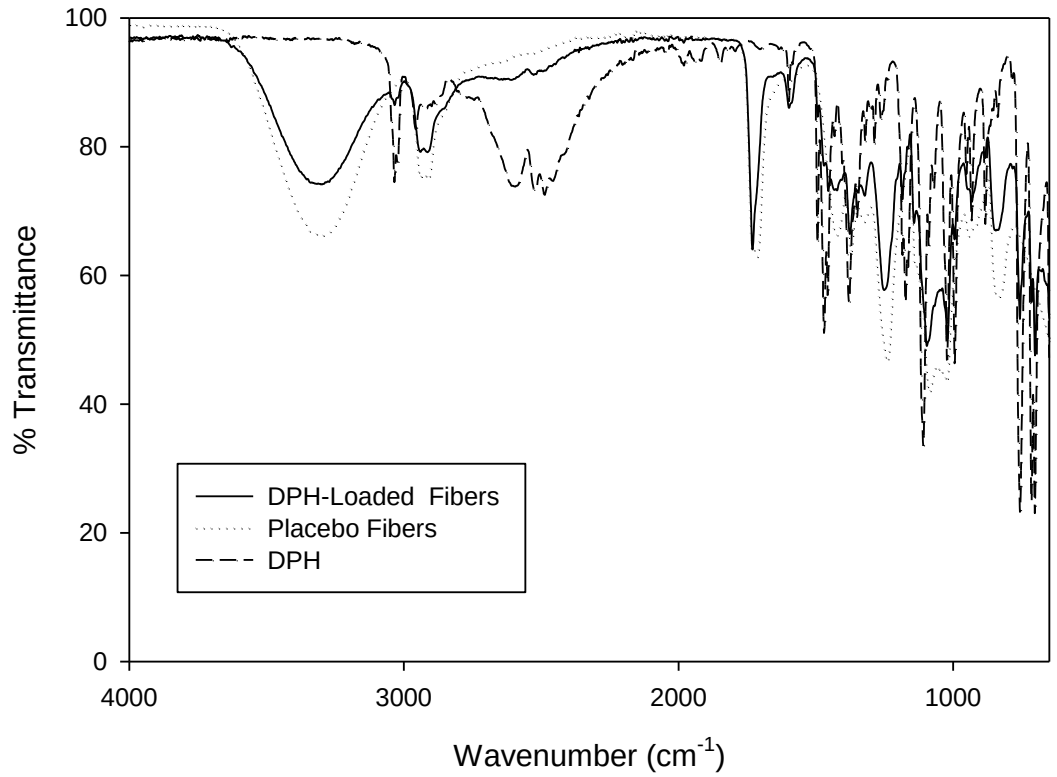


Figure 5.20: FTIR profiles of the drug-loaded fibers (DF), placebo fibers (PF) and DPH

5.4. Concluding Remarks

An optimized FMS formulation was prepared by electrospinning drug-loaded PVA fibers directly onto a thin polymeric film consisting of PVA and HPMC. The physicochemical and physicomechanical characteristics of the FMS were assessed. The FMS exhibited rapid disintegration and drug release, mucoadhesion, oramucosal retention, flexibility

and minimal mucosal irritation due to pH variation. The FMS was found to be flexible and extensible on physicomechanical analysis. Furthermore, upon FTIR analysis, it was elucidated that no significant chemical interactions occurred between drug, polymer and excipients during the process of formulation preparation. The FMS may therefore be deemed suitable for rapid oramucosal drug delivery.

CHAPTER 6

CONCLUSIONS AND RECOMMENDATIONS

6.1. Conclusions

This study designed, developed and analyzed a porous Fibrous Matrix System (FMS), consisting of drug-loaded electrospun fibers incorporated directly onto a polymeric backing film, which has been evidenced to possess considerable potential in rapid oral transmucosal drug delivery.

Preliminary studies were conducted and polyvinylalcohol (PVA) was found to be the most suitable polymer for the formation of the drug-loaded fiber layer for the purposes of this study. Diphenhydramine (DPH) and zidovudine (AZT) were employed as the model drugs. Ideal DPH-loaded PVA fibers were produced by dissolving DPH (10%$^{w}/_{v}$), citric acid (2%$^{w}/_{v}$) and glycerol (5%$^{v}/_{v}$) directly in the 25%$^{w}/_{v}$ PVA solution and subsequently electrospinning. Preliminary studies on the polymeric backing film layer of the FMS revealed that combinations of PVA and hydroxypropylmethylcellulose (HPMC) were optimal for film-formation for the purposes of this study. Variables for the formulation of adequate films were obtained and employed in a 3-factor Box-Behnken experimental design in order to optimize the backing film layer in terms of drug release from the fiber layer, mucoadhesion and disintegration time. The effects of the independent variables on the dependent response variables were assessed and an optimized formulation was mathematically determined.

The optimized FMS exhibited mucoadhesiveness, a rapid rate of disintegration and accelerated drug release. Favorable rheological properties, flexibility, extensibility, minimal pH variation and an absence of significant chemical changes characterized the optimized FMS. From the results of physicochemical and physicomechanical analysis, the FMS was deemed suitable for application in rapid oramucosal drug delivery.

The FMS developed in this study may be regarded as suitable for rapid oramucosal drug delivery and is considered able to overcome some of the inherent disadvantages of oral drug delivery, particularly for pediatric and geriatric patients, who experience difficulty in swallowing large tablets and capsules. The FMS may also be capable of overcoming some of the limitations of current rapidly dissolving systems such as wafers.

6.2. Recommendations

Although the FMS was developed and optimized employing DPH as a model drug, it is not limited in its application to the delivery of this drug, but may be relevant for the oramucosal delivery of a variety of drugs, particularly those requiring a rapid onset of action. Such drugs may include, but should not necessarily be limited to, sleep inducers, anxiolytics, antihistamines, antiemetics, analgesics and antianginal agents. The FMS may also find application in the delivery of drugs that do not necessarily require a rapid onset of action, but tend to be problematic for administration to pediatric or geriatric patients due to poor stability in a liquid formulation as the FMS is a solid delivery system that does not require swallowing. Such drugs may include antibiotics, antiretrovirals and other antiviral agents.

Large variations in drug-loading were observed for the FMS, which were due to the uneven deposition of the drug-loaded fibers during electrospinning. Further electrospinning method and formulation development is therefore required in order to temper the regularity of the fiber layer and, hence, achieve more accurate drug dosing.

Furthermore, the drug-loading capability of the FMS was relatively low and additional studies would thus need to be conducted in order to increase the potential dosing capacity of the FMS.

The present study did not include an *in vivo* component and future work should therefore focus on assessing the FMS for *in vivo* drug release characteristics and suitability.

Zidovudine (AZT), the model drug that was originally applied in this study, exhibited poor permeability, and incorporation of penetration enhancing agents was complicated by their detrimental effect on fiber formation by electrospinning. Further studies involving the incorporation of penetration enhancers into the electrospun fiber layer should therefore be conducted in order to improve the permeation of less permeable drugs.

REFERENCES

1. Abrams, J., 1983. New nitrate delivery systems: Buccal nitroglycerin. American Heart Journal, 105, 848-854.
2. Agarwal, S., Wendorff, J.H., Greiner, A., 2008. Use of electrospinning technique for biomedical applications. Polymer, 49, 5603-5621.
3. Ahn, Y.C., Park, S.K., Kim, G.T., Hwang, Y.J., Lee, C.G., Shin, H.S., Lee, J.K., 2006. Development of high efficiency nanofilters made of nanofibers. Current Applied Physics, 6, 1030-1035.
4. Ali, A.A., 2008. New generation of super absorber nano-fibroses hybrid fabric by electro-spinning. Journal of Materials Processing Technology, 199, 193-198.
5. Allaoui, A., Hoa, S.V., Pugh, M.D., 2008. The electronic transport properties and microstructure of carbon nanofiber/epoxy composites. Composites Science and Technology, 68, 410-416.
6. Andrews, G.P., Laverty, T.P., Jones, D.S., 2009. Mucoadhesive polymeric platforms for controlled drug delivery. European Journal of Pharmaceutics and Biopharmaceutics, 71, 505-518.
7. Arinstein, A., Burman, M., Gendelman, O., Zussman, E., 2007. Effect of supramolecular structure on polymer nanofiber elasticity. Nature Nanotechnology, 2, 59-62.
8. Aungst, B.J., 1999. P-glycoprotein, secretory transport, and other barriers to the oral delivery of anti-HIV drugs. Advanced Drug Delivery Reviews, 39, 105-116.
9. Azarmi, S., Roa, W., Löbenberg, R., 2007. Current perspectives in dissolution testing of conventional and novel dosage forms. International Journal of Pharmaceutics, 328, 12-21.
10. Bai, J., Li, Y., Li, M., Wang, S., Zhang, C., Yang, Q., 2008. Electrospinning method for the preparation of silver chloride nanoparticles in PVP nanofiber. Applied Surface Science, 254, 4520-4523.
11. Baji, A., Mai, Y.-W., Wong, S.-C., Abtahi, M., Chen, P., 2010. Electrospinning of polymer nanofibers: Effects on oriented morphology, structures and tensile properties. Composites Science and Technology, 70, 703-718.
12. Barnes, H.A., 1997. Thixotropy – a review. Journal of Non-Newtonian Fluid Mechanics, 70,1-33.
13. Baumgarten, P.K., 1971. Electrostatic spinning of acrylic microfibers. Journal of Colloid and Interface Science, 36, 71-79.

14. Beachley, V., Wen, X., 2009. Effect of electrospinning parameters on the nanofiber diameter and length. Materials Science and Engineering C, 29, 663-668.
15. Bhardwaj, N., Kundu, S.C., 2010. Electrospinning: A fascinating fiber fabrication technique. Biotechnology Advances, 28, 325-347.
16. Bottenberg, P., Cleymaet, R., De Muynck, C., Remon, J.P., Coomans, D., Michotte, Y., Slop, D., 1991. Development and testing of bioadhesive, fluoride-containing slow-release tablets for oral use. Journal of Pharmacy and Pharmacology, 43, 457-464.
17. Bourtoom, T., Chinnan, M.S., 2008. Preparation and properties of rice starch-chitosan blend biodegradable film. LWT – Food Science and Technology, 41, 1633-1641.
18. Box, G.E.P., Behnken, D.W., 1960. Some new three level designs for the study of quantitative variables. Technometrics, 2, 455-475.
19. Bredenberg, S., Duberg, M., Lennernäs, B., Lennernäs, H., Pettersson, A., Westerberg, M., Nyström, C., 2003. In vitro and in vivo evaluation of a new sublingual tablet system for rapid oromucosal absorption using fentanyl citrate as the active substance. European Journal of Pharmaceutical Sciences, 20, 327-334.
20. Bruner, L., Tolloczko, St., 1901. Über die Auflösungsgeschwindigkeit fester Körper. Zeitschrift für Anorganische Chemie, 28, 314-330.
21. Cappello, B., De Rosa, G., Giannini, L., La Rotonda, I.M., Mensitieri, G., Miro, A., Quaglia, F., Russo, R., 2006. Cyclodextrin-containing poly(ethylene oxide) tablets for the delivery of poorly soluble drugs: Potential as buccal delivery system. International Journal of Pharmaceutics, 319, 63-70.
22. Carli, F., Capone, G., Colombo, I., Magarotto, L., Motta, A., 1984. Surface and transport properties of acrylic polymers influencing drug release from porous matrices. International Journal of Pharmaceutics, 21, 317-329.
23. Casper, C.L., Stephens, J.S., Tassi, N.G., Chase, D.B., Rabolt, J.F., 2004. Controlling surface morphology of electrospun polystyrene fibers: Effect of humidity and molecular weight on the electrospinning process. Macromolecules, 37, 573-578.
24. Chan, B.P., Leong, K.W., 2008. Scaffolding in tissue engineering: general approaches and tissue-specific considerations. European Spine Journal, 17, S467-S479.
25. Chandrasekhar, R., Hassan, Z., AlHusban, F., Smith, A.M., Mohammed, A.R., 2009. The role of formulation excipients in the development of lyophilised fast-disintegrating tablets. European Journal of Pharmaceutics and Biopharmaceutics, 72, 119-129.

26. Chen, Q.Z., Thompson, I.D., Boccaccini, A.R., 2006. 45S5 Bioglass®-derived glass-ceramic scaffolds for bone tissue engineering. Biomaterials, 27, 2414-2425.
27. Chen, J.-P., Chang, G.-Y., Chen, J.-K., 2008. Electrospun collagen/chitosan nanofibrous membrane as wound dressing. Colloids and Surfaces A: Physicochemical and Engineering Aspects, 313-314, 183-188.
28. Chew, S.Y., Wen, J., Yim, E.K.F., Leong, K.W., 2005. Sustained release of proteins from electrospun biodegradable fibers. Biomacromolecules, 6, 2017-2024.
29. Chew, S.Y., Mi, R., Hoke, A., Leong, K.W., 2008. The effect of the alignment of electrospun fibrous scaffolds on Schwann cell maturation. Biomaterials, 29, 653-661.
30. Chopra, S., Motwani, S.K., Iqbal, Z., Talegaonkar, S., Ahmad, F.J., Khar, R.K., 2007. Optimisation of polyherbal gels for vaginal drug delivery by Box-Behnken statistical design. European Journal of Pharmaceutics and Biopharmaceutics, 67, 120-131.
31. Chu, B., Liang, D., Hadjiargyrou, M., Hsiao, B.S., 2006. A new pathway for developing *in vitro* nanostructured non-viral gene carriers. Journal of Physics: Condensed Matter, 18, S2513-S2525.
32. Chunder, A., Sarkar, S., Yu, Y., Zhai, L., 2007. Fabrication of ultrathin polyelectrolyte fibers and their controlled release properties. Colloids and Surfaces B: Biointerfaces, 58, 172-179.
33. Coates, J., 2000. Interpretation of infrared spectra, a practical approach. In: Meyers, R.A. (Ed.), Encyclopedia of Analytical Chemistry, John Wiley and Sons, Ltd, Chichester, pp. 10815-10837.
34. Coviello, T., Alhaique, F., Parisi, C., Matricardi, P., Bocchinfuso, G., Grassi, M., 2005. A new polysaccharidic gel matrix for drug delivery: preparation and mechanical properties. Journal of Controlled Release, 102, 643-656.
35. Deitzel, J.M., Kleinmeyer, J., Harris, D., Beck Tan, N.C., 2001. The effect of processing variables on the morphology of electrospun nanofibers and textiles. Polymer, 42, 261-272.
36. Deng, X.-L., Sui, G., Zhao, M.-L., Chen, G.-Q., Yang, X.-P., 2007. Poly(L-lactic acid)/hydroxyapatite hybrid nanofibrous scaffolds prepared by electrospinning. Journal of Biomaterials Science. Polymer Edition, 18, 117-130.
37. Deschepper, E., Thas, O., Ottoy, J.P., 2006. Regional residual plots for assessing the fit of linear regression models. Computational Statistics and Data Analysis, 50, 1995-2013.

38. Ding, B., Kim, J., Miyazaki, Y., Shiratori, S., 2004. Electrospun nanofibrous membranes coated quartz crystal microbalance as gas sensor for NH_3 detection. Sensors and Actuators B, 101, 373-380.
39. Dixit, R.P., Puthli, S.P., 2009. Oral strip technology: Overview and future potential. Journal of Controlled Release, 139, 94-107.
40. Dokoumetzidis, A., Macheras, P., 2006. A century of dissolution research: From Noyes and Whitney to the Biopharmaceutics Classification System. International Journal of Pharmaceutics, 321, 1-11.
41. Doshi, J., Reneker, D.H., 1995. Electrospinning process and applications of electrospun fibers. Journal of Electrostatics, 35, 151-160.
42. Eggers, J., Villermaux, E., 2008. Physics of liquid jets. Reports on Progress in Physics, 71, 036601.
43. Eouani, C., Piccerelle, Ph., Prinderre, P., Bourret, E., Joachim, J., 2001. In-vitro comparative study of buccal mucoadhesive performance of different polymeric films. European Journal of Pharmaceutics and Biopharmaceutics, 52, 45-55.
44. Ferreira, S.L.C., Bruns, R.E., Ferreira, H.S., Matos, G.D., David, J.M., Brandão, G.C., da Silva, E.G.P., Portugal, L.A., dos Reis, P.S., Souza, A.S., dos Santos, W.N.L., 2007. Box-Behnken design: An alternative for the optimization of analytical methods. Analytica Chimica Acta, 597, 179-186.
45. Figueiras, A., Hombach, J., Veiga, F., Bernkop-Schnürch, A., 2009. In vitro evaluation of natural and methylated cyclodextrins as buccal permeation enhancing system for omeprazole delivery. European Journal of Pharmaceutics and Biopharmaceutics, 71, 339-345.
46. Fong, H., Chun, I., Reneker, D.H., 1999. Beaded nanofibers formed during electrospinning. Polymer, 40, 4585-4592.
47. Formhals, A., 1934. Process and apparatus for preparing artificial threads. US Patent 1 975 504, 2 Oct.
48. Formhals, A., 1939. Method and apparatus for spinning. US Patent 2 160 962, 6 Jun.
49. Formhals, A., 1940. Artificial thread and method of producing same. US Patent 2 187 306, 16 Jan.
50. Formhals, A., 1943. Production of artificial fibers from fiber forming liquids. US Patent. 2 323 025, 29 Jun.
51. Frenot, A., Chronakis, I.S., 2003. Polymer nanofibers assembled by electrospinning. Current Opinion in Colloid and Interface Science, 8, 64-75.
52. Giannola, L.I., De Caro, V., Giandalia, G., Siragusa, M.G., Tripodo, C., Florena, A.M., Campisi, G., 2007. Release of naltrexone on buccal mucosa: Permeation

studies, histological aspects and matrix system design. European Journal of Pharmaceutics and Biopharmaceutics, 67, 425-433.

53. Gong, J., Shao, C.-L., Yang, G.-C., Pan, Y., Qu, L.-Y., 2003. Preparation of ultra-fine fiber mats contained $H_4SiW_{12}O_{40}$. Inorganic Chemistry Communications, 6, 916-918.
54. He, C.-L., Huang, Z.-M., Han, X.-J., Liu, L., Zhang, H.-S., Chen, L.-S., 2006. Coaxial electrospun poly(L-lactic acid) ultrafine fibers for sustained drug delivery. Journal of Macromolecular Science, Part B: Physics, 45, 515-524.
55. He, C.-L., Huang, Z.-M., Han, X.-J., 2009. Fabrication of drug-loaded electrospun aligned fibrous threads for suture applications. Journal of Biomedical Materials Research Part A, 89A, 80-95.
56. Hogan Jr., C.J., Biswas, P., 2008. Narrow size distribution nanoparticle production by electrospray processing of ferritin. Aerosol Science, 39, 432-440.
57. Hoogstraate, J.A.J., Wertz, P.W., 1998. Drug Delivery via the Buccal Mucosa. Pharmaceutical Science and Technology Today, 1, 309-316.
58. Huang, Z.-M., Zhang, Y.-Z., Kotaki, M., Ramakrishna, S., 2003. A review on polymer nanofibers by electrospinning and their applications in nanocomposites. Composites Science and Technology, 63, 2223-2253.
59. Huang, Z.-M,. He, C.-L., Yang, A., Zhang, Y., Han, X.-J., Yin, J., Wu, Q., 2006. Encapsulating drugs in biodegradable ultrafine fibers through co-axial electrospinning. Journal of Biomedical Materials Research Part A, 77A, 169-179.
60. Jarusuwannapoom, T., Hongrojjanawiwat, W., Jitjaicham, S., Wannatong, L., Nithitanakul, M., Pattamaprom, C., Koombhongse, P., Rangkupan, R., Supaphol, P., 2005. Effect of solvents on electro-spinnability of polystyrene solutions and morphological appearance of resulting electrospun polystyrene fibers. European Polymer Journal, 41, 409-421.
61. Jaworek, A., 2007. Micro- and nanoparticle production by electrospraying. Powder Technology, 176, 18-35.
62. Ju, Y.-W., Park, J.-H., Jung, H.-R., Cho, S.-J., Lee, W.-J., 2008. Electrospun $MnFe_2O_4$ nanofibers: Preparation and morphology. Composites Science and Technology, 68, 1704-1709.
63. Kalayci, V.E., Patra, P.K., Kim, Y.K., Ugbolue, S.C., Warner, S.B., 2005. Charge consequences in electrospun polyacrylonitrile (PAN) nanofibers. Polymer, 46, 7191-7200.
64. Kang, X., Pan, C., Xu, Q., Yao, Y., Wang, Y., Qi, D., Gu, Z., 2007. The investigation of electrospun polymer nanofibers as a solid-phase extraction

sorbent for the determination of trazodone in human plasma. Analytica Chimica Acta, 587, 75-81.

65. Karavas, E., Georgarakis, E., Bikiaris, D., 2006. Application of PVP/HPMC miscible blends with enhanced mucoadhesive properties for adjusting drug release in predictable pulsatile chronotherapeutics. European Journal of Pharmaceutics and Biopharmaceutics, 64, 115-126.
66. Kenawy, E.-R., Bowlin, G.L., Mansfield, K., Layman, J., Simpson, D.G., Sanders, E.H., Wnek, G.E., 2002. Release of tetracycline hydrochloride from electrospun poly(ethylene-co-vinylacetate), poly(lactic acid), and a blend. Journal of Controlled Release, 81, 57-64.
67. Kenawy, E.-R., Abdel-Hay, F.I., El-Newehy, M.H., Wnek, G.E., 2007. Controlled release of ketoprofen from electrospun poly(vinyl alcohol) nanofibers. Materials Science and Engineering A, 459, 390-396.
68. Kenawy, E.-R., Abdel-Hay, F.I., El-Newehy, M.H., Wnek, G.E., 2009. Processing of polymer nanofibers through electrospinning as drug delivery systems. Materials Chemistry and Physics, 113, 296-302.
69. Khil, M.-S., Cha, D.-I., Kim, H.-Y., Kim, I.-S., Bhattarai, N., 2003. Electrospun nanofibrous polyurethane membrane as wound dressing. Journal of Biomedical Materials Research Part B: Applied Biomaterials, 67B, 675-679.
70. Kim, K., Luu, Y.K., Chang, C., Fang, D., Hsiao, B.S., Chu, B., Hadjiargyrou, M., 2004. Incorporation and controlled release of a hydrophilic antibiotic using poly(lactide-co-glycolide)-based electrospun nanofibrous scaffolds. Journal of Controlled Release, 98, 47-56.
71. Kim, T.G., Lee, D.S., Park, T.G., 2007. Controlled protein release from electrospun biodegradable fiber mesh composed of poly(ε-caprolactone) and poly(ethylene oxide). International Journal of Pharmaceutics, 338, 276-283.
72. Langoth, N., Bernkop-Schnürch, A., Kurka, P., 2005. In vitro evaluation of various buccal permeation enhancing systems for PACAP (pituatary adenylate cyclase-activating polypeptide). Pharmaceutical Research, 22, 2045-2050.
73. Lee, C.H., Shin, H.J., Cho, I.H., Kang, Y.-M., Kim, I.A., Park, K.-D., Shin, J.-W., 2005. Nanofiber alignment and direction of mechanical strain affect the ECM production of human ACL fibroblast. Biomaterials, 26, 1261-1270.
74. Li, D., Xia, Y., 2004. Electrospinning of nanofibers: Reinventing the wheel? Advanced Materials, 16, 1151-1170.
75. Li, M., Han, G., Yang, B., 2008a. Fabrication of the catalytic electrodes for methanol oxidation on electrospinning-derived carbon fibrous mats. Electrochemistry Communications, 10, 880-883.

76. Li, X., Zhang, H., Li, H., Tang, G., Zhao, Y., Yuan, X., 2008b. Self-accelerated biodegradation of electrospun poly(ethylene glycol)-poly(L-lactide) membranes by loading proteinase K. Polymer Degradation and Stability, 93, 618-626.
77. Li, Z.-F., Blum, F.D., Bertino, M.F., Kim, C.-S., Pillalamarri, S.K., 2008c. One-step fabrication of a polyaniline nanofiber vapor sensor. Sensors and Actuators B, 134, 31-35.
78. Liang, D., Luu, Y.K., Kim, K., Hsiao, B.S., Hadjiargyrou, M., Chu, B., 2005. *In vitro* non-viral gene delivery with nanofibrous scaffolds. Nucleic Acids Research, 33, e170.
79. Liang, D., Hsiao, B.S., Chu, B., 2007. Functional electrospun nanofibrous scaffolds for biomedical applications. Advanced Drug Delivery Reviews, 59, 1392-1412.
80. Liao, S., Wang, W., Uo, M., Ohkawa, S., Akasaka, T., Tamura, K., Cui, F., Watari, F., 2005. A three-layered nano-carbonated hydroxyapatite/collagen/PLGA composite membrane for guided tissue regeneration. Biomaterials, 26, 7564-7571.
81. Liao, S., Murugan, R., Chan, C.K., Ramakrishna, S., 2008. Processing nanoengineered scaffolds through electrospinning and mineralization suitable for biomimetic bone tissue engineering. Journal of the Mechanical Behaviour of Biomedical Materials, 1, 252-260.
82. Liu, X., Won, Y., Ma, P.X., 2006. Porogen-induced surface modification of nano-fibrous scaffolds for tissue engineering. Biomaterials, 27, 3980-3987.
83. Llabot, J.M., Palma, S.D., Manzo, R.H., Allemandi, D.A., 2007. Design of novel antifungal mucoadhesive films Part II. Formulation and in vitro biopharmaceutical evaluation. International Journal of Pharmaceutics, 336, 263-268.
84. Loh, X.J., Peh, P., Liao, S., Sng, C., Li, J., 2010. Controlled drug release from biodegradable thermoresponsive physical hydrogel nanofibers. Journal of Controlled Release, 143, 175-182.
85. Lu, J.-W., Zhang, Z.-P., Ren, X.-Z., Chen, Y.-Z., Yu, J., Guo, Z.-X., 2008. High-elongation fiber mats by electrospinning of polyoxymethylene. Macromolecules, 41, 3762-3764.
86. Luong-Van, E., Grøndal, L., Chua, K.N., Leong, K.W., Nurcombe, V., Cool, S.M., 2006. Controlled release of heparin from poly(ε-caprolactone) electrospun fibers. Biomaterials, 27, 2042-2050.
87. Ma, Z., Kotaki, M., Yong, T., He, W., Ramakrishna, S., 2005. Surface engineering of electrospun polyethylene terephthalate (PET) nanofibers towards development of a new material for blood vessel engineering. Biomaterials, 26, 2527-2536.

88. Ma, K., Chan, C.K., Liao, S., Hwang, W.Y.K., Feng, Q., Ramakrishna, S., 2008. Electrospun nanofibers scaffolds for rapid and rich capture of bone marrow-derived hematopoietic stem cells. Biomaterials, 29, 2096-2103.
89. MacDiarmid, A.G., Jones Jr., W.E., Norris, I.D., Gao, J., Johnson Jr., A.T., Pinto, N.J., Hone, J., Han, B., Ko, F.K., Okuzaki, H., Llaguno, M., 2001. Electrostatically-generated nanofibers of electronic polymers. Synthetic Materials, 119, 27-30.
90. Madhav, N.V.S., Shakya, A.K., Shakya, P., Singh, K., 2009. Orotransmucosal drug delivery systems: A review. Journal of Controlled Release, 140, 2-11.
91. Malone, M.E., Appelqvist, I.A.M., Norton, I.T., 2003. Oral behaviour of food hydrocolloids and emulsions. Part 1. Lubrication and deposition considerations. Food Hydrocolloids, 17, 763-773.
92. Maquet, V., Boccaccini, AR., Pravata, L., Notingher, I., Jérôme, R., 2004. Porous poly(*α*-hydroxyacid)/Bioglass® composite scaffolds for bone tissue engineering. I: preparation and in vitro characterisation. Biomaterials, 25, 4185-4194.
93. Maretschek, S., Greiner, A., Kissel, T., 2008. Electrospun biodegradable nanofiber nonwovens for controlled release of proteins. Journal of Controlled Release, 127, 180-187.
94. McCarron, P.A., Donnelly, R.F., Zawislak, A., Woolfson, A.D., Price, J.H., McClelland, R., 2005. Evaluation of a water-soluble bioadhesive patch for photodynamic therapy of vulval lesions. International Journal of Pharmaceutics, 293, 11-23.
95. McKee, M.G., Wilkes, G.L., Colby, R.H., Long, T.E., 2004. Correlations of solution rheology with electrospun fiber formation of linear and branched polyesters. Macromolecules, 37, 1760-1767.
96. Meechaisue, C., Dubin, R., Supaphol, P., Hoven, V.P., Kohn, J., 2006. Electrospun mat of tyrosine-derived polycarbonate fibers for potential use as tissue scaffolding material. Journal of Biomaterials Science. Polymer Edition, 17, 1039-1056.
97. Megelski, S., Stephens, J.S., Chase, D.B., Rabolt, J.F., 2002. Micro- and nanostructured surface morphology on electrospun polymer fibers. Macromolecules, 35, 8456-8466.
98. Mewis, J., Wagner, N.J., 2009. Thixotropy. Advances in Colloid and Interface Science, 147-148, 214-227.
99. Miao, X., Tan, D.M., Li, J., Xiao, Y., Crawford, R., 2008. Mechanical and biological properties of hydroxyapatite/tricalcium phosphate scaffolds coated with poly(lactic-co-glycolic acid). Acta Biomaterialia, 4, 638-645.

100. Munasur, A.P., Pillay, V., Chetty, D.J., Govender, T., 2006. Statistical optimisation of the mucoadhesivity and characterisation of multipolymeric propranolol matrices for buccal therapy. International Journal of Pharmaceutics, 323, 43-51.
101. Munir, M.M., Suryamas, A.B., Iskandar, F., Okuyama, K., 2009. Scaling law on particle-to-fiber formation during electrospinning. Polymer, 50, 4935-4943.
102. Nafee, N.A., Ismail, F.A., Boraie, N.A., Mortada, L.M., 2003. Mucoadhesive buccal patches of miconazole nitrate: in vitro/in vivo performance and effect of ageing. International Journal of Pharmaceutics, 264, 1-14.
103. Nicolazzo, J.A., Reed, B.L., Finnin, B.C., 2005. Buccal penetration enhancers – How do they really work? Journal of Controlled Release, 105, 1-15.
104. Nieh, S., Nguyen, T., 1988. Effects of humidity, conveying velocity, and particle size on electrostatic charges of glass beads in a gaseous suspension flow. Journal of Electrostatics, 21, 99-114.
105. Oh, G.-Y., Ju, Y.-W., Kim, M.-Y., Jung, H.-R., Kim, H.J., Lee, W.-J., 2008. Adsorption of toluene on carbon nanofibers prepared by electrospinning. Science of the Total Environment, 393, 341-347.
106. Park, S.H., Kim, C., Choi, Y.O., Yang, K.S., 2003. Preparations of pitch-based CF/ACF webs by electrospinning. Carbon, 41, 2655-2657.
107. Patel, V.M., Prajapati, B.G., Patel, M.M., 2007. Formulation, evaluation and comparison of bilayered and multilayered mucoadhesive buccal devices of propranolol hydrochloride. AAPS PharmSciTech, 8, E147-E154.
108. Pawlowski, K.J., Belvin, H.L., Raney, D.L., Su, J., Harrison, J.S., Siochi, E.J., 2003. Electrospinning of a micro-air vehicle wing skin. Polymer, 44, 1309-1314.
109. Perioli, L., Ambrogi, V., Angelici, F., Ricci, M., Giovagnoli, S., Capuccella, M., Rossi, C., 2004. Development of mucoadhesive patches for buccal administration of ibuprofen. Journal of Controlled Release, 99, 73-82.
110. Pillay, V., Danckwerts, M.P., Bhatt, R., Setshedi, R., Patel, R., 2005. Preparation of hydroxypropylcellulose membranes using slow ionotropic reactions configured in an experimental design. Journal of Bioactive and Compatible Polymers, 20, 395-414.
111. Ponchel, G., 1994. Formulation of oral mucosal drug delivery systems for the systemic delivery of bioactive materials. Advanced Drug Delivery Reviews, 13, 75-87.
112. Qi, H., Hu, P., Xu, J., Wang, A., 2006. Encapsulation of drug reservoirs in fibers by emulsion electrospinning: morphology characterization and preliminary release assessment. Biomacromolecules, 7, 2327-2330.

113. Ramakrishna, S., Fujihara, K., Teo, W.-E., Lim, T.-C., Ma, Z., 2005. An introduction to electrospinning and nanofibers, World Scientific Publishing Co., London.
114. Ranganath, S.H., Wang, C.-H., 2008. Biodegradable microfiber implants delivering paclitaxel for post-surgical chemotherapy against malignant glioma. Biomaterials, 29, 2996-3003.
115. Rathbone, M.J., Drummond, B.K., Tucker, I.G., 1994. The oral cavity as a site for systemic drug delivery. Advanced Drug Delivery Reviews, 13, 1-22.
116. Reneker, D.H., Chun, I., 1996. Nanometre diameter fibres of polymer, produced by electrospinning. Nanotechnology, 7, 216-223.
117. Reneker, D.H., Yarin, A.L., 2008. Electrospinning jets and polymer nanofibers. Polymer, 49, 2387-2425.
118. Rodriguez, C.F., Bruneau, N., Barra, J., Alfonso, D., Doelker, E., 2000. Hydrophilic cellulose derivatives as drug delivery carriers: influence of substitution type on the properties of compressed matrix tablets. In: Wise, D.L. (Ed.), Handbook of Pharmaceutical Controlled Release Technology, Marcell Dekker, New York, pp. 1–30.
119. Rossi, S., Sandri, G., Caramella, C.M., 2005. Buccal drug delivery: A challenge already won? Drug Discovery Today: Technologies, 2, 59-65.
120. Sahoo, S., Ouyang, H., Goh, J.C.-H., Tay, T.E., Toh, S.L., 2006. Characterization of a novel polymeric scaffold for potential application in tendon/ligament tissue engineering. Tissue Engineering, 12, 91-99.
121. Sastry, S.V., Nyshadham, J.R., Fix, J.A., 2000. Recent technological advances in oral drug delivery – a review. Pharmaceutical Science and Technology Today, 3, 138-145.
122. Sawicka, K., Gouma, P., Simon, S., 2005. Electrospun biocomposite nanofibers for urea biosensing. Sensors and Actuators B, 108, 585-588.
123. Schek, R.M., Taboas, J.M., Hollister, S.J., Krebsbach, P.H., 2005. Tissue engineering osteochondral implants for temporomandibular joint repair. Orthodontics & Craniofacial Research, 8, 313-319.
124. Schnell, E., Klinkhammer, K., Balzer, S., Brook, G., Klee, D., Dalton, P., Mey, J., 2007. Guidance of glial cell migration and axonal growth on electrospun nanofibers of poly-ε-caprolactone and a collagen/poly-ε-caprolactone blend. Biomaterials, 28, 3012-3025.
125. Scholz, O.A., Wolff, A., Schumacher, A., Giannola, L.I., Campisi, G., Ciach, T., Velten, T., 2008. Drug delivery from the oral cavity: focus on a novel mechatronic delivery device. Drug Discovery Today, 13, 247-253.

126. Şenel, S., Hıncal, A.A., 2001. Drug permeation enhancement via buccal route: possibilities and limitations. Journal of Controlled Release, 72, 133-144.
127. Shenoy, S.L., Bates, W.D., Frisch, H.L., Wnek, G.E., 2005. Role of chain entanglements on fiber formation during electrospinning of polymer solutions: good solvent, non-specific polymer-polymer interaction limit. Polymer, 46, 3372-3384.
128. Shukla, S., Brinley, E., Cho, H.J., Seal, S., 2005. Electrospinning of hydroxypropyl cellulose fibers and their application in synthesis of nano and submicron tin oxide fibers. Polymer, 46, 12130-12145.
129. Sibeko, B., Pillay, V., Choonara, Y.E., Khan, R.A., Modi, G., Iyuke, S.E., Naidoo, D., Danckwerts, M.P., 2009. Computational molecular modeling and structural rationalization for the design of a drug-loaded PLLA/PVA biopolymeric membrane. Biomedical Materials, 4, 015014.
130. Sill, T.J., von Recum, H.A., 2008. Electrospinning: Applications in drug delivery and tissue engineering. Biomaterials, 29, 1989-2006.
131. Simpson, D.M., Messina, J., Xie, F., Hale, M., 2007. Fentanyl buccal tablet for the relief of breakthrough pain in opioid-tolerant adult patients with chronic neuropathic pain: a multicenter, randomized, double-blind, placebo-controlled study. Clinical Therapeutics, 29, 588-601.
132. Singh, B., Kumar, R., Ahuja, N., 2004. Optimizing drug delivery systems using systematic "Design of Experiments." Part I: Fundamental aspects. Critical Reviews™ in Therapeutic Drug Carrier Systems, 22, 27-105.
133. Sjökvist, E., Nyström, C., 1991. Physicochemical aspects of drug release. XI. Tableting properties of solid dispersions, using xylitol as carrier material. International Journal of Pharmaceutics, 67, 139-153.
134. Son, W.K., Youk, J.H., Lee, T.S., Park, W.H., 2004. The effects of solution properties and polyelectrolyte on electrospinning of ultrafine poly(ethylene oxide) fibers. Polymer, 45, 2959-2966.
135. Song, M., Pan, C., Li, J., Zhang, R., Wang, X., Gu, Z., 2008. Blends of TiO_2 nanoparticles and poly(*N*-isopropylacrylamide)-*co*-polystyrene nanofibers as a means to promote the biorecognition of an anticancer drug. Talanta, 75, 1035-1040.
136. Standing, J.F., Tuleu, C., 2005. Paediatric formulations – Getting to the heart of the problem. International Journal of Pharmaceutics, 300, 56-66.
137. Stanley, T.H., Ashburn, M.A., 1992. Novel delivery systems: Oral transmucosal and intranasal transmucosal. Journal of Pain and Symptom Management, 7, 163-171.

138. Stewardson, D.J., Whitfield, R.I., 2004. A demonstration of the utility of fractional experimental design for finding optimal genetic algorithm parameter settings. Journal of the Operational Research Society, 55, 132-138.
139. Sudhakar, Y., Kuotsu, K., Bandyopadhyay, A.K., 2006. Buccal bioadhesive drug delivery – A promising option for orally less efficient drugs. Journal of Controlled Release, 114, 15-40.
140. Suwantong, O., Opanasopit, P., Ruktanonchai, U., Supaphol, P., 2007. Electrospun cellulose acetate fiber mats containing curcumin and release characteristic of the herbal substance. Polymer, 48, 7546-7557.
141. Szepes, A., Ulrich, J., Farkas, Z., Kovács, J., Szabó-Révész, P., 2007. Freeze-casting technique in the development of solid drug delivery systems. Chemical Engineering and Processing, 46, 230-238.
142. Taepaiboon, P., Rungsardthong, U., Supaphol, P., 2006. Drug-loaded electrospun mats of poly(vinyl alcohol) fibers and their release characteristics of four model drugs. Nanotechnology, 17, 2317-2329.
143. Taepaiboon, P., Rungsardthong, U., Supaphol, P., 2007. Vitamin-loaded electrospun cellulose acetate nanofiber mats as transdermal and dermal therapeutic agents of vitamin A acid and vitamin E. European Journal of Pharmaceutics and Biopharmaceutics, 67, 387-397.
144. Tan, E.P.S., Ng, S.Y., Lim, C.T., 2005. Tensile testing of a single ultrafine polymeric fiber. Biomaterials, 26, 1453-1456.
145. Tan, E.P.S., Lim, C.T., 2006. Mechanical characterization of nanofibers – A review. Composites Science and Technology, 66, 1102-1111.
146. Tan, S., Feng, X., Zhao, B., Zou, Y., Huang, X., 2008. Preparation and photoluminescence properties of electrospun nanofibers containing PMO-PPV and $Eu(ODBM)_3$phen. Materials Letters, 62, 2419-2421.
147. Tao, J., Shivkumar, S., 2007. Molecular weight dependent structural regimes during the electrospinning of PVA. Materials Letters, 61, 2325-2328.
148. Taylor, G., 1969. Electrically driven jets. Proceedings of the Royal Society of London. Series A, Mathematical and Physical Sciences, 313, 453-475.
149. Theron, S.A., Zussman, E., Yarin, A.L., 2004. Experimental investigation of the governing parameters in the electrospinning of polymer solutions. Polymer, 45, 2017-2030.
150. Tiwari, S.K., Tzezana, R., Zussman, E., Venkatraman, S.S., 2010. Optimizing partition-controlled drug release from electrospun core-shell fibers. International Journal of Pharmaceutics, 392, 209-217.

151. Tripatanasuwan, S., Zhong, Z., Reneker, D.H., 2007. Effect of evaporation and solidification of the charged jet in electrospinning of poly(ethylene oxide) aqueous solution. Polymer, 48, 5742-5746.
152. Tsai, P.P., Schreuder-Gibson, H., Gibson, P., 2002. Different electrostatic methods for making electret filters. Journal of Electrostatics, 54, 333-341.
153. Tungprapa, S., Jangchud, I., Supaphol, P., 2007. Release characteristics of four model drugs from drug-loaded electrospun cellulose acetate fiber mats. Polymer, 48, 5030-5041.
154. US Pharmacopeia 32, 2009. US Pharmacopeial Convention, Rockville, MD.
155. Vaz, C.M., van Tuijl, S., Bouten, C.V.C., Baaijens, F.P.T., 2005. Design of scaffolds for blood vessel tissue engineering using a multi-layering electrospinning technique. Acta Biomateriala, 1, 575-582.
156. Verreck, G., Chun, I., Rosenblatt, J., Peeters, J., Van Dijck, A., Mensch, J., Noppe, M., Brewster, M.E., 2003a. Incorporation of drugs in an amorphous state into electrospun nanofibers composed of a water-insoluble, nonbiodegradable polymer. Journal of Controlled Release, 92, 349-360.
157. Verreck, G., Chun, I., Peeters, J., Rosenblatt, J., Brewster, M.E., 2003b. Preparation and characterization of nanofibers containing amorphous drug dispersions generated by electrostatic spinning. Pharmaceutical Research, 20, 810-817.
158. Vidaurre, A., Cortázar, I.C., Ribelles, J.L.G., 2007. Polymeric scaffolds with a double pore structure. Journal of Non-Crystalline Solids, 353, 1095-1100.
159. Viswanath, B., Ravishankar, N., 2007. Porous biphasic scaffolds and coatings for biomedical applications via morphology transition of nanorods. Nanotechnology, 18, 475604.
160. Viswanathamurthi, P., Bhattarai, N., Kim, H.Y., Lee, D.R., 2003. Vanadium pentoxide nanofibers by electrospinning. Scripta Materiala, 49, 577-581.
161. Winfield, A.J., 2004. Solutions. In: Winfield, A.J., Richards, R.M.E. (Ed.), Pharmaceutical practice, 3rd ed., Churchill Livingstone, London, p. 18.
162. World Health Organization, 2007. Antiretroviral therapy for HIV infection in infants and children: Towards universal access. Recommendations for a public health approach. WHO Press, World Health Organization, Switzerland.
163. World Health Organization, 2008. The International Pharmacopoeia, 4th ed.
164. Wu, C., McGinity, J.W., 2000. Influence of relative humidity on the mechanical and drug release properties of theophylline pellets coated with an acrylic polymer containing methylparaben as a non-traditional plasticizer. European Journal of Pharmaceutics and Biopharmaceutics, 50, 277-284.

165. Xin, Y., Huang, Z., Li, W., Jiang, Z., Tong, Y., Wang, C., 2008. Core-sheath functional polymer nanofibers prepared by co-electrospinning. European Polymer Journal, 44, 1040-1045.
166. Xu, C.Y., Inai, R., Kotaki, M., Ramakrishna, S., 2004. Aligned biodegradable nanofibrous structure: a potential scaffold for blood vessel engineering. Biomaterials, 25, 877-886.
167. Xu, X., Yang, L., Xu, X., Wang, X., Chen, X., Liang, Q., Zeng, J., Jing, X., 2005. Ultrafine medicated fibers electrospun from W/O emulsions. Journal of Controlled Release, 108, 33-42.
168. Xu, X., Chen, X., Liu, A., Hong, Z., Jing, X., 2007. Electrospun poly(l-lactide)-grafted hydroxyapatite/poly(L-lactide) nanocomposite fibers. European Polymer Journal, 43, 3187-3196.
169. Xu, X., Chen, X., Ma, P., Wang, X., Jing, X., 2008. The release behavior of doxorubicin hydrochloride from medicated fibers prepared by emulsion-electrospinning. European Journal of Pharmaceutics and Biopharmaceutics, 70, 165-170.
170. Yang, Q., Li, Z., Hong, Y., Zhao, Y., Qiu, S., Wang, C., Wei, Y., 2004. Influence of solvents on the formation of ultrathin uniform poly(vinyl pyrrolidone) nanofibers with electrospinning. Journal of Polymer Science: Part B: Polymer Physics, 42, 3721-3726.
171. Yang, F., Murugan, R., Wang, S., Ramakrishna, S., 2005. Electrospinning of nano/micro scale poly(L-lactic acid) aligned fibers and their potential in neural tissue engineering. Biomaterials, 26, 2603-2610.
172. Yang, D., Li, Y., Nie, J., 2007. Preparation of gelatin/PVA nanofibers and their potential application in controlled release of drugs. Carbohydrate Polymers, 69, 538-543.
173. Yang, F., Wolke, J.G.C., Jansen, J.A., 2008. Biomimetic calcium phosphate coating on electrospun poly(ε-caprolactone) scaffolds for bone tissue engineering. Chemical Engineering Journal, 137, 154-161.
174. Yao, W.-L., Wang, J.-L., Yang, J., Du, G.-D., 2008a. Novel carbon nanofiber-cobalt oxide composites for lithium storage with large capacity and high reversibility. Journal of Power Sources, 176, 369-372.
175. Yao, W., Yang, J., Wang, J., Tao, L., 2008b. Synthesis and electrochemical performance of carbon nanofiber-cobalt oxide composites. Electrochimica Acta, 53, 7326-7330.

176. Yoshimoto, H., Shin, Y.M., Terai, H., Vacanti, J.P., 2003. A biodegradable nanofiber scaffold by electrospinning and its potential for bone tissue engineering. Biomaterials, 24, 2077-2082.
177. Zaman, M.A., Martin, G.P., Rees, G.D., 2008. Mucoadhesion, hydration and rheological properties of non-aqueous delivery systems (NADS) for the oral cavity. Journal of Dentistry, 36, 351-359.
178. Zeleny, J., 1914. The electrical discharge from liquid points, and a hydrostatic method of measuring the electric intensity at their surfaces. The Physical Review, 3, 69-91.
179. Zeleny, J., 1917. Instability of electrified liquid surfaces. The Physical Review, 10, 1-7.
180. Zeleny, J., 1935. The role of surface instability in electrical discharges from drops of alcohol and water in air at atmospheric pressure. Journal of the Franklin Institute, 219, 659-675.
181. Zeng, J., Xu, X., Cheng, X., Liang, Q., Bian, X., Yang, L., Jing, X., 2003. Biodegradable electrospun fibers for drug delivery. Journal of Controlled Release, 92, 227-231.
182. Zeng, J., Yang, L., Liang, Q., Zhang, X., Guan, H., Xu, X., Chen, X., Jing, X., 2005. Influence of the drug compatibility with polymer solution on the release kinetics of electrospun fiber formulation. Journal of Controlled Release, 105, 43-51.
183. Zong, X., Kim, K., Fang, D., Ran, S., Hsiao, B.S., Chu, B., 2002. Structure and process relationship of electrospun bioabsorbable nanofiber membranes. Polymer, 43, 4403-4412.
184. Zong, X., Li, S., Chen, E., Garlick, B., Kim, K.-S., Fang, D., Chiu, J., Zimmerman, T., Brathwaite, C., Hsiao, B.S., Chu, B., 2004. Prevention of postsurgery-induced abdominal adhesions by electrospun bioabsorbable nanofibrous poly(lactide-co-glycolide)-based membranes. Annals of Surgery, 240, 910-915.